Politecnico di Milano

SCHOOL OF INDUSTRIAL AND INFORMATION ENGINEERING
Master of Science – Mechanical Engineering

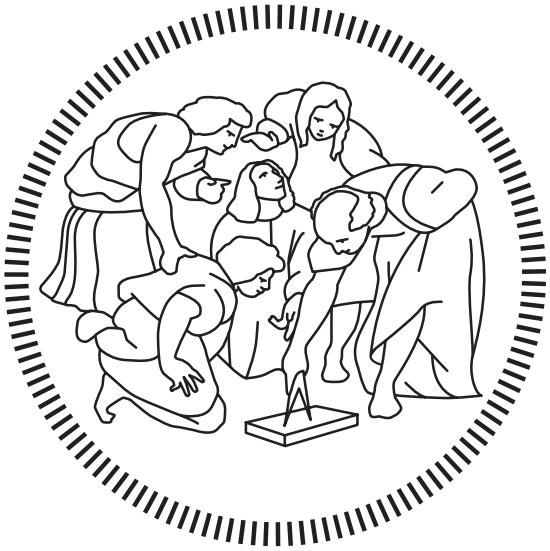

Car and caravan dynamic stability under crosswind

Supervisor
Prof. Paolo SCHITO

Co-Supervisor
Prof. Michele VIGNATI

Candidate
Andrea DELLAVEDOVA – 920865

Academic Year 2019 – 2020

Acknowledgements

Voglio ringraziare in primo luogo il Professor Paolo Schito per avermi supportato durante tutto il lavoro e per avermi aiutato con prontezza.
Un ringraziamento va anche al Professor Michele Vignati per avermi guidato durante le fasi relative alla dinamica del veicolo, al Dottorando Antonio Cioffi per avermi supportato per la fase di realizzazione del modello implementato sul simulatore di guida e, infine, al Dottorando Fabio Semeraro per avermi guidato nella parte di analisi aerodinamiche.
Il più grande ringraziamento va alla mia famiglia per avermi supportato economicamente, ma sopratutto, moralmente durante tutto il percorso di studio; senza la quale non avrei potuto raggiungere questo grande traguardo.
Un grosso grazie anche ai miei nonni per l'immenso amore che mi hanno regalato e che è ricambiato completamente.
Ringrazio anche i miei zii e zia per avermi guidato durante la crescita e per essere sempre presenti nei momenti importanti del mio percorso.
Un enorme ringraziamento va alla mia ragazza Arianna che mi ha supportato nei momenti difficili e che ha reso speciale questi ultimi anni.
Per ultimi, ma non per importanza, voglio ringraziare i miei amici e amiche storiche e i miei amici universitari, grazie per avermi fatto passare dei momenti stupendi pieni di divertimento e emozioni uniche.

Abstract

The work of this thesis concerns the behaviour of a car towing a caravan in crosswind condition. This situation is of particular interest because it can lead to dangerous situations. In fact, especially at high speed, it can affect the stability of the system and it can cause crashes.
Even if there is not a strong wind and a high speed, this system is more prone to instability than a single car due to the fact that the motion of the trailer affects the behaviour of the car. As a consequence, on the road there are particular restrictions for this type of vehicle like lower speed limit.
The aerodynamic of a car towing a caravan has been studied a lot in the past in order to avoid this problem and to find solutions that were able to reduce the drag coefficient and so the fuel consumption.
A few studies have been dedicated to the analysis of the effect of crosswind on such systems, however this dangerous situation, that can lead to the instability, is not solved yet.
In this thesis the behaviour of a car towing a caravan with different crosswinds and different speeds has been analysed through a mathematical model describing the dynamic of the system. The forces that have been generated by the action of the wind are calculated by CFD computation.
Then the aerodynamic models have been validated comparing them with experimental results obtained through wind tunnel tests.

Contents

List of Figures

List of Tables

Chapter 1

Introduction

During 2019, 172,183 road accidents occurred on Italian roads with 3,173 victims and 241,384 total incidents (ISTAT [1]). 333 accidents were caused by strong wind conditions that caused 11 deaths and 455 injuries.
This is what happens in Italy, as regards England, an area most subject to strong winds, the number of accidents caused by strong winds rises to 2700 out of a total of 152158 accidents.
The greatest number of wind-related accidents occur on country roads and highways were high vehicle's speeds increase the cross-wind effect.
In the past, several solutions have been studied to limit the crosswind effects, especially on vehicles with large side surface. Wind barriers and vehicle's shape modifications have been studied in order to reduce the aerodynamic influence under cross-wind. L. Salati [2] studied cross-wind loads on large side surfaces vehicles, in particular they studied the aerodynamic loads on heavy trucks. They carried out a double research, studying both barriers to be installed on the carriageway and changes in the truck's shape in order to reduce the cross-wind effects.
Numerous studies have also been carried out studying the behaviour of vehicles with smaller side surfaces such as cars. Wojciak et al. [3] studied the sedan car dynamic response during variable wind conditions in order to study the aerodynamic loads variations and therefore their effects on the car dynamic behaviour.
According to Thordarson, Researcher, and Olafsson [4] 31% of accidents occur in strong wind conditions (wind with gusts above 10 m/s) of which 64% involve vehicles with trailers. For this vehicle category only two studies have been found related to the aerodynamic analysis of a car towing a caravan.
This type of vehicles are particularly interesting as they are equipped with a large lateral surface, therefore the aerodynamic loads created by the crosswind are considerable. Moreover, the vehicle dynamic configuration make them more sensitive to external loads and they are more prone to instability. The effects of the aerodynamic loads generated on the caravan have strong repercussions on the towing car and consequently on the driver's response, who have to be able to react promptly in order to keep the vehicle on the desired trajectory.
Despite these considerations there are few studies in the literature. Weir, Klein, and Zellner [5] performed a study regarding the behaviour of a car towing an utility trailer under cross-wind conditions. They used a dynamic model in order to study the response of the vehicle and several wind tunnel experiments to study the aerodynamic

loads due to cross-wind.
Darling and Staden [6] studied the particular case of a car towing a caravan by several wind tunnel experiments. They studied the response of the vehicle in presence of cross-wind performing dynamic tests in the wind tunnel.
Therefore, in this work, the aim is to study the aerodynamic loads variation at different wind speeds and angles. In order to compute the aerodynamic coefficients associated with the car and the caravan, several CFD simulations were done and the caravan model was validated using a wind-tunnel experimentation.
Subsequently it has been analysed the aerodynamic effects on the vehicle dynamics, identifying which conditions are the most critical. In particular, it has been analysed a lateral gust, as a critical condition that takes the driver by surprise and it can easily cause instability. In the dynamic analysis, particular attention have been paid to variations in the vertical load on the wheels in order to define safety conditions for overturning. In fact, one of the most common accidents for this type of vehicle in such condition is the rollover caused by strong side winds. The trajectory of the vehicle has also been analysed to verify the critical conditions for the sliding and define the conditions in which the driver is not able to keep the vehicle in the correct carriage.

1.1 State of the art

Cross-wind stability analysis has become very important in recent years. This is due to the fact that strong cross-wind gust could cause accidents or at least increase the discomfort perceived by the driver. In case of simple vehicle, cross-wind influences the driver's perception but in most cases it does not represent critical safety conditions. Cross-wind starts to became a dangerous condition when car is travelling at high speeds, because the driver could take a wrong reaction on the steering wheel and so could lose the car control and so end into an accident (Wojciak et al. [7]).
There are vehicles for which cross-wind is not anymore a comfort issue but became to be a safety problem. In case of trucks, buses, vans or trains, the lateral surface has a grate extensions so cross-wind can generate huge forces that alter the dynamic conditions of the vehicle. In the past there were many examples of accidents caused by cross-wind like what happened in United States on March 2019 for a train or On January 7, 2003, a tractor-trailer rans off the Interstate 81 in Frederick County, Virginia, due to the strong winds (Chen and Cai [8]).
In the case of articulated vehicles the crosswind has a greater effect on stability. Cross-wind is an huge problem for articulated trucks in different situations (traveling on a bridge or leaving a tunnel) in this conditions the high speed of the truck and presence of cross-wind conditions can lead to instability phenomena or to accidents. The articulated vehicle sensibility to cross-wind is increased in the last years due to the fact that, in order to reduce the consumptions and the emissions, lighter and lighter vehicles were produced. Reducing the weight, the relationship between aerodynamic forces and inertia increases and therefore the rollover risk becomes an important factor to be kept under control (Wojciak et al. [3]).
Lateral area plays a fundamental role as it increases the forces generated by the wind on the vehicle. Therefore there are three factors that most influence crosswind sensitivity: weight, side area and the presence of a trailer. Considering these three

factors the car-caravan combination is very sensitive to cross-wind as the trailer has a large side area combined with a low weight.
In this case, the driver's response is particularly difficult as had to control not only the car but also the trailer. In addition, the effects that the trailer has on the car dynamics can be non-intuitive for an inexperienced driver which can cause an incorrect response and the consequent loss of control of the vehicle.
In order to analyse the vehicle behaviour and quantify the risk of accidents, it is necessary to analyse the data that best represent dangerous situations such as the risk of rollover and loss of control of the vehicle.
For the risk of turnover is possible to inspect the roll motion, it is clear that if the roll angle became too big a rollover can happen. While for lateral motion it is well known that articulated vehicles are prone to snaking instability in which the angle between the trailer axis and the car axis experiences an oscillatory behaviour and can lead to loss of control on the towing car (Sharp and Fernández [9]).
Darling and Staden [6] performed an experimental evaluation regarding the stability of a car-caravan combination by coupling a mathematical model with a wind tunnel experiment. They used a 1/12 scale model (figure 1.1) developed by themselves. They did the study based on different aerodynamic conditions and different vehicle positioning configurations, varying not only the wind's speed and incidence angle but also the relative angle between car and caravan. The most of their tests were performed with a wind speed of 20 m/s. They noted that the aerodynamic coefficients vary greatly according to the wind angle of incidence and the relative positioning between the car and the trailer. They also highlighted that the main instability phenomenon concerns the oscillation of the relative angle between the axes of the car and the trailer (defined as snaking). In conclusion they reported that this unstable oscillation can be strongly influenced by aerodynamic effects and therefore can leads to a large deterioration of the vehicle stability.

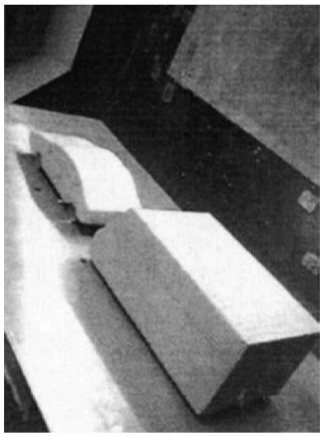

Figure 1.1. Darling et Standen model

Zhang et al. [10] made a numerical investigation regarding a tractor semi-trailer under cross-wind. The aerodynamic behaviour of a tractor with semi-trailer is close to the behaviour of a car towing a caravan. They used a computational model to simulate the aerodynamic characteristics of the vehicle, simulating different wind incidence

angles and they developed a mathematical relationship to predict the aerodynamic coefficients variation with respect to the wind incidence angle variation. While, as far as vehicle dynamics are concerned, they used a multi-body model in order to simulate the vehicle dynamic response. By analysing the dynamic results they were able to correlate the crosswind effects on the vehicle's dynamic behaviour. In particular they analysed the lateral movement, the lateral acceleration and the yaw rate, concluding that the aerodynamic characteristics have a marked influence on the dynamic behaviour of the vehicle.
Weir, Klein, and Zellner [5] used a six degree of freedom model (figure 1.2) coupled with a wind tunnel test to study the response of a car towing a utility trailer under cross-wind. They used different types for both the car and the trailer. They tested both a sedan and station wagon, and as for the trailer, a single-axle trailer and a dual-axle trailer were used. In order to simulate the vehicle dynamic behaviour they used a six degrees of freedom model considering lateral dynamic and roll motion for both subsystems. In order to carry out the aerodynamic test they used a 1/10 scale model by modifying the wind's incidence angle up to 30 deg. They concluded that, as far as aerodynamic characteristics are concerned, the car rear shape has a marginal influence and little effect on the yaw stability of the trailer. While, from a dynamic point of view, the double axle trailer has better behaviour and greater stability. So from this study is possible to understand that the rear shape of the car is not a fundamental parameter like in the drag reduction analysis but the distance between the car and the caravan is the most important aspect.

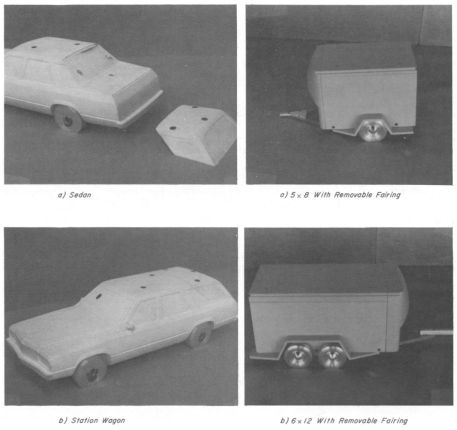

Figure 1.2. Weir et al. models

These are all the studies present on the literature that take in consideration the aerodynamic behaviour of a car towing a caravan in cross-wind conditions. While there are more works concerning the drag reduction on car trailing a caravan. Leon [11] studied the caravan shape influence on the towing car aerodynamic, in particular the aim of his study was the drag reduction. In particular in this work has been studied different caravan shapes and different car-caravan configurations. The conclusion was that, in order to reduce the drag, the caravan needs to have an height similar to the one of the towing car. If the caravan has not an height similar to the one of the towing car, the caravan should be positioned within 0.9 m from the towing car. It has been

noted that, in order to reduce the drag, the caravan should have a front and a rear chamfer.
Huemer et al. [12] studied the influence of unsteady aerodynamics on driving dynamics of passenger cars. In this study CFD simulations have been used in order to find aerodynamic loads acting on the vehicle. With the aerodynamics loads obtained from CFD a multy-body simulation have been used to study the behaviour of the vehicle. It has been done a study on the driver perception using a dynamic driving simulator, concluding that the main parameters that affect the driver's perception are the lateral acceleration and the yaw velocity.
Zhang [13] studied the non-stationary crosswind stability of ground vehicles. He studied different vehicles responses under cross-wind conditions, considering both railway vehicles and road vehicles. In this work has been used a non-stationary wind model based on NONAR method. It was studied the car towing a caravan behaviour under cross-wind and made a risk analysis based on the lateral displacement, the yaw angle variation and the vertical load changes. It has been found different situations in which the vehicle is unstable and concluded that the driver response is a fundamental parameter. As can be imagined, a driver with experience can control the vehicle much better.

1.2 Dynamic model

A mathematical model is necessary in order to understand the dynamic behaviour of the system. The mathematical model must be able to reproduce the motion of the system and it must output the positions, speeds and accelerations related to system's particular points.
There is a wide range of choices regarding which mathematical model to use. The choice ranges from simple models with few degrees of freedom, easy to implement but not very accurate, to complex multi-body models that represent the real behaviour in a very truthful way but they require the use of dedicated software. In the choice of the model it is necessary to consider its application, therefore it is necessary to adopt a model that reproduce accurately the behaviour that has to be study without unnecessary complexity. He and Ren [14] carried out a comparison between different models, considering both very simple and complex models, in order to find the right tradeoff between complexity and accuracy. They used as reference a multi-body model developed with CarSim software that uses 21 degrees of freedom and that reproduces very accurately the real behaviour of the vehicle. The models that have been analysed were: a linear model with three degrees of freedom, a non-linear model with 4 degrees of freedom and a non-linear model with 6 degrees of freedom. They tested the models by simulating different maneuvers to get the widest possible overview. They considered a single-lane change maneuver at low speed, a single-lane change maneuver at high speed and a Fishhook maneuver. They concluded that the three degrees of freedom linear model can only be used if the aim is to analyse the lateral behaviour of the vehicle at low speeds and there is not the intend to study the roll. While, if the intent is to analyse maneuvers at high speeds and the rolling behaviour of the vehicle, as in the case of this work, it is necessary to use a more complex model such as a non-linear model with six degrees of freedom.

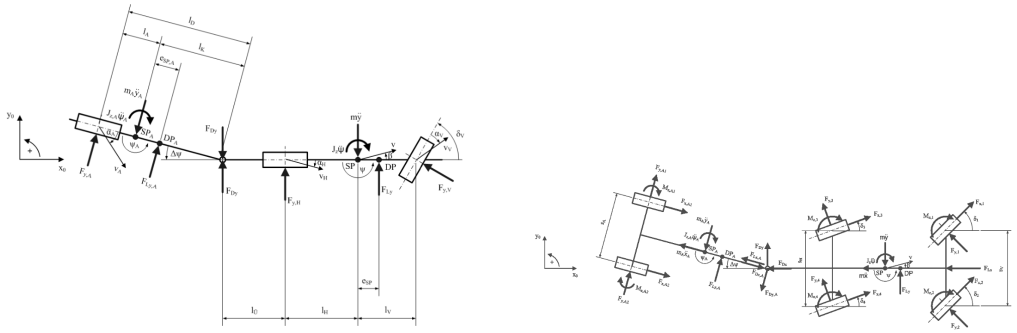

(a) *Linear single track model* (b) *Non-linear double track model*

Figure 1.3. Hubner et al.'s models

The aim of the work made by Hubner et al. [15] was to develop a control to stabilise the car-caravan combination by means of a sliding-control. For the development of the control they used two different models: a linear single track model and a non-linear double track model. The linear single-track model considers only one wheel per axle, no vertical load changes during maneuvers and the lateral forces exchanged at the wheel road contact point are considered linear with the side slip angle. This model is usable up to 0.4 g of lateral acceleration and does not consider roll, so in order to improve the simulation they resorted to a more complex model that also included loads transfers. The non-linear double track model considers two wheels for each axle, the center of gravity is no longer on the ground but at it is at a certain height making it possible to consider also the loads transfers and the forces exchanged with the ground are no longer linear. The scheme that they used is reported in figure 1.3. This model allows to analyse the roll dynamics and the lateral forces variation due to the vertical load variation thus ensuring a more accurate simulation.

Robert Tafner [16] presented two methods in order to identify roll dynamics parameters. They used a four degrees of freedom model considering the lateral dynamics and the roll dynamics in order to evaluate the roll angle. In their model (represented in figure 1.4) a linear behaviour is assumed for what concern the suspensions, the slope of the road surface is neglected, the pitch and the roll centers heights are negligible.

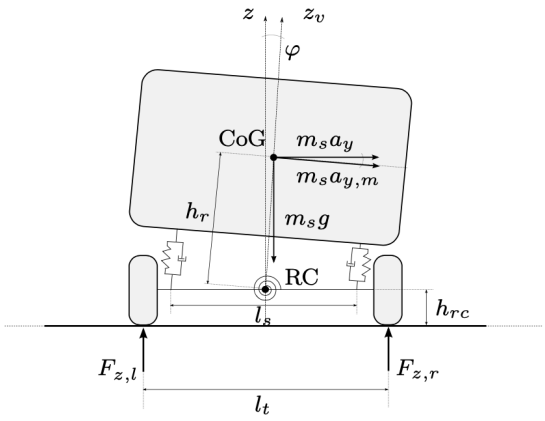

Figure 1.4. Roll model by Tafner et al.

1.3 Aerodynamic model

An aerodynamic model for both the car and the caravan are needed in order to be able to perform an aerodynamic simulation. The choice of the two models is not trivial as there is the possibility to choose between numerous car and caravan models. During the choice of the models, it is necessary to consider which cars are most used to tow caravans and which caravans are most used on the roads. The shape that most influences the aerodynamic characteristics is the one of the caravan, due to the fact that it has a larger surface, especially the lateral one, and it is less tapered, thus it produces great resistance with the air. For this reason it is necessary to choose the caravan model correctly, while as regards the shape of the car, especially the rear of the car, as noted by Weir, Klein, and Zellner [5], it is possible to have a big margin in the choice. Another very important aspect in the choice of the model to be used in CFD simulations is the number of studies that are present in the literature in order to have different results needed to validate the model. Regarding the car model is very simple to find several aerodynamic studies that have been carried out both with longitudinal wind and with cross wind on different types of cars. Different models have been created and some of them are worldwide recognised; such as the DrivAer model and the Ahmed Body model. While it is difficult to find a caravan standard model worldwide recognised because there are few studies in the literature and each of them uses a on-off model created by the author.

1.3.1 Car model

The aerodynamics of cars has always been studied; this discipline has a fundamental role in the automotive field as by knowing the phenomenon in depth, cars can be developed with great advantages like drag reduction and downforce improvement.
Drag force has been studied a lot in the past, numerous studies have been carried out to study which are the aspects that most influence the drag force. The drag study was born from the aim of increasing the car speed and subsequently found great success also for the consumption reduction. One of the most used models, thanks to its simplicity is the Ahmed Body model (figure 1.5). The purpose of the Ahmed Body

model is to analyse the rear shape of the car effects, in particular paying attention to the drag forces.

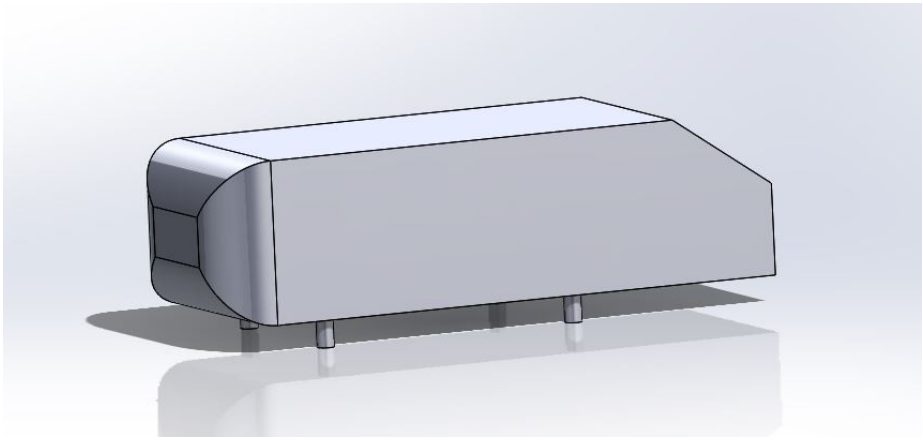

Figure 1.5. Ahmed body model

With the evolution of aerodynamic analysis methods, this model has become too simple to carry out an accurate analysis and therefore there was the necessity to develop more complex models . One of the most complex models and which allows a more refined analysis is the DrivAer model developed by TUM (TUM [17]). This model has the advantage of being modular and therefore allows to modify some components to study different phenomena. For example, it allows to modify the rear shape of the car, allows to consider both a smooth bottom and a detailed bottom, allows the study of the flow inside the engine compartment also considering the pressure drops due to the presence of radiators etc.
This model is also used for study crosswind conditions effects as in the case studied by Wojciak et al. [3]. In this study, a non-stationary aerodynamic analysis was conducted to evaluate the effects of wind dynamics. A 1:2 scale model was used to carry out the analysis, which had an oscillating trend respect to the vertical axis during the acquisitions in the wind tunnel test. The results obtained indicate that, in non-stationary conditions, the aerodynamic loads are significantly different from the stationary ones, but, as far as lateral forces and roll moments are concerned, they are over-predicted by the quasi-static approximation. For this reason, quasi-static aerodynamic analysis are used in this study. When choosing the car model it was considered also the car types that are most used for towing a caravan. According to Hevans [18] the most used models for this purpose are either SUVs or sedans. Therefore, the DrivAer model (figure 1.6) is particularly useful for this purpose.

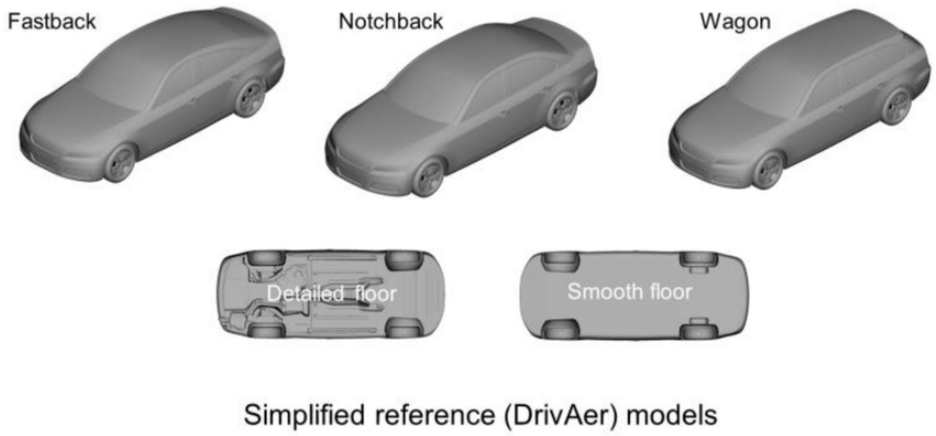

Figure 1.6. DrivAer model

Howell and Panigrahi [19] studied the influence of crosswinds, under different angles of attack, on the behaviour of different car types. They studied different vehicles for each topology in order to have a large number of results. They performed several tests for each vehicle type concerning different wind angles. In this way they were able to obtain the variation of lateral forces as a function of the wind incidence angle. They studied the side forces trend at different wind's angles and for different vehicle shape. The results show that the most important parameter for what concern the side forces is the vehicle height and that the vehicle length has a lower influence. Their result were used in order to validate the results from the DrivAer model CFD analysis.

1.3.2 Caravan model

There is a large variety of caravans on the market, each model differs in size, weight, number of axles and shape (Leon [11]). Some examples are given below:

- Conventional single axle;
- Twin axle;
- Pop Top caravan;
- GRP fiberglass;
- Camper Trailer;
- Fifth Wheelers.

The most used model is the Conventional single axle caravan model (figure 1.7), this model is characterised by a single axle, a length ranging from 3 to 6 meters and can accommodate from two to six people with all utilities.

Figure 1.7. Caravan Standard

Double axle caravans (figure 1.8) have greater stability and greater load capacity, however they are more difficult to maneuver especially in tight maneuvers.

Figure 1.8. Double axle caravan

An interesting model is the Pop-Top model (figure 1.9), this model is equipped with an extendable roof. This particularity allows to maintain a reduced frontal area while driving, thus reducing drag and improving consumption; once arrived at destination, the roof is lifted, regaining the internal volume.

Figure 1.9. Pop-Top model

The GRP type caravans are among the smallest on the market, their goal is to guarantee a minimum capacity with the advantage of a high cost reduction.
The camper-trailer models are the evolution of the Pop-Top as they reduce the overall dimensions to a minimum during freight, reducing fuel consumption more markedly than the Pop-Tops and allow better maneuverability and stability when towing. Once positioned, they allow to expand the internal volume not only thanks to the lifting of the roof but also to the expansion of all the walls.
Finally, the Fifth-Wheelers models are the most bulky, with very large living volumes at the expense of ease of towing. These models can have up to three axis and are difficult to tow by standard cars as they have a considerable mass.
For the purpose of this work, the model that is best suited is the Standard single-axis model, as it is the most widespread model and does not present any type of aerodynamic device.

1.3.3 Wind model

The definition of the wind model is one of the most important aspects of the study. During the motorway travel different wind conditions can occur. Therefore, it is necessary to define a model that replicates the most critical conditions such as side gusts. In the literature there are several models able to define this phenomenon.
According to Carrarini [20] the wind can be defined according to two macro models: steady and unsteady wind. The first is defined in the case in which the fluctuations are low compared to the average value and, in this case, the wind speed is considered constant and equal to its average value. In the second case the fluctuations are large compared to the average value and can no longer be neglected. In this case the *frozen turbolence* hypothesis is widely used and therefore the fluctuations are added to the average speed value.
According to Wetzel and Proppe [21] it is possible to define a simplified model that defines the turbulent component as an ideal gust. This definition allows to define a gust profile fixed in space.
The fixed wind gust method can be used with different profiles as known from Carrarini [20]; can be characterised by impulse or step profiles. Some of the possible profiles are reported in figure 1.10 and are: *rugby-ball*, mainly used for aeronautical purposes;

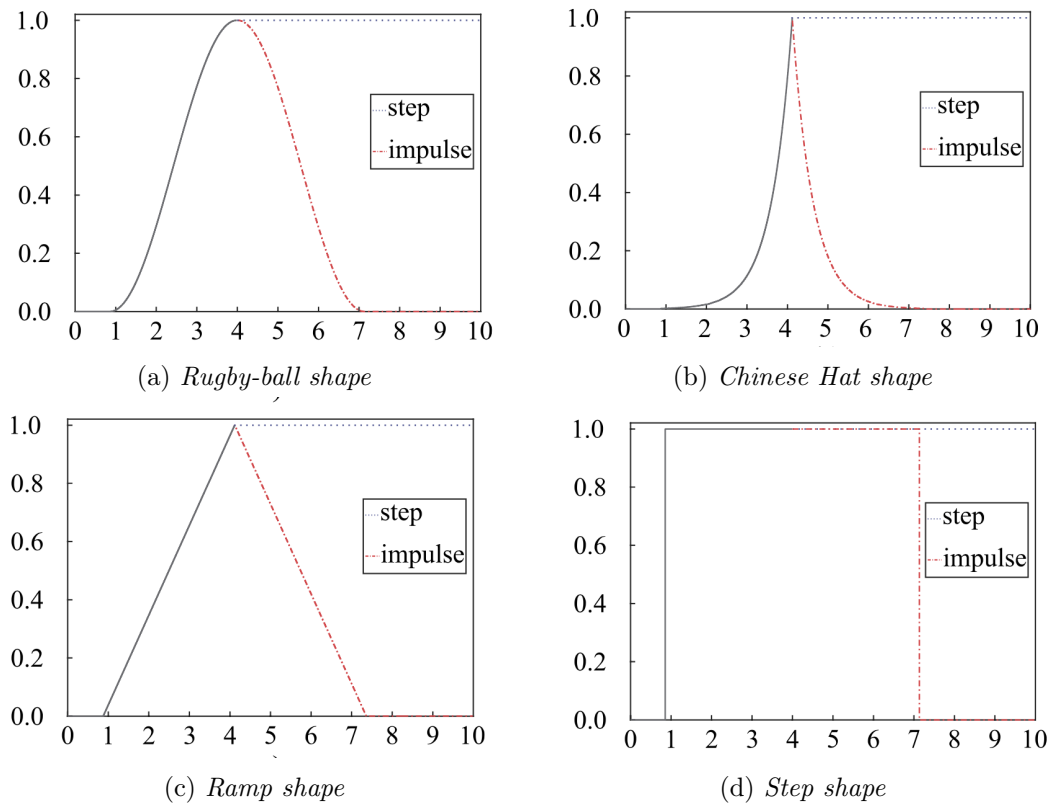

(a) *Rugby-ball shape* (b) *Chinese Hat shape*

(c) *Ramp shape* (d) *Step shape*

Figure 1.10. Wind models

exponential shape; *ramp* shape and the *step* shape. In this study the *Chinese Hat* shape is used. The *Chinese Hat* shape has a fixed width and a direction transversal to the movement of the vehicle. This model does not consider the wind angle variations during the vehicle motion.

Once the wind profile has been defined, it is important to study which speeds are encountered while driving and to evaluate the most critical conditions. One way to understand which speeds are to be considered is to analyse the statistical characterisation of the wind speeds in a fixed geographical area as was done by Burlando et al. [22]. In this work a statistical analysis was carried out on the Ligurian-Tuscan region using data collected from anemometric stations over a period of 58 years. These data were processed to take into account the incompleteness of long-standing data and various discontinuities in acquisitions. The final results reported average speeds, with a return period of 50 years, up to $58.89 m/s$ in the locality of Cap Sagro located on the east coast of Corsica. As regards more populated locations, therefore with a greater number of infrastructures such as motorways, the average speeds recorded are equal to 23.59 m/s in Florence, $23.18 m/s$ in Pisa and $27.97 m/s$ in Albenga.

Chapter 2

Mathematical model

The aim of this chapter is to explain the mathematical model used to simulate the dynamic behaviour of the system. The model is used to simulate the response of the vehicle under the effect of cross-wind and to find the threshold over which the the vehicle became unstable. The model has been implemented in MATLAB™and SIMULINK™.

2.1 Vehicle model

In order to describe the behaviour of the system a non-linear model was used for both the car and the caravan. The car and the caravan are described by simple scheme (figure 2.1) highlighting the fundamental points to describe the motion of the system.

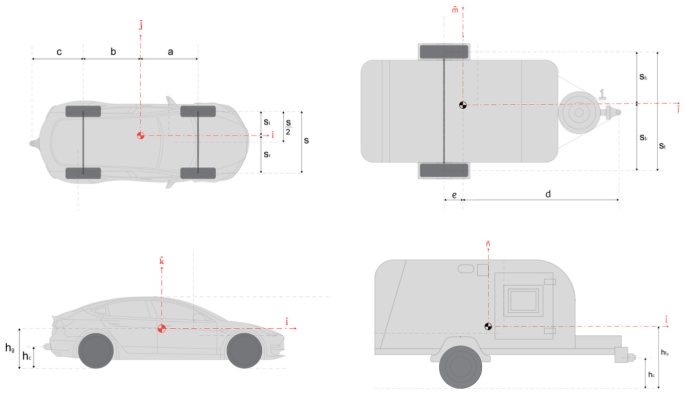

Figure 2.1. Model scheme

The motion of the system is describe within two plane, the first one is parallel to the ground, it describes the lateral dynamic of the car and trailer, while the second one is perpendicular to the ground and it is used to describe the roll motion of the system (figure 2.2). The car has four contact points with ground while the caravan has two contact points due to the fact that a single axle caravan is considered. The two are connected by pin joint that allow only the rotation while the translation is fixed. In oder to consider the roll motion the suspensions characteristic have been

considered including the anti-roll bar both for front and rear axis of the car.

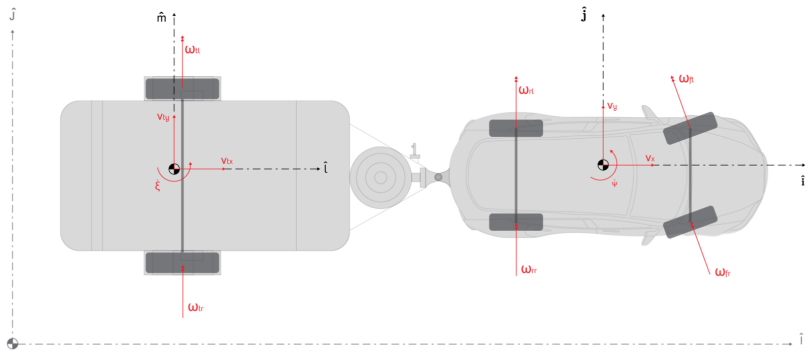

Figure 2.2. Reference systems and degree of freedom

The following assumptions have been made:

1. The road is assumed to be perfectly smooth. This assumption has been made due to the fact that comfort analysis is not considered in this work;
2. Pitch motion and vertical motion have been used only to evaluate the vertical forces acting on the wheels caused by loads transfer;
3. The external forces acting on the system are limited to the one caused by wind action and tyre road contact forces. The aligning torque generated by the contact patch has been ignored. Aerodynamic forces have been evaluated by CFD analysis;
4. All the suspensions geometry like caster, toe, camber angles have been neglected and also ply steer conicity of tyres has not been considered;
5. Friction in the pin joint between car and caravan has been ignored;
6. A front wheel drive car has been considered without any type of control except for the driver.

In order to describe the motion of the model fourteen degrees of freedom have been chosen, highlighted in figure 2.3 , that are reported in the following:

1. Lateral motion of the two centers of gravity of the car and the trailer described by means of the lateral coordinate expressed as Y_i where the subscript i distinguish between car (c) and trailer (t);

2. Longitudinal motion of the two centers of gravity described by longitudinal coordinate expressed as X_i where i represent the car (c) or the trailer (t);

3. Yaw motions of the car and of the trailer described by yaw angle expressed as ψ_i where i indicates which vehicle is representing;

4. The roll motions of the car and the trailer described by the roll angle expressed as ϕ_i where i is as previous;

5. Rotation with respect to the wheels axis for all the four wheels of the car and the two wheels of the caravan, for a total of six rotation expressed as ω_{ij} where i explains which axis is consider while j tells which side is considered;

There are three different reference systems in order to describe the model, one absolute reference system and two relative reference systems:

1. Absolute reference system: $\hat{I} - \hat{J} - \hat{K}$;

2. Relative reference system placed on the center of gravity of the car:$\hat{i} - \hat{j} - \hat{k}$;

3. Relative reference system placed on the center of gravity of the caravan:$\hat{l} - \hat{m} - \hat{n}$;

The three reference systems are related by means of the following relations:

$$\begin{Bmatrix} \hat{I} \\ \hat{J} \end{Bmatrix} = \begin{bmatrix} \cos\psi_c & -\sin\psi_c \\ \sin\psi_c & \cos\psi_c \end{bmatrix} \begin{Bmatrix} \hat{i} \\ \hat{j} \end{Bmatrix}; \begin{Bmatrix} \hat{I} \\ \hat{J} \end{Bmatrix} = \begin{bmatrix} \cos\psi_t & -\sin\psi_t \\ \sin\psi_t & \cos\psi_t \end{bmatrix} \begin{Bmatrix} \hat{l} \\ \hat{m} \end{Bmatrix} \tag{2.1}$$

$$\begin{Bmatrix} \hat{l} \\ \hat{m} \end{Bmatrix} = \begin{bmatrix} \cos\psi_c - \psi_t & -\sin\psi_c - \psi_t \\ \sin\psi_c - \psi_t & \cos\psi_c - \psi_t \end{bmatrix} \begin{Bmatrix} \hat{i} \\ \hat{j} \end{Bmatrix} \tag{2.2}$$

2.1.1 Equations of motion

In order to describe the dynamic behaviour of the system it is necessary to compute the equations of motion. This has been done by performing forces and moments balance. There are different types of forces acting on the model:

1. Inertial forces;

2. Contact forces between tyres and ground;

3. Resistance forces, for example rolling resistance;

4. Aerodynamic forces, these forces are computed by using CFD.

In order to represent all the different type of forces the following format has been used : F_{kij}. Where k represent the direction of the force, i and j represent which force is considered, for example fl stays for front left and is referred to the contact force of the front left tyre. The equations of motion calculation of can be carried out by considering car and caravan as a coupled system. This technique is more expensive from an analytical point of view as the forces on the hinge, being internal forces, are not explicit. Another technique is to replace the hinge joint by means of a group of

springs in all directions and using very high stiffnesses in order to reproduce the type of constraint. In this way it is possible to express the forces exchanged by the hinge and decouple the two systems in order to solve the equations of motion individually for both the car and the caravan. The latter method has the advantage of being able to analyse the behaviour of the forces exchanged between car and trailer.

The equations of motion were obtained by calculating the equilibria in the longitudinal and lateral direction and making the moment with respect to the center of gravity of the model in figure 2.3.

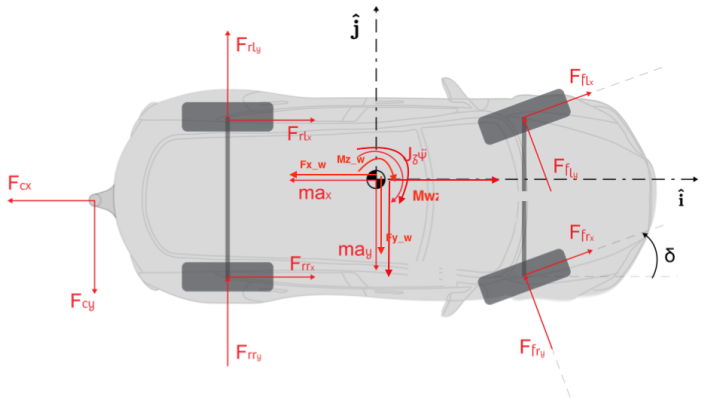

Figure 2.3. Car scheme

$$\begin{cases} a_{xc} = \dfrac{(F_{xfl}+F_{xfr})\cos\delta + (F_{xrl}+F_{xrr}) - (F_{yfl}+F_{yfr})\sin\delta - F_{xc} - F_{xw}}{m_c} \\ a_{yc} = \dfrac{(F_{yfl}+F_{yfr})\cos\delta + (F_{xfl}+F_{xfr})\sin\delta + (F_{yrl}+F_{yrr}) - F_{yc} - F_{yw}}{m_c} \\ \ddot{\psi}_c = ([(F_{xfl}+F_{xfr})\sin\delta + (F_{yfl}+F_{yfr})\cos\delta]\,a - ((F_{yrl}+F_{yrr})b) \\ \qquad +F_{yc}(b+c) - [F_{xfl}\cos\delta - F_{yfl}\sin delta + F_{xrl}]\,s_c \\ \qquad -[F_{yfr}\sin\delta - F_{xfr}\cos\delta - F_{xrr}]\,s_c + M_{zwc})/J_{zc} \end{cases} \tag{2.3}$$

Doing the same for the caravan model represented in figure 2.4 have been obtained the following:

$$\begin{cases} a_{xt} = \dfrac{F_{xtl}+F_{xtr}+F_{xcl}-F_{xwt}}{m_t} \\ a_{yt} = \dfrac{F_{ytl}+F_{ytr}+F_{yct}-F_{ywt}}{m_t} \\ \ddot{\psi}_t = \dfrac{F_{yctl}d - (F_{ytl}+F_{ytr})e - F_{xtl}s_t + F_{xtr}s_t + M_{zwt}}{J_{zt}} \end{cases} \tag{2.4}$$

The forces exchanged by the hinge between car and trailer are linked by the following link:

$$\begin{Bmatrix} F_{xct} \\ F_{yct} \end{Bmatrix} = \begin{bmatrix} \cos\psi_c - \psi_t & -\sin\psi_c - \psi_t \\ \sin\psi_c - \psi_t & \cos\psi_c - \psi_t \end{bmatrix} \begin{Bmatrix} F_{xc} \\ F_{yc} \end{Bmatrix} \tag{2.5}$$

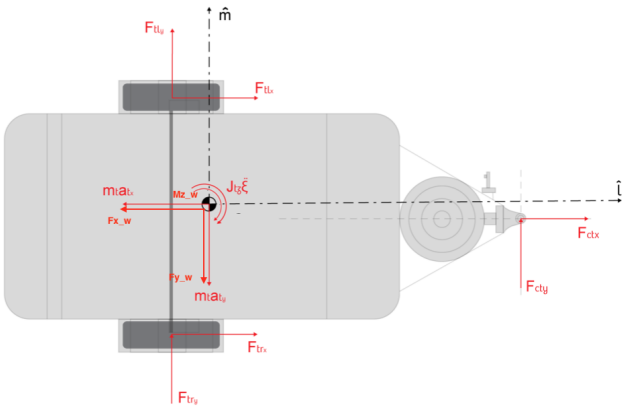

Figure 2.4. Caravan scheme

As regards the rolling behaviour of the two vehicles, it has been decided to consider the vehicle body separately from the suspended masses and consider the deformability of the tires. Then the vertical balances concerning the vehicle body and the suspended masses have been carried out in order to obtain the vertical forces that are exchanged by the wheels and therefore consider the load transfers.

$$\begin{aligned} \ddot{z_{bc}} &= \frac{F_{s1c} + F_{s2c} - F_{zwc} + F_{zc}}{m_c} \\ \ddot{z_{bt}} &= \frac{F_{s1t} + F_{s2t} - F_{zwt} + F_{zct}}{m_t} \end{aligned} \tag{2.6}$$

Where F_{sij} are the suspensions forces and i represent the side of the vehicle (left 1 right 2) and j indicate if the force is of the car or of the trailer. The suspensions forces have been grouped for each side due to the fact that the pitch motion was not considered and only the roll motion has been computed. The suspensions forces have been evaluated considering the vertical motion of the unsprung masses, considering different stiffness and damping for rear and front axle of the car and, obviously, have been considered different stiffness for the caravan suspensions. In the following the equation of motion for each wheel and the formulation of the suspension forces are reported:

$$\ddot{z_{wij}} = \frac{(-F_{sij} - k_t z_{wij})}{m_k} \tag{2.7}$$

$$F_{sij} = -k_i(z_b - z_{wij} - (\frac{s \sin \varphi_k}{2})) - r_i(\dot{z_b} - \dot{z_{wij}} - (\frac{s\dot{\varphi} \cos \varphi}{2})) \tag{2.8}$$

In order to be able to consider the roll angle values during the simulation, two moment balances have been performed with respect to the roll centers of car and

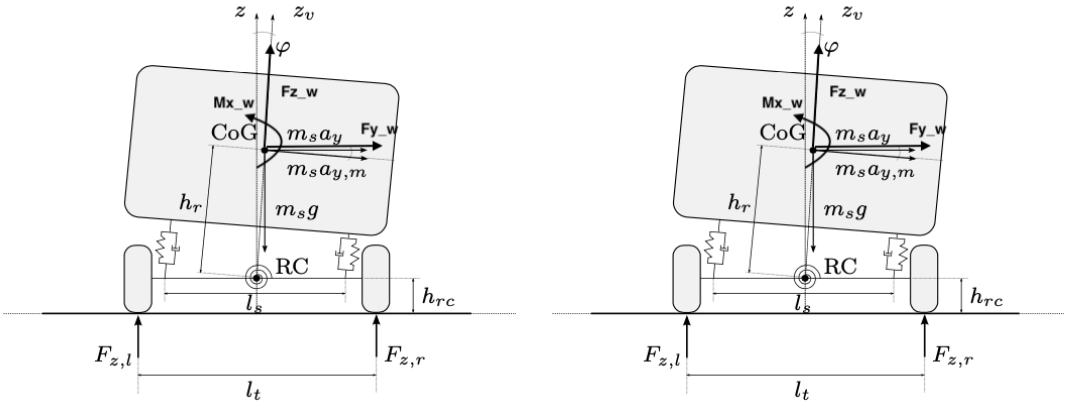

(a) *Roll car's scheme* (b) *Roll caravan's scheme*

Figure 2.5. Roll model

caravan respectively. For the car, anti-roll bars have been considered as they are normally present on road cars while, in the case of the caravan, no anti-roll bars have been considered as usually this type of vehicles are equipped with a more rudimentary type of suspension.
The two equation of motion describing the roll motion are reported in the following for the car and trailer respectively (with reference on the figure 2.5):

$$\begin{aligned}\ddot{\varphi}_c = -(m_c(a_{yc}\cos\varphi_c - g\sin\varphi_c) + F_{ywc}\cos\varphi_c + F_{zwc}\sin\varphi_c)h_r \\ -F_{zc}\sin\varphi_c h_c + F_{yc}\cos\varphi_c h_c + \frac{s_c}{2}(F_{s1c} + F_{s2c}) + M_{rollf} + M_{rollr} - M_{xwt}\end{aligned} \tag{2.9}$$

$$\begin{aligned}\ddot{\varphi}_t = -(m_t(a_{yt}\cos\varphi_t - g\sin\varphi_t + F_{ywt}\cos\varphi_t \\ +F_{zwt}\sin\varphi_t)h_{rt} - F_{zct}\sin\varphi_t h_t + F_{yct}\cos\varphi_t h_t + \frac{s_c}{2}(F_{s1t} + F_{s2t}) - M_{xwt}\end{aligned} \tag{2.10}$$

2.1.2 Kinematic relations

In order to be able to fully analyse the motion of the vehicle it is necessary to know the behaviour of some fundamental points such as the wheels. To do this, it is necessary to identify the kinematic links that link the motion of these points with the free coordinates of the system.
Below are reported these links for both the car and the trailer:

- For the car in longitudinal direction:

$$\begin{aligned} v_{xfl} &= (v_x - \dot{\psi}_c s_c)\cos\delta + (v_y + \dot{\psi}_c a)\sin\delta \\ v_{xfr} &= (v_x + \dot{\psi}_c s_c)\cos\delta + (v_y + \dot{\psi}_c a)\sin\delta \\ v_{xrl} &= v_x - \dot{\psi}_c s_c \\ v_{xrr} &= v_x + \dot{\psi}_c s_c \\ v_{xc} &= v_x \end{aligned} \tag{2.11}$$

- For the car in lateral direction:

$$\begin{aligned} v_{yfl} &= (v_y + \dot{\psi}_c a)\cos\delta - (v_x - \dot{\psi}_c s_c)\sin\delta \\ v_{yfr} &= (v_y + \dot{\psi}_c a)\cos\delta - (v_x + \dot{\psi}_c s_c)\sin\delta \\ v_{yrl} &= v_y - \dot{\psi}_c b \\ v_{yrr} &= v_y - \dot{\psi}_c b \\ v_{xc} &= v_y - \dot{\psi}_c (b + c) \end{aligned} \tag{2.12}$$

- For the trailer in longitudinal direction:

$$\begin{aligned} v_{xt} &= v_{xct} - \dot{\psi}_t (s_t - \frac{s_t}{2}) \\ v_{xtl} &= v_{xt} - \dot{\psi}_t s_t \\ v_{xtr} &= v_{xt} + \dot{\psi}_t s_t \end{aligned} \tag{2.13}$$

- For the trailer in longitudinal direction:

$$\begin{aligned} v_{yt} &= v_{yct} - \dot{\psi}_t d \\ v_{ytl} &= v_{yt} - \dot{\psi}_t e \\ v_{ytr} &= v_{yt} + \dot{\psi}_t e \end{aligned} \tag{2.14}$$

- The relationships that link the speeds of the hinge between car and trailer are:

$$\begin{Bmatrix} v_{xct} \\ v_{yct} \end{Bmatrix} = \begin{bmatrix} \cos\psi_c - \psi_t & -\sin\psi_c - \psi_t \\ \sin\psi_c - \psi_t & \cos\psi_c - \psi_t \end{bmatrix} \begin{Bmatrix} v_{xc} \\ v_{yc} \end{Bmatrix} \tag{2.15}$$

All equations have been developed with reference to the scheme in figure 2.6.

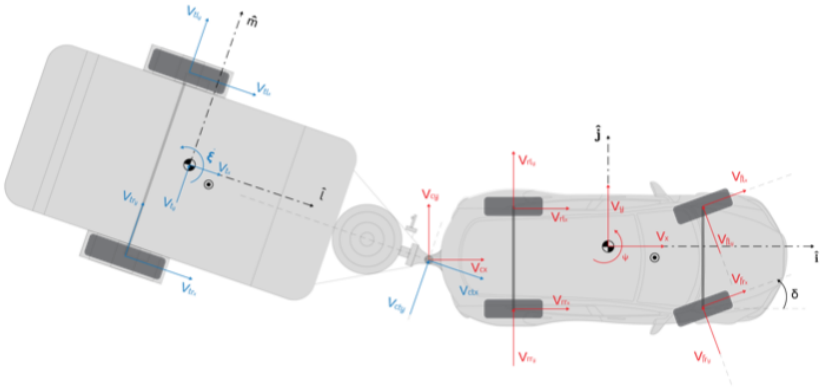

Figure 2.6. Kynematic scheme

It is necessary to introduce a further transformation regarding the accelerations by obtaining it from the derivative of the velocity with respect to time:

- As for the accelerations of the car:

$$\begin{aligned} a_x &= \dot{v_x} - v_y\dot{\psi_c} \\ a_y &= \dot{v_y} + v_x\dot{\psi_c} \end{aligned} \tag{2.16}$$

- As for the accelerations of the caravan:

$$\begin{aligned} a_{xt} &= \dot{v_{xt}} - v_{yt}\dot{\psi_t} \\ a_{yt} &= \dot{v_{yt}} + v_{xt}\dot{\psi_t} \end{aligned} \tag{2.17}$$

2.1.3 Vertical forces

The contact between the tires and the road generates vertical forces which influence the lateral forces generated by the wheels.

Vertical forces are considered as the sum of two components:

- Static load due to weight and its distribution in the car body. This component remains constant;
- Dynamic vertical load due to inertia forces due to the accelerations undergone by the vehicle during maneuvers; these forces are also affected by aerodynamic loads.

As far as the static vertical forces on the car body are concerned, they have been obtained by means of the equilibria from the scheme reported in figure 2.8:

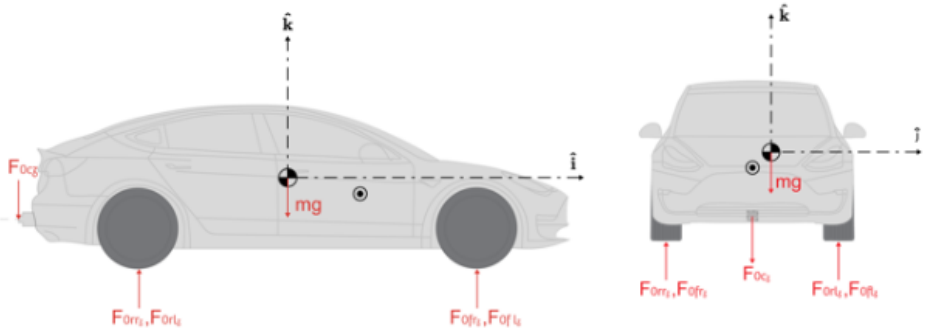

(a) Side view **(b)** Front View

Figure 2.7. Vertical static load of the car

The results are:

$$\begin{aligned} F_{z0fl} &= mg\frac{b}{a+b}\frac{1}{2} - F_{z0c}\frac{c}{a+b}\frac{s}{2} \\ F_{z0fr} &= mg\frac{b}{a+b}\frac{1}{2} - F_{z0c}\frac{c}{a+b}\frac{s}{2} \\ F_{z0rl} &= mg\frac{a}{a+b}\frac{1}{2} + F_{z0c}\frac{a+b+c+}{a+b}\frac{s}{2} \\ F_{z0rr} &= mg\frac{a}{a+b}\frac{1}{2} + F_{z0c}\frac{a+b+c+}{a+b}\frac{s}{2} \end{aligned} \tag{2.18}$$

While, for the dynamic component of the vertical forces of the car the scheme below (figure 2.8) has been considered where have been considered not only the inertia but also the aerodynamic load experienced by the car.
The aerodynamic loads are considered in the center of gravity.

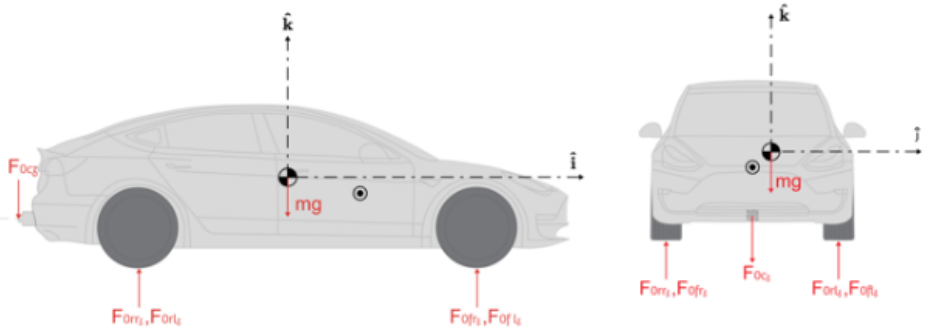

(a) Side view **(b)** Front View

Figure 2.8. Vertical load transfer of the car

The results are:

$$
\begin{aligned}
\delta F_{zrl} &= \frac{F_{xc}h_c + \delta F_{zc}(a+b+c) + M_{yw} + (ma_x + F_{xw})h_g - F_{zw}a}{2(a+b)} \\
&\quad + \frac{M_{xw} + \delta F_{zc}\frac{s}{2} - F_{yc}h_c - F_{zw}\frac{s}{2}}{s}\frac{K_{roll-r}}{K_{roll-r}+K_{roll-f}}; \\
\delta F_{zrr} &= \frac{F_{xc}h_c + \delta F_{zc}(a+b+c) + M_{yw} + (ma_x + F_{xw})h_g - F_{zw}a}{2(a+b)} \\
&\quad - \frac{M_{xw} + \delta F_{zc}\frac{s}{2} - F_{yc}h_c - F_{zw}\frac{s}{2}}{s}\frac{K_{roll-r}}{K_{roll-r}+K_{roll-f}}; \\
\delta F_{zfl} &= \frac{-F_{xc}h_c - \delta F_{zc}c - M_{yw} - (ma_x + F_{xw})h_g + F_{zw}b}{2(a+b)} \\
&\quad + \frac{M_{xw} + \delta F_{zc}\frac{s}{2} - F_{yc}h_c - F_{zw}\frac{s}{2}}{s}\frac{K_{roll-f}}{K_{roll-r}+K_{roll-f}}; \\
\delta F_{zfr} &= \frac{-F_{xc}h_c - \delta F_{zc}c - M_{yw} - (ma_x + F_{xw})h_g + F_{zw}b}{2(a+b)} \\
&\quad - \frac{M_{xw} + \delta F_{zc}\frac{s}{2} - F_{yc}h_c - F_{zw}\frac{s}{2}}{s}\frac{K_{roll-f}}{K_{roll-r}+K_{roll-f}};
\end{aligned}
\tag{2.19}
$$

For the trailer is the same, first are reported the static load and after that there are the load transfer with reference on the scheme in figure 2.9:

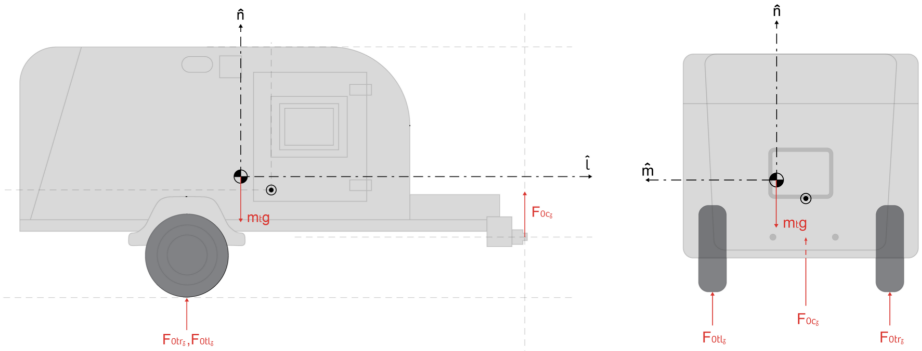

(a) Side view **(b)** Rear View

Figure 2.9. Vertical static load of the caravan

$$
\begin{aligned}
F_{z0tr} &= m_t g \frac{d}{d+e}\frac{1}{2} \\
F_{z0tr} &= m_t g \frac{d}{d+e}\frac{1}{2} \\
F_{z0c} &= m_t g \frac{e}{d+e}
\end{aligned}
\tag{2.20}
$$

And for the loads transfer the scheme is reported in the figure 2.10:

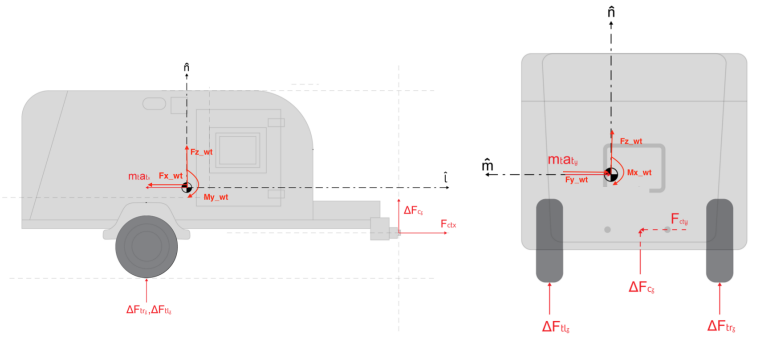

(a) Longitudinal load transfer (Side View)

(b) Lateral load transfer (Rear View)

Figure 2.10. Vertical load transfer of the caravan

$$
\begin{aligned}
\delta F_{ztr} = & \frac{-F_{zw} + M_{yw} + (F_{xw} + ma_x)(h_{gt} - h_c) + (F_{xtr} + F_{xtl})h_c}{2(d+e)} \\
& - \frac{-(F_{ytl} + F_{ytr})h_c + M_{xw} - (F_{yw} + ma_y)(h_{gt} - h_c)}{s}; \\
\delta F_{ztl} = & \frac{-F_{zw} + M_{yw} + (F_{xw} + ma_x)(h_{gt} - h_c) + (F_{xtr} + F_{xtl})h_c}{2(d+e)} \\
& + \frac{-(F_{ytl} + F_{ytr})h_c + M_{xw} - (F_{yw} + ma_y)(h_{gt} - h_c)}{s}; \\
\delta F_{zct} = & -F_{zw} - \delta F_{ztr} - \delta F_{ztl};
\end{aligned}
\tag{2.21}
$$

2.1.4 Contact forces

When studying the dynamics of a vehicle, a fundamental, if not the most important, element covers the contact between the ground and the tire. In order to describe this phenomenon it is necessary to calculate the contact forces in both directions.

Several studies have been conducted that have led to the formulation of different models, one of the most used is the Pacejka model that compute tires forces based on tire slippages and vertical forces. The general model that is used for both lateral and longitudinal forces using the relative slip is shown in the following:

$$
y = D \sin\left(C \arctan\left(Bx - E(Bx - \arctan bc)\right)\right) \tag{2.22}
$$

with $Y(x) = y(x) + S_v$ and $x = X * S_H$ in order to translate the curve and all the other parameters are:

- Y is the output of the model and can be F_x or F_y;
- X is the input of the model and can be the lateral slip α or the longitudinal slip κ;

- B is the stiffness factor that influence the slope of the first part of the curve;
- C is the shape factor that influence the asimptotic value;
- D is the peak value;
- E is the curvature factor;
- S_H is the horizontal shift;
- S_v is the vertical shift.

The result of such model il represented in figure 2.11:

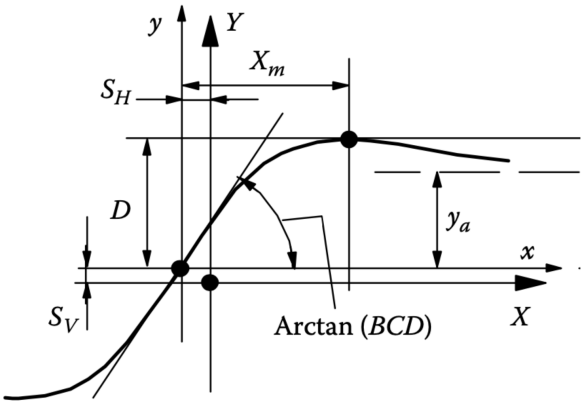

Figure 2.11. Tyre contact forces in accordance with Pacejka

So in order to use this model it is necessary to calculate the slippages in the two longitudinal and lateral directions.

$$\begin{aligned} \alpha_{ij} &= -\arctan\frac{v_{yih}}{v_{yij}} \\ \kappa_{ij} &= \frac{\omega_{ij} r_{ij} - v_{xij}}{v_{xij}} \end{aligned} \tag{2.23}$$

Where α_{ij} represent the lateral slip for each tyre and κ_{ij} represent the longitudinal slip for each tyre.

Therefore it is necessary to calculate the rotation speed of the wheels and therefore it is necessary to introduce an equation of motion for each wheel considering the torques acting on the wheels. They can be of two types: drive torque (only for the front wheels of the car) and braking torque (present on each wheel).

In the equilibrium there are also the rolling resistance moments due to the tire hysteresis that are generated by the translation forward of the vertical force in the contact patch.

$$M_{res} = F_{zig} f r_{ij} \tag{2.24}$$

Where f is a constant that depends on the tyre and on the surface.

Finally, the equation of motion is calculated by means of an equilibrium with respect to the center of the wheel, explaining the rotational acceleration of the latter

$$\dot{\omega_{ij}} = \frac{T_{ij} - F_{xij} - M_{resij}}{J_{wij}} \tag{2.25}$$

Once the rotational acceleration of the wheel has been obtained, it is sufficient to integrate its expression over time in order to obtain the rotational speed:

$$\omega_{ij} = \int_{t_0}^{t} \dot{\omega_{ij}}, dt + \omega_{0ij} \tag{2.26}$$

ω_{0ij} represent the angular velocity of the wheel at initial conditions.

Using the slippages just obtained, it is possible to calculate a first output from the model but without considering a very important aspect: the combined slip scheme reported in figure 2.12. This phenomenon is due to the fact that the longitudinal and lateral forces created in the contact patch are not independent from each other, so this influence must also be considered.

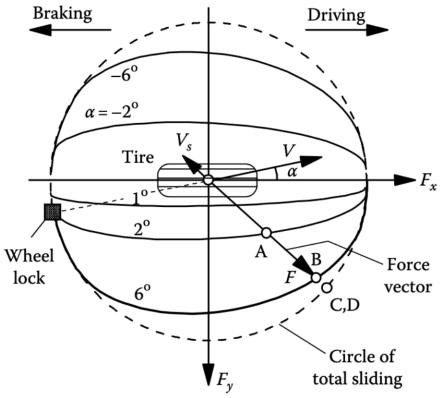

Figure 2.12. Combined slip ellipse

In accordance with Pacejka and Besselink [23] it is possible to take this phenomenon into account by means of two weighting functions that modify the response of the Pacejka model in relation to the force in the other direction.

- For the longitudinal direction the weighting functions are:

$$\begin{aligned} H_{x\alpha_{ij}} &= B_{x1_{ij}} \cos\left(\arctan\left(B_{x2-ij}\kappa ij\right)\right) \\ G_{x\alpha_{ij}} &= \cos\left(C_{x\alpha_{ij}} \arctan\left(H_{x\alpha_{ij}}\alpha_{ij}\right)\right) \\ F_{xij} &= F_{0xij} G_{x\alpha_{ij}} \end{aligned} \tag{2.27}$$

- For the lateral direction the weighting functions are:

$$\begin{aligned} H_{y\kappa_{ij}} &= B_{y1_{ij}} \cos\left(\arctan\left(B_{y2-ij}\alpha ij\right)\right) \\ G_{y\kappa_{ij}} &= \cos\left(C_{y\kappa_{ij}} \arctan\left(H_{y\kappa_{ij}}\kappa_{ij}\right)\right) \\ F_{yij} &= F_{0yij} G_{y\kappa_{ij}} \end{aligned} \tag{2.28}$$

Where B and C present in this formulae are other parameters different from the one seen for the Pacejka formulation and F_{0kij} are the output of the Pacejka model.

As a last modification of the model it is necessary to introduce the phenomena of transitory, as the Pacejka model is a static model. The rubber, as a mechanical system, is characterised by transients that have to be included in the model, these transients are obtained by introducing the so-called *relaxation length*.

$$\begin{aligned} \dot{\alpha_{ij}} \frac{\lambda y}{v_{xij}} + \alpha_{ij} &= -\arctan\frac{v_{yij}}{v_{xij}} \\ \dot{\kappa_{ij}} \frac{\lambda_x}{v_{xij}} + \kappa_{ij} &= \frac{\omega_{ij} r_{ij}}{v_{xij}} - 1 \end{aligned} \tag{2.29}$$

Where λ_x and λ_y are the longitudinal relaxation length and lateral relaxation length respectively.

2.1.5 Driver model

In order to simulate the behaviour of the vehicle with greater realism, it is necessary to introduce a model that reproduces the behaviour of a driver on board. The model has to control the steering angle applied by the driver on the steering wheel while, as regards speed control, it has been decided to opt for a simple cruise control in order to keep the speed constant and prevent it from being decreased due to resistance forces.

The characterisation of the driver is complex as it is necessary to reproduce in mathematical form a human behaviour that is not entirely predictable. The model that has been used is based on a simple PI control (figure 2.13) that acts on the steering angle according to the error between the ideal and actual trajectory of the vehicle. This errors is evaluated on two different points, one at a fixed distance from the center of gravity in the longitudinal direction the other is placed in the center of gravity.

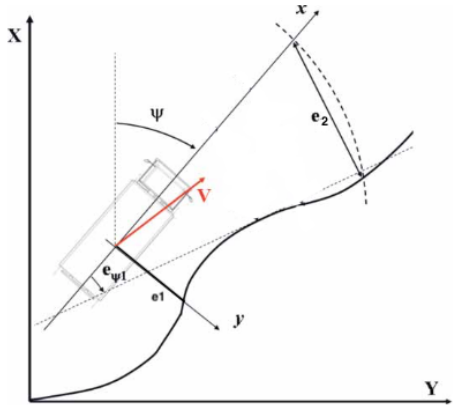

Figure 2.13. Scheme of the driver's model

The main parameters of the control are the gains used to weigh the error on the trajectory and the preview length or the distance from the vehicle that the driver considers during the driving. By manipulating these parameters it is possible to modify the driver's response ranging from a very attentive and reactive driver to a distracted driver with slow reflexes. In this work it has been tried to reproduce the behaviour of an average driver without unbalancing on either side.
The driver model is based on a simple PI controller based on the distance error and the heading error defined as :

$$\begin{aligned} \epsilon_d &= (Y_{ref} - (Y_G + L_{prev} \sin\psi)) \cos\psi - (X_{ref} - (X_G + L_{prev} \cos\psi)) \sin\psi \\ \epsilon_\psi &= \psi_{ref} - \psi \end{aligned} \tag{2.30}$$

Where ϵ_d is the distance error, ϵ_ψ is the heading error and L_{prev} is the preview length. So the model computing each instant these errors apply a steering angle on the steering wheel in order to follow a predefined trajectory.

The model was tested by performing a lane change maneuver and the result is reported in the following figure 2.14.

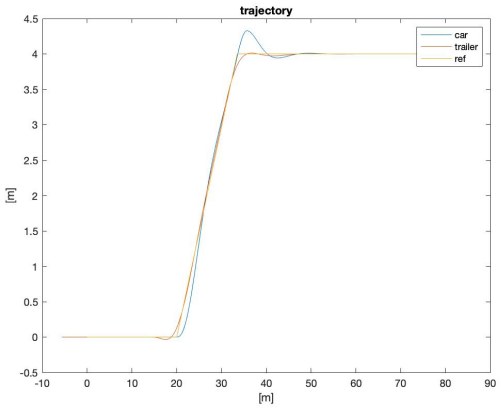

Figure 2.14. Lane change manuver test

As for the cruise control, a simple PI controller has been adopted which analyses the error on the longitudinal speed with respect to a reference speed and acts on the torque delivered by the engine to the wheels. As already mentioned, this model is considered a front-wheel drive vehicle as it is the type of vehicle that is most widespread on the market.

The error between longitudinal speed and reference speed $\varepsilon = v_{xc} - v_{xref}$ is used in order to compute the torque necessary to be delivered by the engine:

$$T_{cruisecontrol} = k_P \varepsilon + k_I \int \varepsilon dt \tag{2.31}$$

2.1.6 Test trajectory

In order to analyse different situations and find the most critical condition, it is necessary to define reference trajectories. The trajectories that are followed most frequently while driving on the motorway have been studied.

The most common and simplest trajectory that has been analysed is the straight one, in order to analyse the behaviour of a vehicle that is traveling at constant speed along a straight and is hit by a crosswind gust.
In addition to this type of trajectory, a vehicle may need to move to another lane, for example for a slower vehicle in front of it, so, the lane change trajectory (figure 2.15) has also been considered to simulate this maneuver. To model this trajectory, have been considered the time span used to move from one lane to another and, knowing the advancement speed, the space traveled. Typically, it takes 10 s and, considering a maximum speed of 80 Km/h, 222 m to face a lane change with a caravan towed.

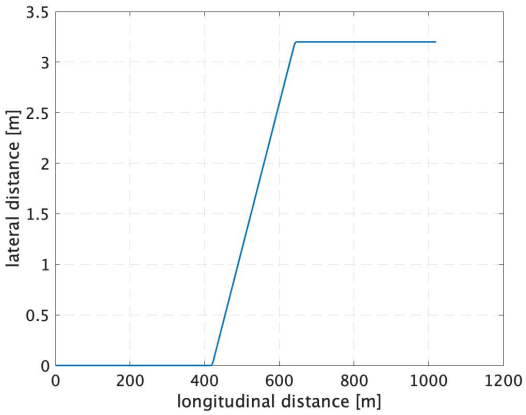

Figure 2.15. Lane change manuver test

A vehicle not only needs to change lanes but also to overtake, so the double lane change maneuver (figure 2.16) has also been implemented, with the aim of analysing the response to overtaking.

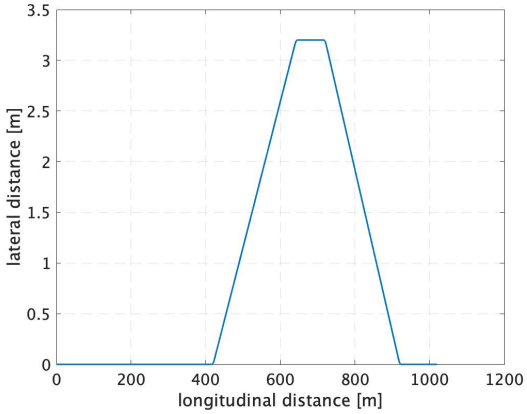

Figure 2.16. Double lane change manuver test

Finally, a vehicle could find itself facing a motorway curve, therefore of a wide radius, while being hit by a gust of side wind. Therefore a curve with a radius of 500 m (figure 2.17) has been implemented.

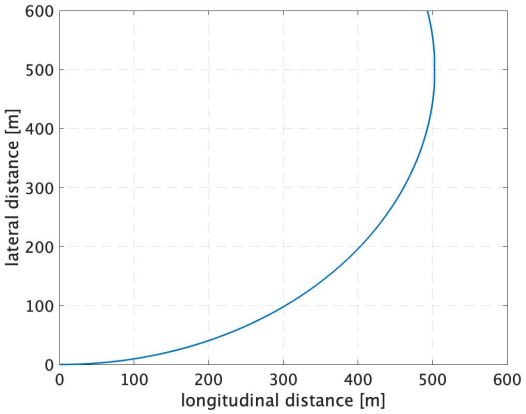

Figure 2.17. Highway curve

2.1.7 Wind model

There are several ways to define a wind gust. Different forms can be used and can be characterised by impulses or steps. Typical forms of ideal winds are: rugby-ball, ramp shape and step shape. For this work it has been decided to use the exponential shape or Chinese-hat shape (Neto et al. [24]). For this model it is assumed that the gust has a component exclusively perpendicular to the vehicle and that the incidence angles variations during the gust are absent. This model is based on the average speed of the gust while the maximum speed is obtained thanks to the following:

$$U_{mean} = \frac{U_{max}}{G} \tag{2.32}$$

Where G is equal to 1.6946 in accordance with Neto et al. [24]. The definition of

the model starts from the standard deviation of the turbulence defined as:

$$\sigma_u = 0.2446 U_{mean} \tag{2.33}$$

The normalised frequency is then calculated with a range of frequencies ranging from $n_1 = 1/300$ Hz up to $n_2 = 1$ Hz.

$$f_u = \frac{n L_u^y}{U_{mean}} \tag{2.34}$$

Where L_u^y is the characteristic length equal to 6 m. From this it is possible to obtain the average time constant T.

$$\begin{aligned} \bar{T} &= \frac{1}{2}\left[\frac{\int_{n_1}^{n_2} n^2 S_u(n)\ , dn}{\int_{n_1}^{n_2} S_u(n)\, dn}\right]^{0.5} \\ S_u(n) &= \frac{4 f_u \sigma_u^2}{(1 + 70.7 f_u^2)^{\frac{5}{6}}} \frac{1}{n} \end{aligned} \tag{2.35}$$

Then the time constant and the characteristic frequency f are calculated with:

$$\begin{aligned} T &= \bar{T} 4.1825 \\ f &= \frac{1}{2T} \end{aligned} \tag{2.36}$$

After that the longitudinal and transversal components, u_x and u_y, function of the longitudinal distance and dependent on the wind yaw angle β_w are computed:

$$\begin{cases} u_x(\tilde{x}) = f\tilde{x} \cos\beta_w \frac{1}{U_{mean}} \\ u_y(\tilde{x}) = f\tilde{x} \sin\beta_w \frac{1}{U_{mean}} \end{cases} \tag{2.37}$$

From these components the coherence function is computed:

$$C = e^{-\sqrt{25u_x^2 + 256u_y^2}} \tag{2.38}$$

Finally the wind profile is determined by:

$$V_w = U_{mean} + 2.84 \sigma_u C \tag{2.39}$$

After that, in order to does not introduce instability caused by the sudden increase of the wind speed, a ramp is introduced in first part of the gust. Finally it is need to smooth the result in order to avoid sharp change.
The results are reported in the following figure 2.18:

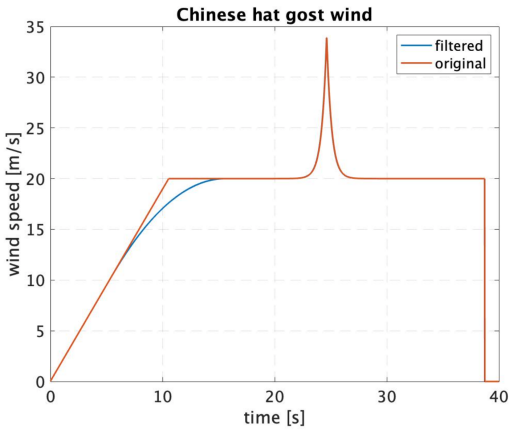

Figure 2.18. Chinese hat wind profile

In this case a mean velocity of 20 m/s has been used but for the various analysis different speeds and wind angle were tested.

2.1.8 Safety indexes

In order to check the safety of the vehicle, some indicators are needed. Since the vehicle in question is subject to the risk of overturning, it is necessary to define indices that indicate whether the vehicle is close to this dangerous conditions. In order to analyse the risk of rollover, the variations of the vertical forces on the individual wheels and the roll angle have been analysed. For the first check, two parameters have been defined, the first simply indicates when one or more wheels lose contact with the ground and therefore the relative vertical forces cancel out.

$$\delta F_{zi} = \frac{F_{zi}}{F_{zistat}} \tag{2.40}$$

Where F_z mean the instantaneous vertical force of the wheel while F_{zistat} mean the static vertical force of the wheel. In this way the variation of the vertical force is normalised with respect to the static case and an indication of the risk of lifting it can be obtained.

Another often used coefficient is that adopted by L. Salati [2]. This index takes into consideration the difference between the two sides of the vehicle, thus considering the lateral load transfers.

$$\eta = \frac{F_{zleft} - F_{zright}}{F_{zaxle}} \tag{2.41}$$

Thanks to this index it is possible to evaluate the risk of rollover and verify that it is below a certain threshold that guarantees safety for the vehicle. This threshold is considered equal to 0.9, i.e. if the coefficient is lower than this value, the vehicle can be considered safe as the lateral load transfer is limited, while above this threshold there are very marked load transfers and so it is very close to a rollover situation and the vehicle cannot be considered to be in a safe condition.

Another very important parameter that has to be analysed is the maximum lateral displacement achieved due to external forcing. To analyse this value, it was considered a motorway carriageway, a situation more prone to accidents due to side winds, with a width of 3.5 m. The vehicle width is considered equal to 2 m to maintain a certain generality and it is verified that the distance between the lateral limit of the vehicle and the limit of the carriageway is less than 0.25 m. In this way, it is possible to analyse the risk of the vehicle invading other carriageways, or in the worst case, leaving the road.

$$\delta_y = \frac{3,5}{2} - (Y + \frac{s}{2}) \tag{2.42}$$

Where 3,5 is the carriageway width, Y is the lateral position of the vehicle center of gravity, considering an offset of 0 m, and s is the gauge of the vehicle.

Chapter 3

Aerodynamic model

The aim of this chapter is to explain the aerodynamic model that has been used and its validation. OpenFOAM™software has been used for aerodynamic simulations.
OpenFOAM™is an open source software developed by OpenCFD Ltd™since 2004.
OpenFOAM™allows to perform all kinds of fluid dynamics simulations, from open fields, as in this case, to simulations that include thermal exchanges and chemical reactions.
As regards the visualisation of the results, ParaView™software has been used in order to analyse the flow behaviour around the two vehicles, while Matlab™software has been used for the forces analysis and the relative aerodynamic coefficients calculation.
In order to carry out the simulations, the two clusters of the Politecnico di Milano have been used as the computational burden was too high to allow the usage of a simple laptop.
For the validation of the results, a grid independence study has been carried out to eliminate the results dependence on the mesh quality, then the results have been compared with the results obtained from experimental campaigns. In particular, as regards the validation of the caravan model, the experimental validation has been carried out at the Politecnico di Milano in the wind tunnel used by exercises of the vehicle aerodynamics course.

3.1 Computational Fluid Dynamics

The most traditional ways to carry out aerodynamic analyses are wind tunnel tests and road tests (Hucho [25]).
In road tests, full-size models are used in real operating conditions, this allows to obtain extremely truthful results but at the expense of cost.
Regarding the analysis in the wind tunnel, scale models are used in order to reduce costs compared to a full-scale model, however they present difficulties in recreating realistic conditions, one of the main problems that is faced is to reproduce a realistic Reynolds number.
An alternative method, which thanks to the evolution of computers has become competitive, is Computational Fluid Dynamic (CFD). Thanks to this methodology it is possible to carry out simulations without creating a physical model which allows to keep costs down. The only limits of this methodology are represented by the computers

computing capacity, the execution speed and the incomplete knowledge of the physical phenomenon involved. All the methods used are based on the approximation of the Navier-Stokes equations and on the use of finite element methods for spatial and temporal discretisation.

3.1.1 Modelling approaches

In general, there are three different methods for modelling the motion of a fluid (Medina et al. [26]):

1. Direct Numerical Simulations (DNS);
2. Large Eddy Simulations (LES);
3. Reynolds Averaged Navier- Stokes (RANS).

Using the first method, the Navier-Stokes equations are solved directly (without using turbulence models) and all turbulent scales must be included in the mesh. For this reason they are very expensive at a computational level and with current technologies they are used exclusively in research without finding space in the industrial field.
In the case of LES (Large Eddy Simulation) the large eddies are simulated while for the small scales sub-grid models are used. In this case the computational cost is more accessible, in fact they are also used on an industrial level, but they present difficulties in defining the mesh due to the separation of the scales. To soften this separation and improve the results, spatial filters, depending on the mesh size, are applied.
Finally, RANS (Reynolds-Averaged Navier-Stokes) are the most used as they have a relatively low computational cost. With this method the flow filed is averaged after being decomposed into mean and fluctuations component. This process introduces a series of unknown quantities, known as the Reynolds stresses, which are modelled based on statistical information about the flow.
Using the RANS method it is necessary to define a model for the turbulence description. The different turbulence models differ in how they model the flow close to walls, the number of additional variables solved for, and what these variables represent (Frei [27]).
The most used models are:

1. **Spalart-Allmaras (S-A)**: this model uses a transport equation to define kinematic eddy turbulent viscosity and is mainly used in the aerospace field;
2. k-ϵ: This is one of the most used models and is based on the calculation of two variables: k the turbulence kinetic energy; and ϵ the rate of dissipation of turbulence kinetic energy. This model has a good convergence speed and requires low memory. It is not excellent in the case of flow fields that have marked pressure gradients and it behaves very well in the case of bluff-body.
3. k-ω: It is similar to k-ϵ model, but it solves for ω (the specific rate of dissipation of kinetic energy). It is more nonlinear, and thereby more difficult to converge than the k-ϵ model, and it is quite sensitive to the initial guess of the solution. This model is used for internal flows, flows with marked curvatures and jets.

4. k-ω **SST**: It is a combination of the k-ϵ model in the free stream and the k-ω model near the walls. It has similar resolution requirements to the k-ω model and the low Reynolds number k-ϵ model, but its formulation eliminates some weaknesses displayed by pure k-ω and k-ϵ models.

For this work the RANS method has been used to model the air motion around the two geometries. This has been done in order have good results without an extreme computational cost and because, for this type of applications, is the most used.
For what concern the turbulence model, the SST model has been used. It has been used because is the most used and produce a good modelling of the turbulence.

All aerodynamic simulations have been performed using the SimpleFOAM algorithm. This algorithm present in OpenFOAM™is used for the simulation of incompressible fluids in steady state conditions. The solver uses this algorithm to solve the continuity equations and momentum equations:

$$\begin{aligned} \nabla \cdot u &= 0; \\ \nabla(u \otimes u) - \nabla R &= -\nabla p + S_u \end{aligned} \tag{3.1}$$

Where u is the velocity, p is the kinematic pressure, R is the stresses tensor and S_u is the momentum source.
As for turbulence, the SST model was used. This model combines the k-ω model in the inner boundary layer; while, in the free shear flow area, it uses the k-ϵ model. The model is based on the the turbulent kinetic energy calculation k and the turbulent specific dissipation rate ω. The model needs to be initialised by imposing initial conditions on both k and ω. Both can be estimated using the following formulas once the flow conditions are known:

$$\begin{aligned} k &= \frac{3}{2}(I|u_{ref}|)^2 \\ \omega &= \frac{k^{0.5}}{C_\mu^{0.25} L} \end{aligned} \tag{3.2}$$

where I is the intensity, and u_{ref} a reference velocity, C_μ is a constant equal to 0.009 and L is a length reference scale. In the present work the following values have been chosen:

- Intensisty I : 0.002;
- Reference velocity: 40 m/s for validations;
- Reference length scale L: 0.2 m.

As regards the aerodynamic coefficients, the following formulas have been used, considering the frontal area for all coefficients.

$$C_x = \frac{2F_x}{\rho V^2 A} \; C_y = \frac{2F_y}{\rho V^2 A} \; C_z = \frac{2F_z}{\rho V^2 A} \tag{3.3}$$

3.2 CFD set up and simulations

The simulation set up is the follows:

- Simulation domain and vehicle scale 1:1;
- Stationary wind conditions;
- Moving floor to reproduce the vehicle motion on the ground;
- Forces and moments calculated in the center of gravity;
- Wind speed: $40 m/s$;
- Wind angle respect to the axis of the car: 10 (for the validation phase).

3.2.1 Car aerodynamic model

Several simulations have been carried out in order to find the right compromise between computational cost and truthfulness of the simulations. During the choice of the domain, particular attention was paid to the wake phenomena in order to obtain a sufficiently large domain that would allow the complete wake development and that it would allow the complete windward conditions settlement. The final domain chosen extends in length by 60 m in width by 40 m and in height by 10 m and is shown in figure 3.1.

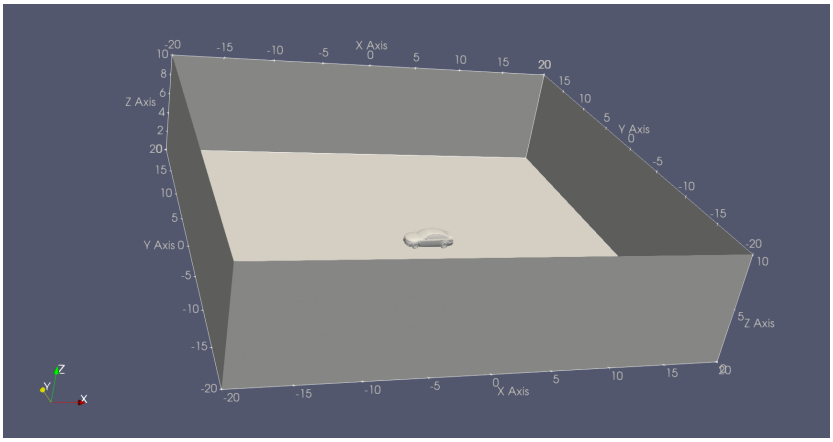

Figure 3.1. Simulation domain

For the car model the DrivAer notchback variant model has been chosen as it was considered the right compromise between the type of car used for towing a caravan and the vast presence of past studies in order to have good values for the validation. The model, being a modular model, has been equipped with a smooth underbody, smooth wheels and the ducts for cooling the engine and the corresponding pressure drops have been eliminated in order to have a simple model and reduce the computational cost. These abstractions from reality were made possible by the fact that the objective of the analysis is to derive the forces and moments generated by the

wind on the vehicle so these details are secondary and have a minimal influence on the results. The model is shown in figure 3.2.

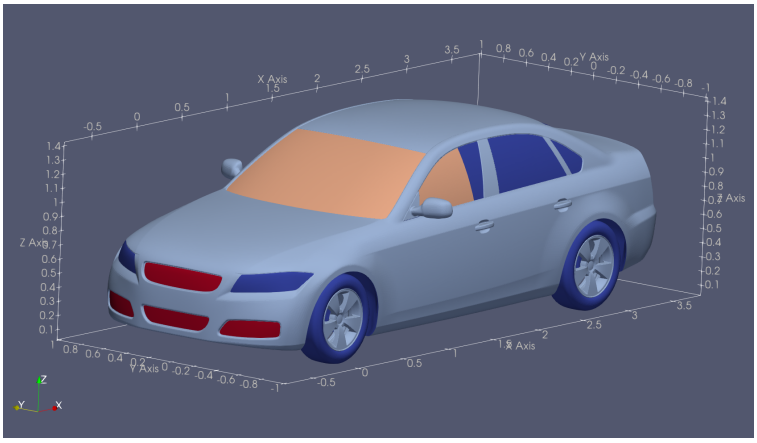

Figure 3.2. DrivAer model

The last phase was the definition of the mesh. The base cells are cubes with side of 1 m. Finally, the mesh was analysed. First of all, the resolution of the model has been chosen in order to obtain a mesh that correctly represents the surface of the model without aggravating the computational cost, reaching a mesh of 0.0039 m for the vehicle (figure 3.3). The choice not to consider details such as the bottom and the grooves of the tires has made it possible to use a coarser mesh, saving computational cost but at the same time able to accurately reproduce the geometry of the vehicle.

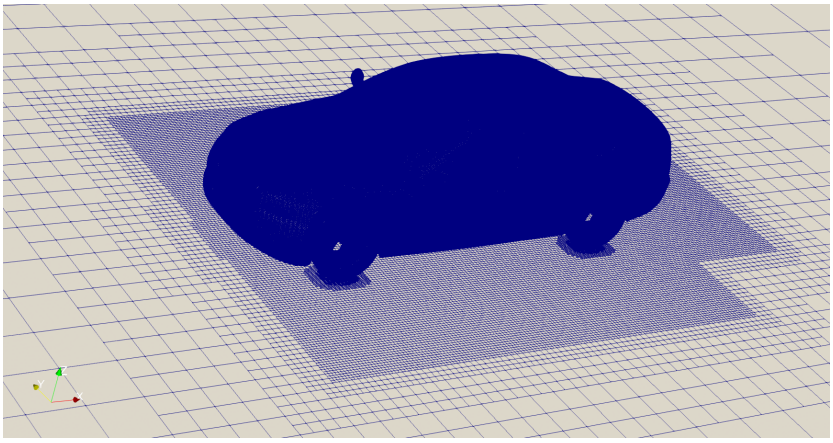

Figure 3.3. DrivAer's surface mesh

After defining the mesh for the geometry, the simulation behaviour was studied as the number of layers varies. To optimise this parameter, the yPlus has been analysed. yPlus is defined as: $y^+ = \frac{yu_\tau}{\nu}$ where y is the absolute distance from the wall, ν is the kinematic viscosity and u_τ is the friction velocity. yPlus is a parameter used to analyse the behaviour of the simulation near the wall. To have a good simulation this parameter has to be between 30 and 300. In order to obtain these values a number of layers equal to 5 has been used.

The simulations carried out with this value have reported a correct value of the yPlus in the vicinity of the surfaces as can be seen in figure 3.4.

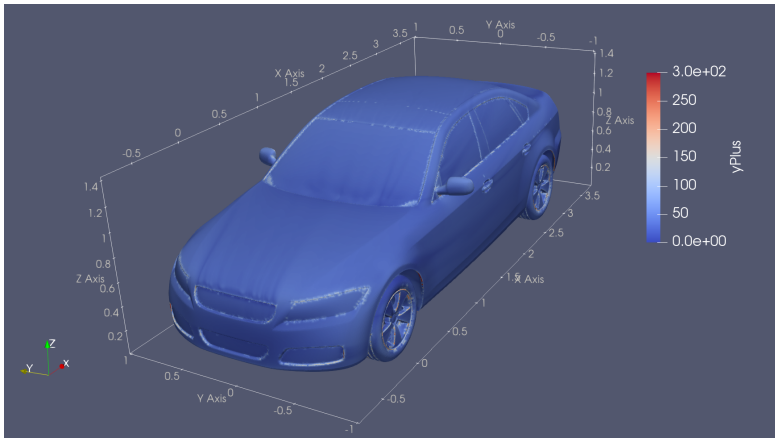

Figure 3.4. yPlus result

Finally, the size of the mesh surrounding the model was adjusted using different refinement boxes in order to have a more refined mesh in the neighborhood of the model and a coarser one in the most remote areas of the domain. The result are showed in figure 3.5.

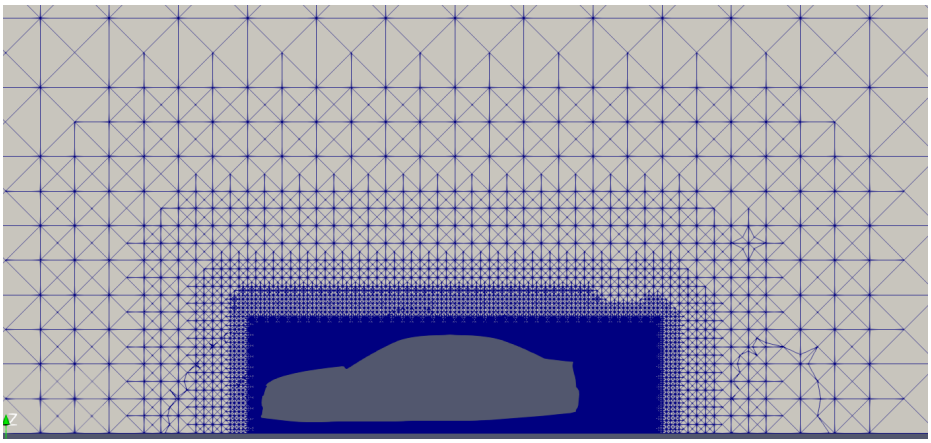

Figure 3.5. Refinement Box

In order to validate the simulation, the variation of the results with the mesh was first analysed in order to obtain results that were independent on the mesh quality. To do this, the cells number of the mesh have been increased and the aerodynamic coefficients have been analysed. It has been noted that from values higher than 19.4 million cells the results are almost constant and therefore it was possible to conclude that from this value onwards a further mesh refinement would only lead to an increase in the computational cost without improving the mesh results.

Finally the results have been compared with the studies of Wojciak et al. [3] and Howell and Panigrahi [19] in order to validate the results (figure 3.6 and figure 3.7).

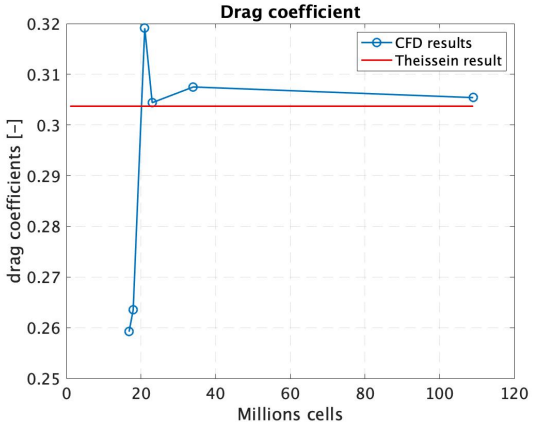

Figure 3.6. Drag coefficient of DrivAer model with 10° yaw angle variation with mesh resolution

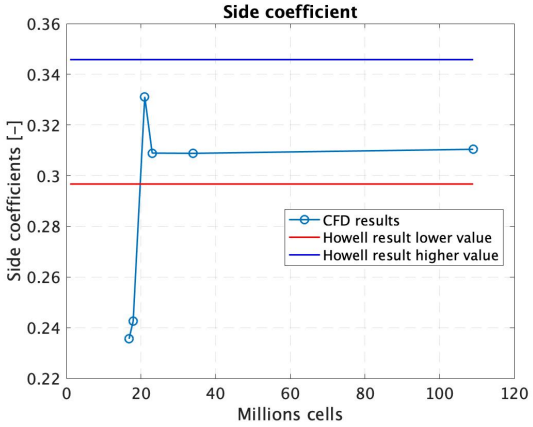

Figure 3.7. Side coefficient of DrivAer model with 10° yaw angle variation with mesh resolution

As regards the drag coefficient, it can be noted that the results obtained have a small deviation from the results obtained by Theissen. The difference between the 34 million cell CFD results and the results used for validation is 1.23%.
While for what concerns the lateral coefficients Howell reports a lower limit and an upper limit based on the statistical analysis he has carried out, and it is noted that the results of CFDs are between the two limits.

3.2.2 Caravan aerodynamic model

As regards the caravan model validation, the procedure was similar to what has been done for the car. The simulation setting process is identical to what was written in the previous case, the same solution algorithm, the same turbulence model with the corresponding parameters have been used.
Thanks to various simulations it has been possible to conclude that the simulation domain that was used for simulations on the DrivAer model was sufficient for the simulations concerning the caravan, as the wake phenomena evolve completely.

The substantial difference with respect to the car case lies in the model choice and in the validation procedure. In this case, since, in the literature, there are not many previous studies on this type of geometry, if not for drag reduction purposes only; it has been decided to create a model based on the typical caravan geometries and to validate the CFD simulation through wind tunnel experiments.
The model has been created using AutoDesk's INVENTOR™software by reproducing the relevant geometric aspects and neglecting the details that play a secondary role in the aerodynamic analysis such as windows. The geometry of the model was inspired by the typical caravan shape. The model has a length of $5.93m$ (excluding towbar), a width of $2.32m$ and a height of $2.57m$ for a total frontal area of $5.884m^2$.
The model created, with some modifications to simplify the geometry and reduce the computational cost, is shown in figure 3.8

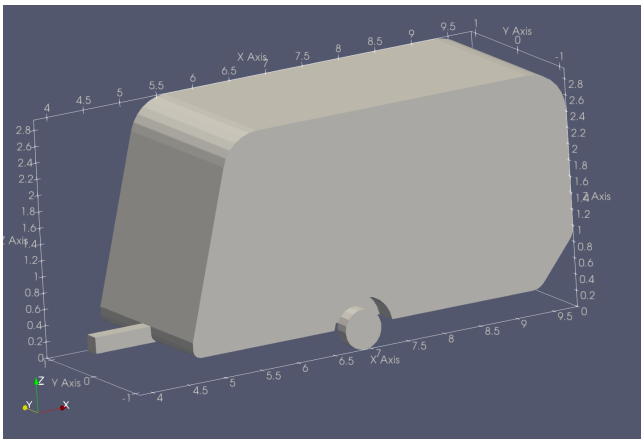

Figure 3.8. Caravan's model

The same simulation setup used for the DrivAer model has also been used for the validation of the caravan model simulation. The process of defining the domain and the mesh is identical to what was seen previously. Also in this case, has been used a cubic base cell with side equal to 1 m and a surface dimension of $0.00781m$ has been reached compared to $0.0039m$ for the DrivAer.
In order to obtain a correct yPlus, the same number of layers used previously has been used as the results obtained were within the limits. The results are reported in figure 3.9.

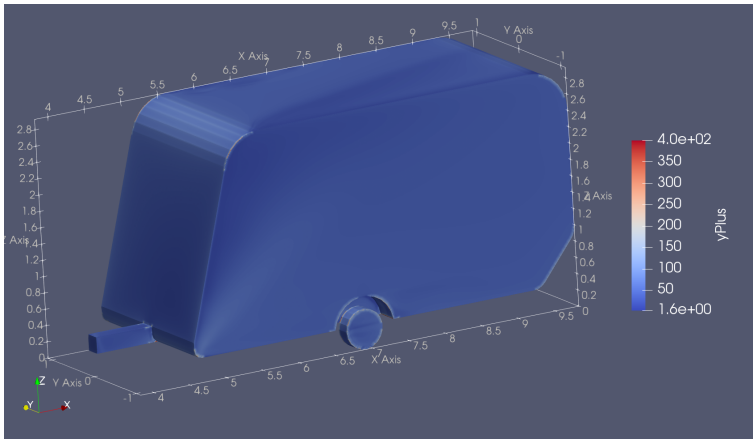

Figure 3.9. Caravan's yPlus results

Finally, the number of refinement boxes has been chosen equal to the previous case as the mesh has to be used for the simulation of both vehicles. Also in this case, five refinement boxes of the same size as the previous case have been used. However, an analysis was carried out by reducing the number of refinement boxes in order to see the influence of the mesh on the simulation results and it has been noted that in this case fewer refinement boxes are required, consequently a smaller number of cells, to obtain correct values of aerodynamic coefficients as reported in figure 3.10.

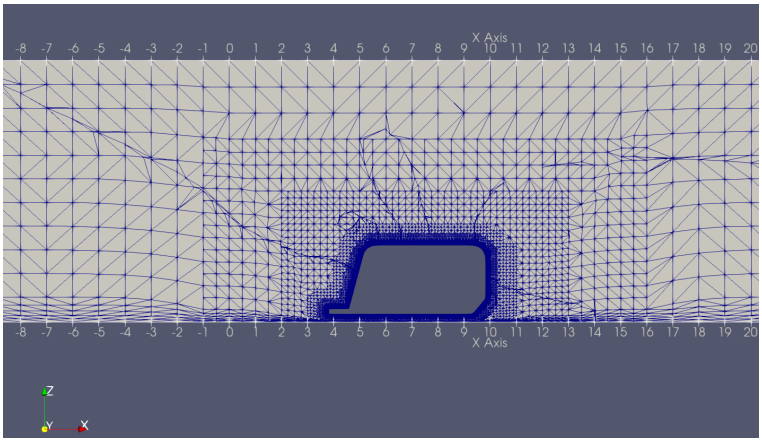

Figure 3.10. Refinement boxes

In the following is reported the trend of the aerodynamic coefficients as function of the cells number (figure 3.11):

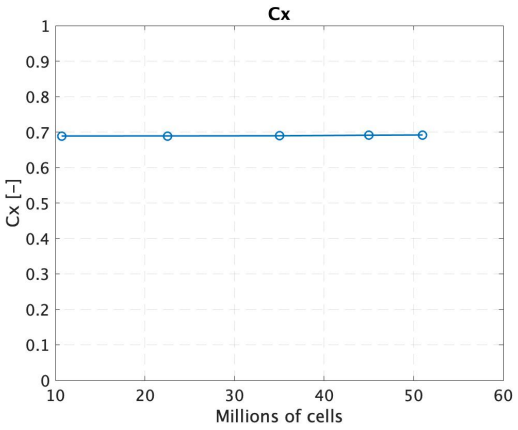

Figure 3.11. Drag coefficient of caravan model with 10° yaw angle variation with mesh resolution

Clearly, thanks to the simple shape of the caravan, it is not needed a big cells number. It is possible to notice that the variation of the drag coefficient is quite small and is almost the same also for small cells number.

3.3 Complete model aerodynamic simulation

In this section are discussed the CFD simulations in order to find the car and caravan aerodynamic loads. The aim of the simulations is to compute the car and caravan aerodynamic coefficients separately in order to introduce the aerodynamic loads caused by different wind conditions in the dynamic simulations . The models that have been used are the previous described, the DrivAer model for the towing car and the caravan model tested in the wind tunnel. The two model have been placed aligned on the longitudinal axis in order to simulate the vehicle motion in a straight way and the relative angle between car and caravan was kept to zero. The simulations were done with different yaw angles in order to map the aerodynamic coefficients as function of the incidence angle.

3.3.1 Simulation domain and mesh set up

As was done for the validation of the DrivAer model and the caravan model, at the beginning the simulation domain was defined. In this part a particular attention was done in the wake and inflow region, in order to consider a domain large enough to simulate well the wake phenomena and to have enough space for the complete stabilisation of the inflow.
The simulation domain consist in a box shape of dimension (60x40x10 m) where the front and left patches are the boundary from where there is the input of the flow, whereas the right and rear patches are where there is the output of the flow. The upper patch is set to have the same velocity and direction of the wind present in the domain while the lower patch has only a longitudinal component set to be equal to the absolute velocity of the flow in order to simulate the motion of the vehicle over the ground. Another important aspect in the definition of the domain is the

computational cost, the domain could not be too large in order to keep low the cells number and so the computational time.
The domain and its dimensions are shown in the figure 3.12 .

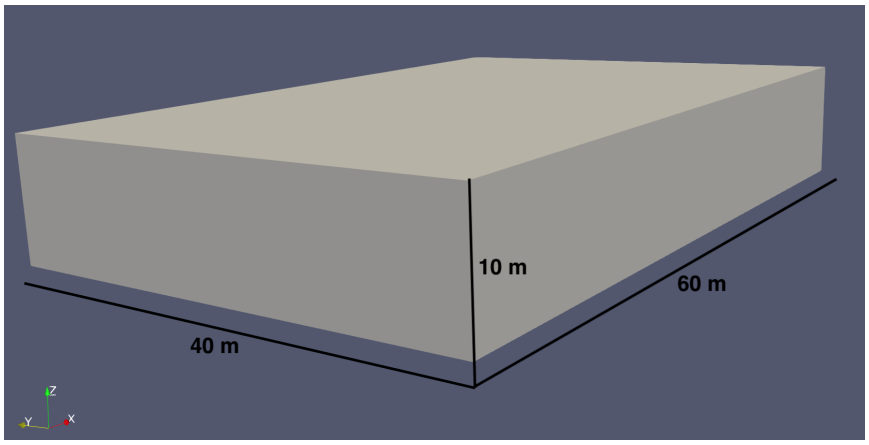

Figure 3.12. CFD Domain for the complete model

The domain has been then discretised along the three main directions (x, y, z) in order to define the base cell dimensions. The discretisation was obtained considering a cells number equal to 60 along the longitudinal direction, 40 along the lateral direction and 10 cells along the vertical direction; in this way hexahedral cells with a side length of 1 m were obtained.
After defining the base cells size, the vehicle has been considered and the internal mesh has ben defined.
The model has been positioned with the longitudinal axis coinciding with the x-axis of the domain and with a distance between the front of the car and the front wall of 19 m (figure 3.13).

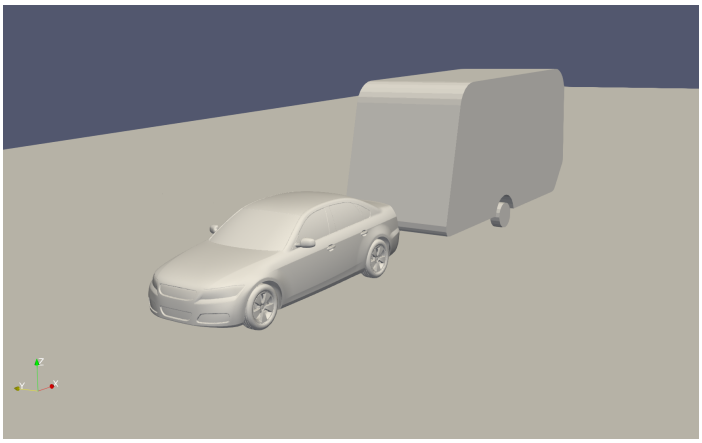

Figure 3.13. Position of the model in the domain

To create the mesh, the OpenFoam™SnappyHexMesh tool was used which allows to create a hexahedral mesh fitting the vehicle geometry.
In order to obtain a good mesh without excessively increasing the computational cost, refinement boxes have been used in order to thicken the mesh in the most delicate

areas, such as the wake area and the area between the car and the caravan (figure 3.14). A total of 5 refinement boxes have been used positioned as follows:

1. **Box 1**: dimensions (27x12x6 m) including the whole model and a large part of the wake;
2. **Box 2**: dimensions (24x10x5.5 m) including the whole model and a part of the wake;
3. **Box 3**: dimensions (20x9.6x4.5 m) including the whole model and a small part of the wake;
4. **Box 4**: dimensions (16.7x3.6x3.5 m) defined to create a very dense mesh in the vicinity of the model;
5. **Box 5**: dimensions (7.7x3.2x3 m) placed in the area between car and caravan in order to further thicken this area which is one of the most critical.

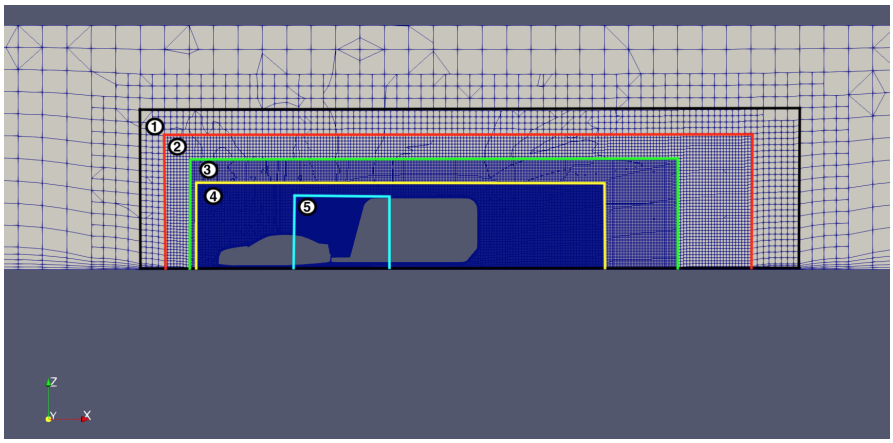

Figure 3.14. Refinement boxes

Finally, 5 layers have been used to accurately define the boundary layer on the model surfaces and allow a correct yPlus.

The domain boundary conditions have been set in order to analyse a flow with different angles of attack. To do this, the front surface and the left surface (with respect to the orientation of the vehicle), were considered as inputs for the flow, while the rear surface and the right surface as output. As previously mentioned, the upper patch reproduces the flow trend while the lower patch has exclusively a speed component in the longitudinal direction in order to reproduce the motion of the vehicle on the road surface. The input speeds have been evaluated starting from the wind speed and orientation and have been decomposed respect to the x and y axes.

$$V_x = V_w \cos(\phi) V_y = V_w \sin(\phi) \tag{3.4}$$

Where V_w represents the absolute wind velocity and ϕ represents the relative angle between the wind direction and the x axis. The scheme of the inlet flow in the domain is reported in figure 3.15

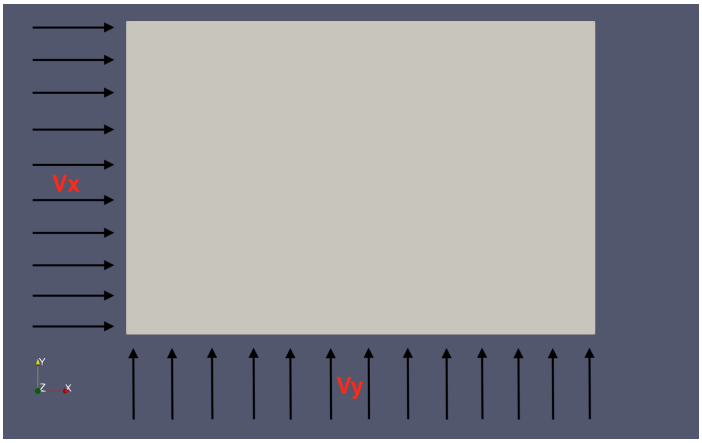

Figure 3.15. Inflow boundary conditions

For what concern the pressure has been set equal to zero on the outflow boundary patch, while for the inflow boundary patch the gradient of the pressure has been set equal to zero.
Finally the boundary conditions for the turbulence model have been defined according to the following:

$$\begin{aligned} k &= \frac{3}{2}(I|u_{ref}|)^2 \\ \omega &= \frac{k^{0.5}}{C_{\mu}^{0.25}L} \end{aligned} \tag{3.5}$$

Considering a turbulence intensity equal to 0.2%, an absolute reference velocity of $40m/s$, in order to keep the Re number hight, and a reference scale length of 0.2 m. In the final phase the results have been analysed as the mesh resolution changed to obtain a mesh that guarantees the independence of the results from the cells number. To do this, various simulations have been carried out with the same conditions, wind speed equal to 40 m/s and inclination of 10°, varying the cells number for the definition of the mesh. Once the results have been obtained, the drag coefficients of the car and the trailer were analysed in order to independently analyse the behaviour of the two vehicles. The results are shown in figure 3.16.

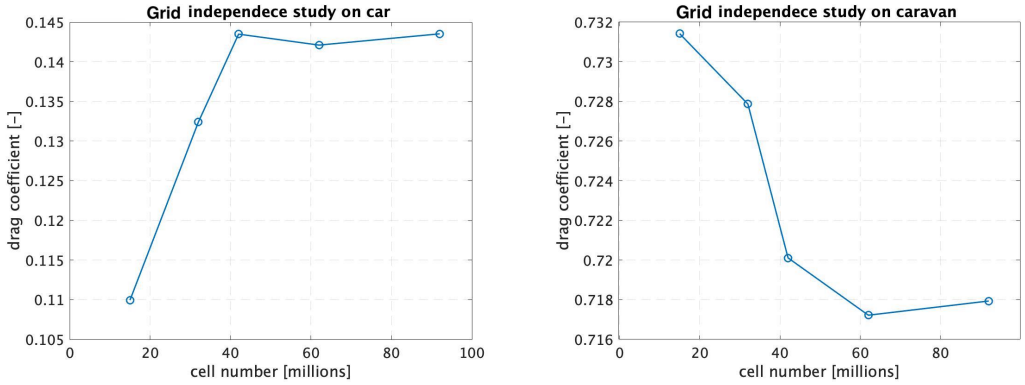

(a) *Drag coefficients of the car at 10° yaw angle variation with mesh resolution*

(b) *Drag coefficients of the caravan at 10° yaw angle variation with mesh resolution*

Figure 3.16. Grid independence study

Analysing the results it is possible to notice that the drag coefficient stabilises after a mesh with a cells number equal to 42 million. Further refinements therefore lead to an increase in the computational cost without increasing the accuracy of the simulation, which is therefore unnecessary.

Chapter 4

Wind tunnel experiment

This chapter presents the caravan model experimental validation and the discussion of the modifications made to the wind tunnel in order to simulate conditions with different air flow angles of incidence.

4.1 Wind tunnel modifications and creation of the model

The wind tunnel that has been used in this phase of the work was designed by a graduated student of the Politecnico di Milano Yılmazer [28] and, before the modifications, only allowed simulations with the wind parallel to the vehicle axis. This wind tunnel has been used for the exercises of the automobile aerodynamics course held by Professor Paolo Schito. The wind tunnel has a Solaris motor with a power of 2.20 Kw capable of obtaining a flow rate of 170/250 m^3/min.
The wind tunnel has a chamber length of 1 m and a section of 50x50 cm, with 4 rectangular entrances, one on each side, which allow the positioning of the model and the instrumentation inside.

The instrumentation consists of a Pitot tube for pressure measurement and a 6-axis balance for the acquisition of forces. The balance (5) is supported by a plate (2) connected directly to the lower part of the tunnel by four cylindrical elements (3). While the model, usually made of polystyrene, is supported by a plate connected by four supports to the balance (4). The original structure for supporting the balance is reported in 4.2 while the whole assembly is reported in figure 4.1.

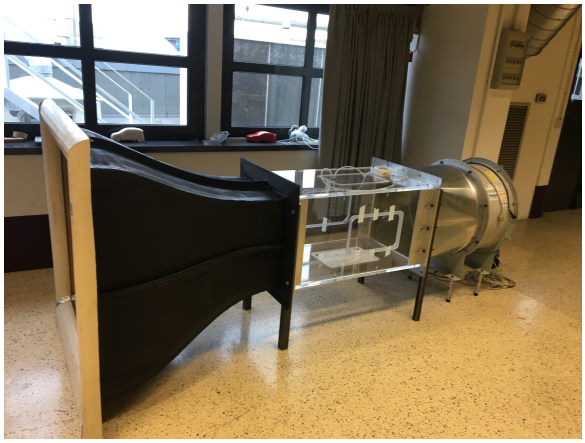

Figure 4.1. Wind tunnel

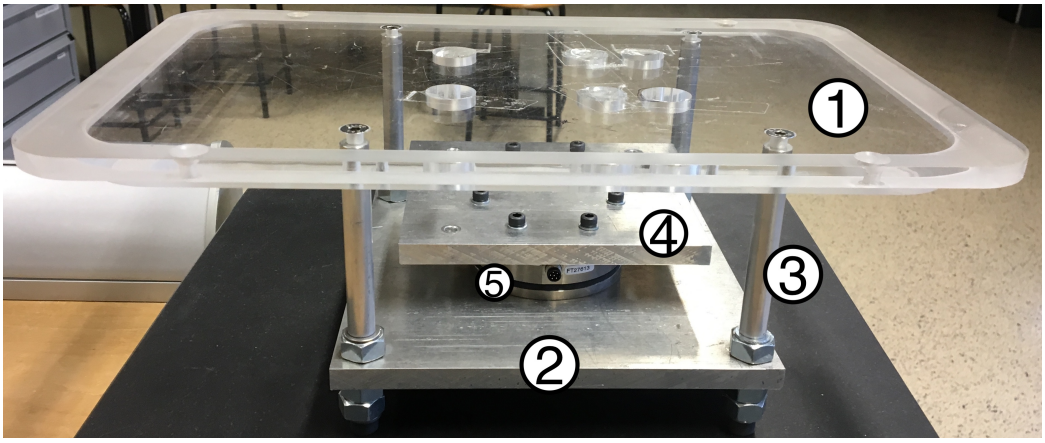

Figure 4.2. Original balance's support structure

In this work, having the need to carry out tests with wind attack angles different from zero, it has been necessary to change the balance support mode. In particular, components 1, 4 and 2 have been modified. The basic idea was to create a support capable of rotating the whole scale-model assembly by the desired quantity while maintaining the center of rotation on the longitudinal axis of the tunnel. The ability to rotate has been made possible thanks to the modification made to component 1. A new component (7) has been created with a hole in the center of radius 85 mm which acts as a guide for a second circular component used as support for the balance (6) (figure 4.3). These components were made in plexiglass by the external company Logis™.

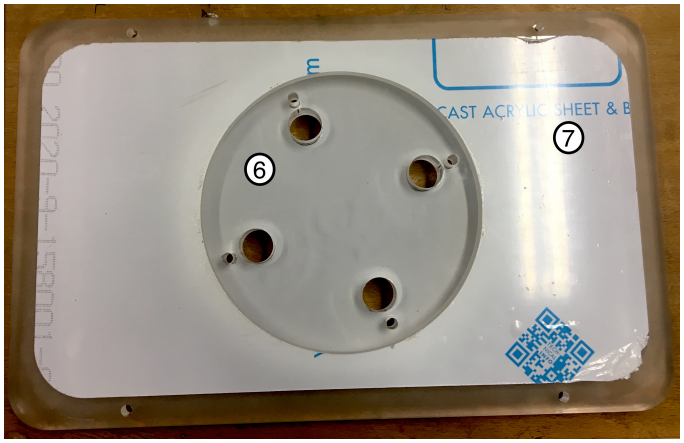

Figure 4.3. New support for the balance

Having to connect the elements (3) to the circular component (6), smaller than the original plate (1), it was necessary to redesign the components (4) and (2) reducing their size. The final result of the entire support structure for the balance is shown in figure 4.4.
The model is connected directly to the balance by means of four screws. It is possible to notice that the balance is connected to the circular element resting on the tunnel plate and therefore it is possible to rotate the whole scale assembly in order to simulate different angles of attack.

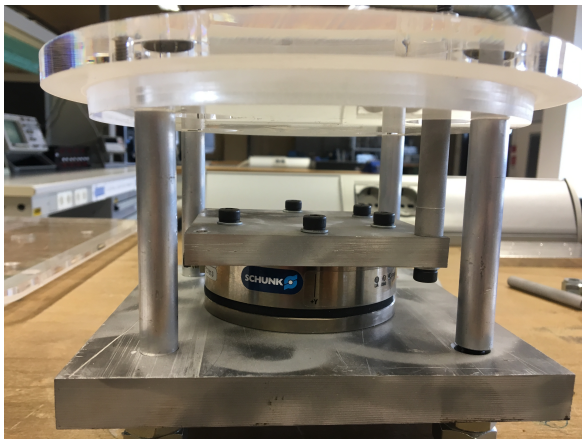

Figure 4.4. New structure for the balance

Once the structure of the wind tunnel used to support the scale has been modified, it was necessary to produce the model of the caravan to be used. A SHAREBOT 3D printer was used for the creation. The material used for printing is PLA, a polymer that does not have strong mechanical characteristics but is excellent for this type of application.

The model is the same used for CFD and it has been scaled. The scale of the model used for the experiment is 1:24 and the frontal area pass from 5.884 m^2 to 0.0121 m^2.

The blockage factor defined as $\frac{Frontalarea}{Crossareaofthetunnel}$ is equal to 0.0484.

Minor changes were made to the model to optimize 3D printing production, the model was made hollow to save material and support guides were created for the insertion of an aluminum plate so as to be able to connect the model to the balance (1).
The 3D printing process has some limitations, it is not able to create overhangs without the aid of supports. To avoid the creation of such supports, and therefore to save material, all critical geometries in the internal part of the model have been readjusted using inclined elements (3). In this way it was possible to obtain the desired geometries externally and it was possible to avoid the production of supports for the internal geometries.
In figure 4.5 it is possible to see the support guides for the aluminum plate and the changes made to avoid the creation of supports.
Four holes have also been introduced to allow a rigid fixing with the aluminum plate by inserting pins (2).

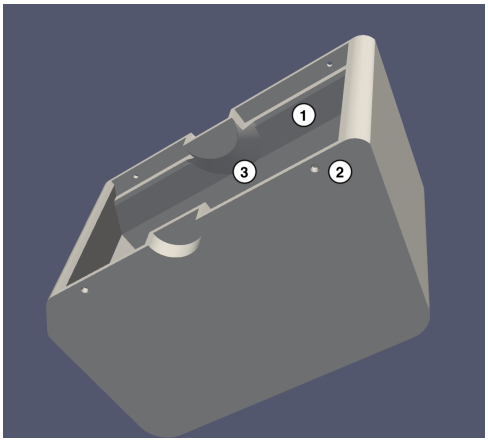

Figure 4.5. Caravan model for 3D printing

Finally, to improve the surface quality and appearance, the external surface was polished and subsequently painted. The final result obtained is shown on the right of figure 4.6.

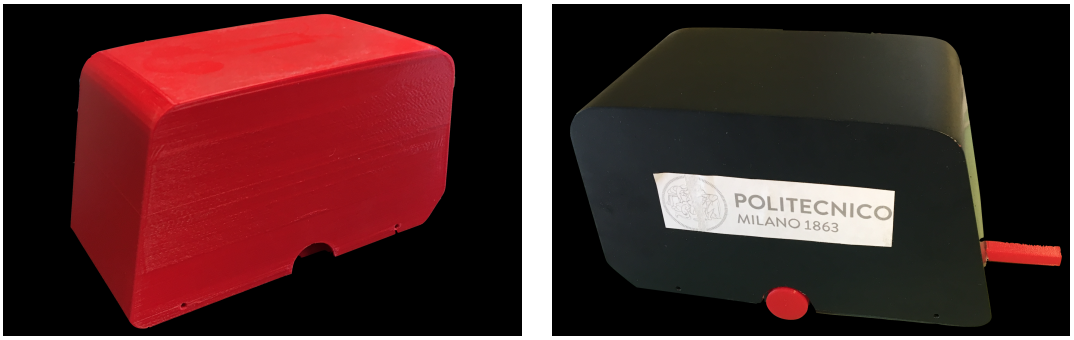

(a) *3D printed model*

(b) *3D printed model after polishing and painting*

Figure 4.6. 3D printed model

4.2 Experimental analysis

In this section is reported all the procedure used for the wind tunnel experiments. First a characterisation of the wind tunnel and its instruments has been carried out, then the tests on the model have been done.

4.2.1 Characterisation of the wind tunnel and instruments

Before being able to proceed with the characterisation of the wind tunnel it was necessary to verify the correct functioning of the instruments and the results are reported in figure 4.7.
First the balance has been analysed, the reference system it uses was noted so that the results could then be compared with the CFD tests. The reference system used by the scale has the x axis in the opposite direction to that of the wind and the z axis directed towards the floor and consequently the y axis directed towards the right side of the model.
Subsequently, a mapping has been made between motor power and flow velocity in order to know in advance the power to be used to obtain a certain speed. The mapping has been carried out considering both the speed and the difference between static and dynamic pressure measured thanks to the pitot tube. This map is dependent on the atmospheric conditions like static pressure and room temperature, in this case the static pressure was 101400 Pa and the temperature was 20,3 °C.

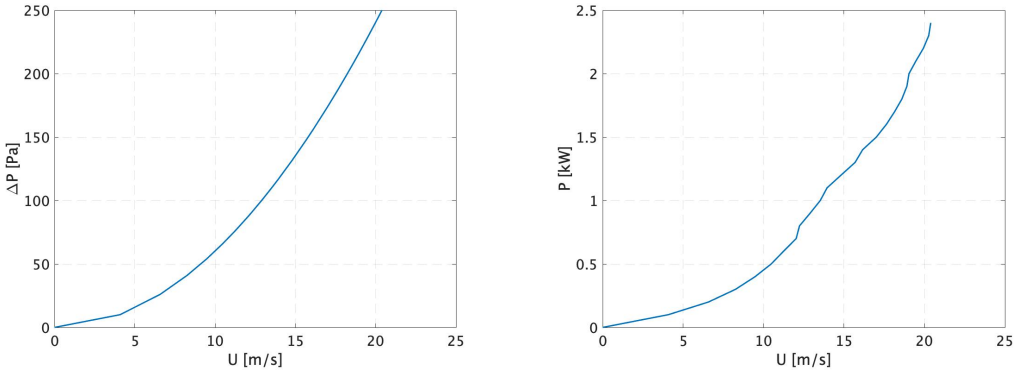

(a) *Correlation between δP and flow speed*

(b) *Correlation between engine power and flow speed*

Figure 4.7. Charachterisation of the wind tunnel

Then, a flow visualisation was carried out in order to see how the flow behaved inside the test chamber. In order to carry out this analysis, wires connected to supports have been used.
The supports have been specifically designed for the purpose and made by 3D printing using the same material as the model. They are composed of two elements, the first one has a rectangular section and a length of 200 *mm* on which there are present 20 holes with a distance of 20 *mm* used for anchoring the wires; and the second one is a plate for the connection to the test chamber walls.
The support is reported in figure 4.8.

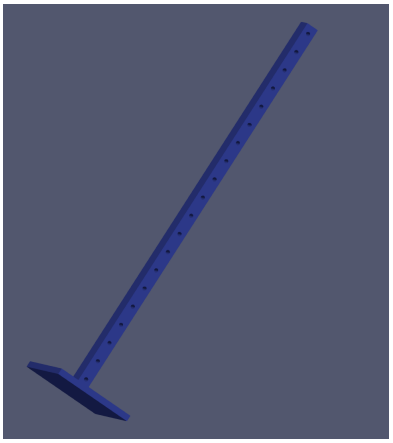

Figure 4.8. Flow visualisation support

Thanks to the use of these supports it has been possible to analyse the flow inside the tunnel. In the figure 4.9 and figure 4.10 are reported the flow visualisation, made using the four supports mounted in the chamber.

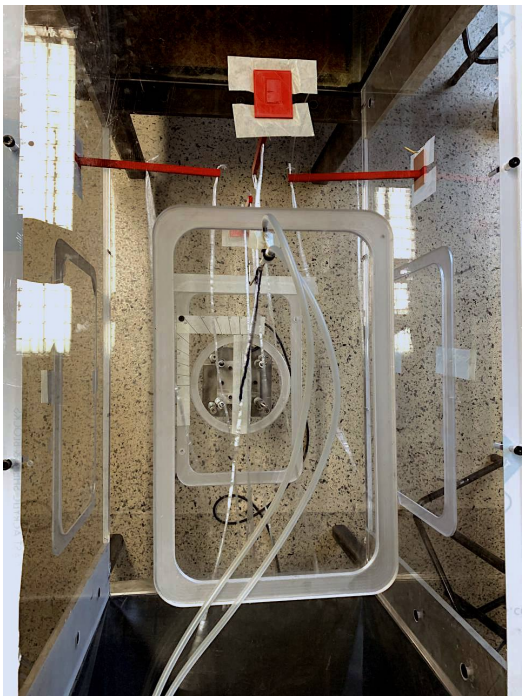

(a) *Flow visualisation from the top*

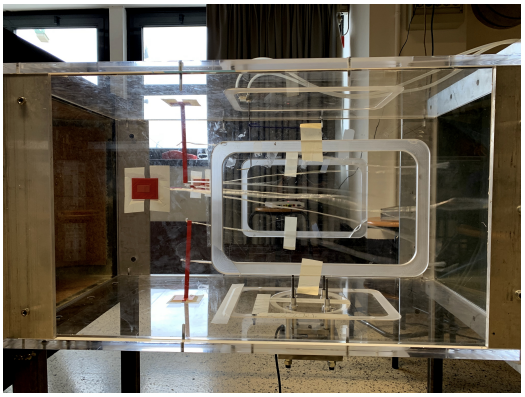

(b) *Flow visualisation from left side*

Figure 4.9. Flow visualisation

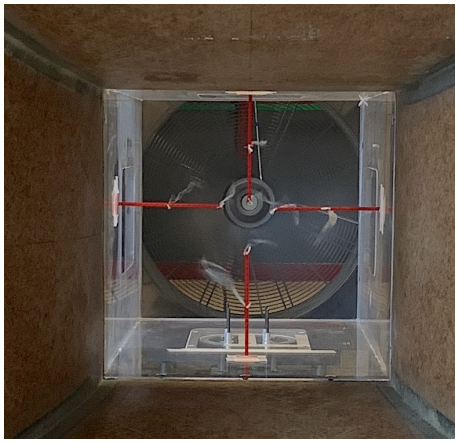

Figure 4.10. Flow visualisation from front inlet

Analysing the behaviour of the wires attached to the supports inside the chamber (figure 4.10), it is possible to notice how the flow is not perfectly parallel to the axis of the wind tunnel but has a rotating trend due to the motor action. The rotation of the flow can be identified thanks to the fact that the left side wires of the tunnel face towards the center and are inclined downwards with respect to the horizontal plane. On the contrary, the right side threads are pointing upwards and also pointing towards the center. These movements of the wires mirror the rotation of the motor which is clockwise. This behaviour differs from the conditions used in the CFD simulations and negatively influences the results obtained during the various tests.

In order to improve this condition and get as close as possible to the conditions simulated in the CFDs, it has been thought to add a very fine mesh net before the tunnel intake duct.

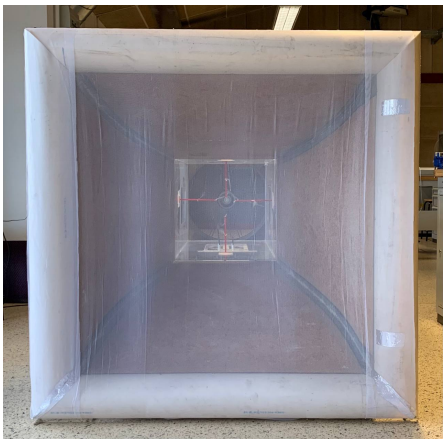

Figure 4.11. Flow visualisation from front inlet with net

By analysing the behaviour of the wires it is possible to notice a slight improvement even if the effects due to the motor rotation are still present. This change led to an improvement also in the measure of the lateral forces that pass to be zero at 3.5° to 2°.

Other improvements have also been hypothesised in order to improve the flow inside the chamber such as lengthening the section between the analysis chamber and the motor or the addition of a stator in order to eliminate the motor rotational effects; unfortunately these changes were not made as they are too expensive.

After that, the drag coefficient of the model was analysed as a function of the Reynolds number in order to know if the tunnel used is able to reach the conditions of the CFD simulations ($Re = 10^6$). The results are shown in figure 4.12.

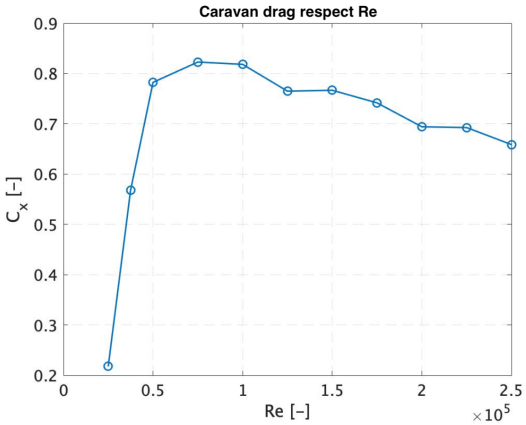

Figure 4.12. Cx function of Re

It is possible to notice that the drag coefficient is quite low for small Re numbers and then, increasing the Re number, it increases to higher values. This is due to the fact that the flow is in the supercritical zone, and the critical zone that exhibit a drag collapse is just ended.
Analysing the second part of the graph is clear that the drag coefficient has a decreasing trend and is not constant, this trend for higher Re number is supposed to become constant.
In order to increase the Re number is possible only to increase the length of the model, because the flow speed is limited by the motor. But due to the high ratio between width and length of the model is not possible to increase the length because the the blockage factor increases and so the effect of the wind tunnel boundary becomes more significant.
For the validation phase it was chosen a Re equal to $2 * 10^5$ in order to be quite far from the critical zone and near the plateau and not too high to be in a condition where the motor fluctuations are minimum.

4.2.2 Calibration of the model

After having characterised the flow inside the tunnel, a calibration of the forces generated by the model has been performed. The model has been placed inside the tunnel and several tests were carried out in stationary conditions with constant Re ($Re = 1.95 * 10^5$) and speed of 14.94 m/s at different angles of attack. The lateral forces values for the different angles were acquired in order to calibrate the reference position. The results are reported in figure 4.13.

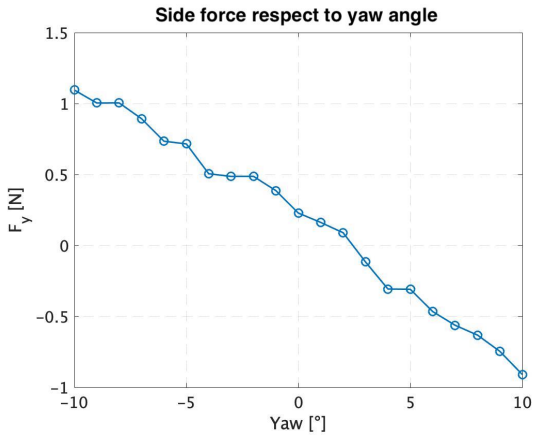

Figure 4.13. Variation of lateral forces respect to yaw angle

Given the symmetry of the model with respect to the longitudinal axis, it would be expected that the lateral forces are zero at a zero angle of attack. This does not occur, the lateral force becomes zero for an angle equal to 2 degrees, as the flow velocity has a component in the y direction due to the motor effects. This discrepancy is compensated by the rotation of the model by 2°. For the validation tests this effect has been taken into account by considering the position rotated by 2 degrees as new zero in order to compensate for the lateral force generated by the flow rotation.

4.2.3 Data acquisition

The procedure followed for data acquisition consists in the following steps:

- Acquisition of temperature and static pressure in order to correctly calculate the air density and consequently the air speed;
- Positioning of the model with the correct inclination in order to compensate the lateral forces caused by the motor rotation;
- Zeroing of the static forces in order to measure only the aerodynamic forces;
- Calculation of the flow velocity to obtain the correct Re and consequently of the pressure difference between static and dynamic:

$$U = \frac{Re * \mu}{\rho * l} \; \delta P = \frac{U^2 \rho}{2}; \tag{4.1}$$

- Motor power setting in order to obtain the correct speed;
- Forces acquisition for a period of 45 sec;
- Forces average over the acquisition period;
- Computation of the aerodynamic coefficients;

With this method, analyses has been made at different angles of attack. The three forces and the three moments have been acquired starting from zero degrees up to a maximum of 40 degrees; each position was corrected by two degrees in order to calibrate the lateral forces.
During the tests, particular attention has been paid to not alter the flow inside the wind tunnel and to monitoring the conditions during the tests. During the acquisition period, the temperature inside the room, the static and dynamic pressure difference have been checked. In this way it has been possible to discard the acquisitions during which there were large variations in temperature and delta pressure.
For each test, despite the precautions, the acquired data have been analysed before proceeding with the average and the calculation of the coefficients in order to ensure that there were not sporadic errors. Once the data have been obtained and the absence of errors have been confirmed, it was proceeded by calculating the average of each single force over the time span and the relative coefficients.

$$C_i = \frac{2F_i}{\rho v^2 A} \tag{4.2}$$

Where i indicates the force or moment considered, ρ the air density during the test and A the model frontal area equal to 0.0121 m^2.
The aerodynamic coefficients have been corrected considering the blockage factor by means of the following:

$$C_{iC} = C_i[\frac{1}{(1+\frac{1}{4}\frac{A}{C})^2}] \tag{4.3}$$

Where C_{iC} represents the corrected coefficient, C_i the coefficient obtained experimentally, A the area of the model and C the area of the tunnel section. In this way the effects of the gallery walls on the model have been considered and the coefficients corrected accordingly.
The results are shown below in figure 4.14:

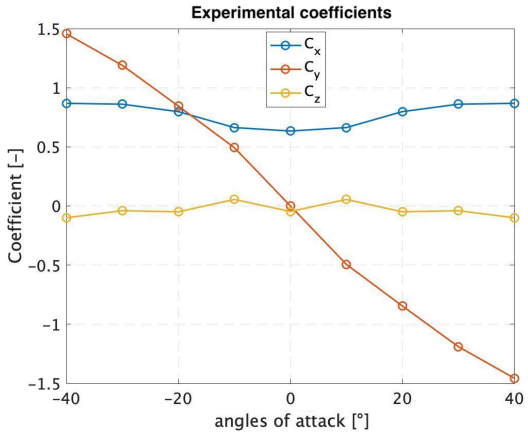

Figure 4.14. Experimental coefficient at various angle of attack

Analysing the results it is possible to note that the lateral forces are about zero for the vehicle positioned at zero degrees, this was possible thanks to the correction of 2 degrees on the position.

The experimental data have been compared to those obtained from CFD simulations. The comparison is reported in the following (figure 4.15 and figure 4.16):

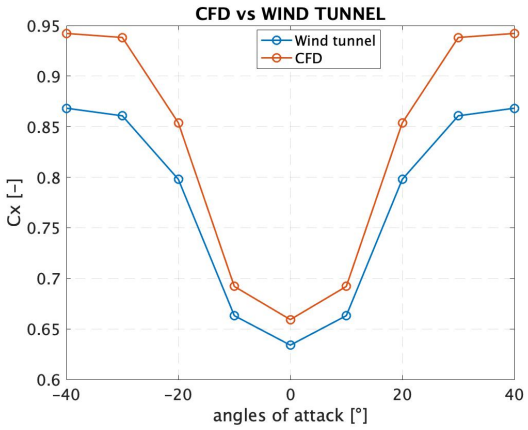

Figure 4.15. Comparison between Cx from CFD and Cx from wind tunnel tests

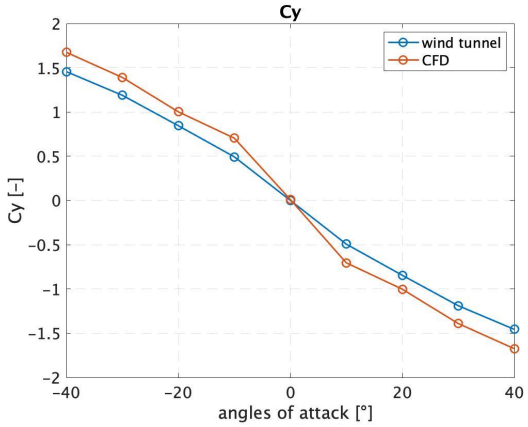

Figure 4.16. Comparison between Cy from CFD and Cy from wind tunnel tests

From these results it can be seen that the maximum deviation between CFD simulation and experimental analysis, as regards the Cx, is equal to 8,5 % for a relative angle equal to 30° and -30°, while as regards the Cy, it is equal to 28% at 10° and -10°. This big difference between the experimental value and the result of the CFDs is due to the fact that the positioning of the model inside the tunnel is affected by uncertainty; and the flow inside the test chamber is not perfectly parallel to its axis but has a rotational component caused by the influence of the motor.

Chapter 5

Results

In this chapter the CFD simulations concerning the car-caravan coupling are discussed and, subsequently, the results of the dynamic simulations are analysed.
As announced, OPENFoam™software has been used for CFD simulations, while MATLAB and SIMULINK™have been used for dynamic simulations.
The CFD simulations have been used in order to find the aerodynamic loads acting on the car and caravan separately at different yaw angle (angle between vehicle and wind). With them it is possible to study the flow around the vehicle and find which are the phenomena that occur.
Once the aerodynamic loads have been computed it is possible to define the aerodynamic coefficients in order to eliminate the dependance on the wind speed. This has been done in order to be able to simulate the vehicle dynamic response in different wind conditions.
With the aerodynamic coefficients it is possible to introduce a wind model, in the dynamic simulation, and evaluate the aerodynamic loads acting on the vehicle at different conditions without the necessity of doing other CFD simulations since they are time consuming. In this way the final simulations are low time consuming and so a quite large situations number can be analysed.
In the dynamic simulations different wind conditions and different trajectory have been tested and, anlysing the results, the most critical conditions have been found.

5.1 CFD simulations and results

Once the basic setup of the simulations has been obtained, it was possible to carry out the simulations useful to define the aerodynamic coefficients at different incidence angles. To obtain the trend of the coefficients as a function of the angle of attack, various simulations have been carried out considering an absolute wind speed equal to 40 m/s and varying the wind incidence angle from -90° to 90° with an interval step of 10°. For each condition, therefore, the wind speed has been decomposed into longitudinal and lateral components as previously reported.
Each simulation has a duration of 1000 iterations in order to achieve the convergence on the residuals. The forces used for the aerodynamic coefficients calculation were averaged over the entire simulation duration, however discarding the first 300 values. This was done in order to not consider the values affected by the initial transient and

by possible numerical errors, thus obtaining the steady-state values.
Also in this case the car and the caravan have been considered separately so that the two vehicles and their interaction could be analysed independently.
The results obtained are reported in figure 5.1.

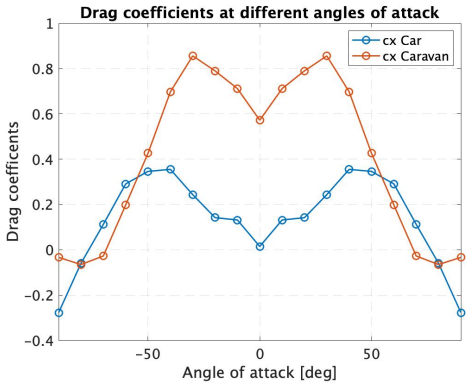

(a) *Drag coefficients of the car and caravan*

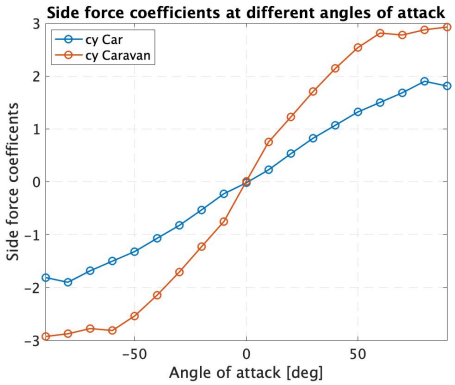

(b) *Side force coefficients of the car and caravan*

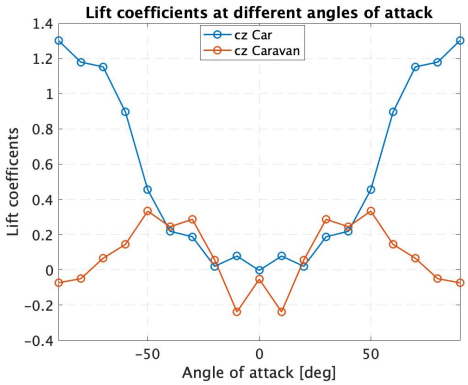

(c) *Lift coefficients of the car and caravan*

Figure 5.1. Trend of aerodynamic coefficients as function of the incidence angles

Analysing the drag coefficient of the car trailing the caravan (reported here) it is possible to notice that for small angles of attack the drag coefficient is lower with respect to the case of the car alone. For the car, this trend can be traced back to the caravan presence which, by modifying the wake flow, avoids the classic pressure reduction in the rear part of the car like it can be seen in figure5.2. This change in the pressure range also affects the drag of the caravan which therefore has lower values compared to higher angles of attack.

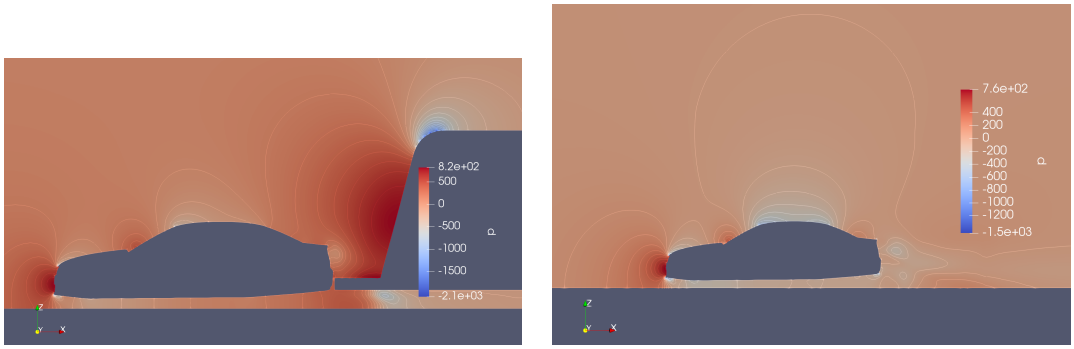

(a) *Pressure field on the rear of the car with the caravan*

(b) *Pressure field on the rear of the car without the caravan*

Figure 5.2. Pressure field on the rear of the car

By increasing the wind incidence angle, up to 25°, the drag coefficient has an increasing trend due to the fact that the flow is no longer influenced by the wake of the car and reaches the front of the caravan undisturbed, like it is possible to see in figure 5.3. The flow generates a high pressure area on the caravan front and a low pressure one at the rear of the car.
While the side force coefficient has a linear trend with the wind incidence angle. This is due to the fact that by increasing the incidence angle the wind interacts more with the vehicle lateral surface.

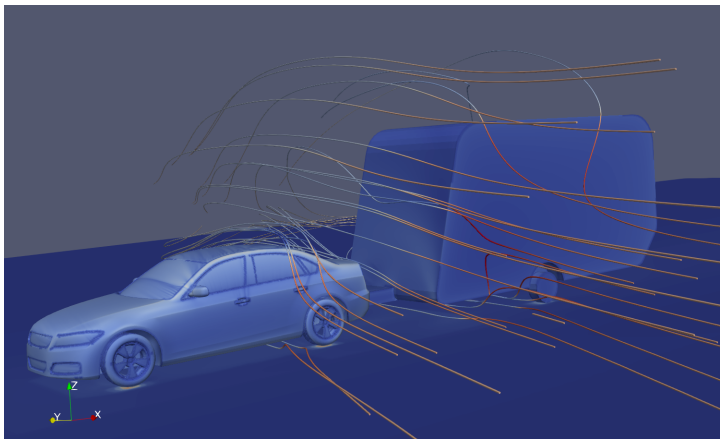

Figure 5.3. Flow at high angles of attack

As regards the use of the CFD results within the dynamic model, the following method has been used:

- Acquisition of the aerodynamic coefficients from CFDs at different angles of attack;
- Wind profile imposition;
- Vehicle trajectory imposition;
- Real time calculation of the relative angle between wind and vehicle axis;

- Interpolation of the aerodynamic coefficients on the basis of the angle of attack;
- Calculation of aerodynamic forces and moments on the basis of the calculated coefficients.

5.2 Dynamic simulations

In this section the results obtained from the dynamic analyses have been reported, that have been carried out with different trajectory and wind conditions. In the first place, the vehicle behaviour for each trajectory and condition have been analysed in order to find the conditions that can cause the vehicle to overturn or lose control by the driver. In particular, have been analysed the variations in vertical load on the wheels for both the caravan and the car, the trajectory that the driver has been able to follow and possible phenomena of instability that occurred.
The simulations have been carried out considering the vehicle at a speed of 80 Km/h as it is the motorway limit for vehicles with trailers. The analysis has been carried out with the following steps:

- Mapping of the safety index of the caravan to different wind conditions;
- Critical situations identification;
- Critical condition analysis;
- Analysis of results in extreme situations.

The caravan safety index has been analysed as a key safety parameter because during the simulations it has been noticed to be the parameter that best identifies the establishment of critical situations.
The mapping was done by setting vehicle speed and trajectory and varying wind conditions. The discretisation of the conditions has been carried out considering a wind speed range from 0 to 20 m/s, with a step of 5 m/s. As regards the absolute wind incidence angle, that is the wind angle with respect to the absolute reference system, a range from 0 ° to 90 ° with a step of 10 ° has been considered. This discretisation has been chosen as the best compromise between computational cost and analysis precision.
Once the critical conditions have been identified, that is the conditions for which the safety index exceeds the limit threshold of 0.9, the behaviour of the vehicle was analysed. The aspects considered are the risk of the caravan overturning, as the component most subject to this phenomenon, and the trajectory followed by the car. Critical conditions have been considered as the minimum wind speed that cause the caravan safety coefficient to exceed the limit threshold of 0.9. For each critical condition the value of the wind speed, wind angle and vehicle speed are reported as key parameter to identify the critical condition.
The safety index map have been made considering the highest absolute value during each simulations, so the values reported in the maps are the worst conditions during each simulations.

5.2.1 Straight trajectory with external gust wind

The most common condition that occurs while driving on the motorway is traveling at a constant speed along a straight. In this condition there are no load transfers due to the maneuver or to particular dynamic conditions, therefore it is possible to analyse in a clear and simple way the effects due to the external wind.
The conditions analysed are shown below in figure 5.4:

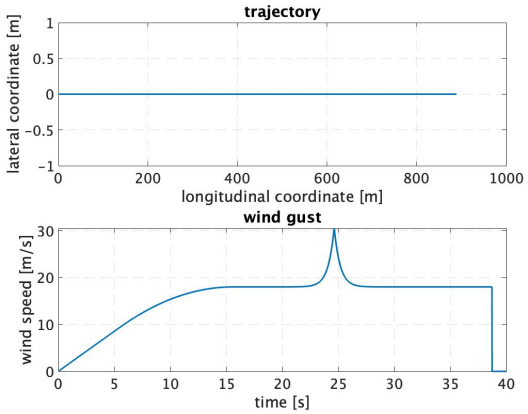

Figure 5.4. Simulation conditions

From figure 5.4 it is possible to notice that the gust lasts about 4 seconds and the peak is located at about 550 m.
With these conditions, a total of 40 simulations have been carried out in order to map the caravan safety index trend as the wind conditions changed. It was thus possible to obtain the map in figure 5.5.

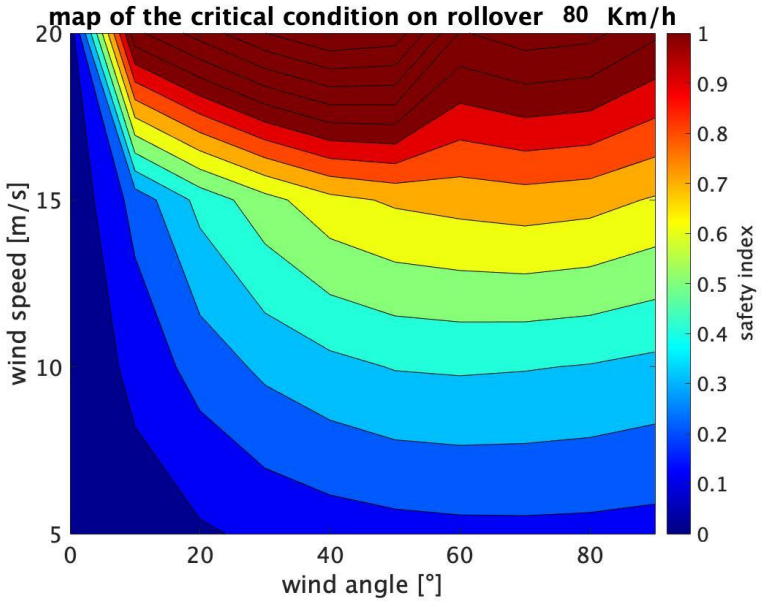

Figure 5.5. Map of safety index of trailer at different wind conditions

Analysing the figure 5.5 it is possible to notice that the safety conditions ($\eta_t < 0.9$)

are reached for wind speeds lower than 18 m/s and angles lower than 35°. It can also be noted that for very small wind angles, the wind speeds that guarantee safety against overturning increase up to a maximum of 20 m/s.
It is important to note that the conditions for which the safety index is higher than 0.9 the caravan has one of the two wheels with a load reduction equal to 90% and if it reaches 1 one of the wheels has lost contact with the ground.
Analysing the map, it can be seen that for speeds greater than 18 m/s and angles greater than 35° the safety index reaches the unit value indicating that a wheel has lost contact with the ground and therefore the caravan is subject to overturning.
Once the critical conditions have been defined, a comparative analysis has been carried out between the limit conditions and critical conditions. The behaviour was analysed for wind of 17 m/s and 30° in which the safety index is lower than 0.9 and wind at 17 m/s and 35° in which the safety index exceeds the limit threshold of 0.9.
The trend of the safety index as a function of the simulation time is shown in figure 5.6:

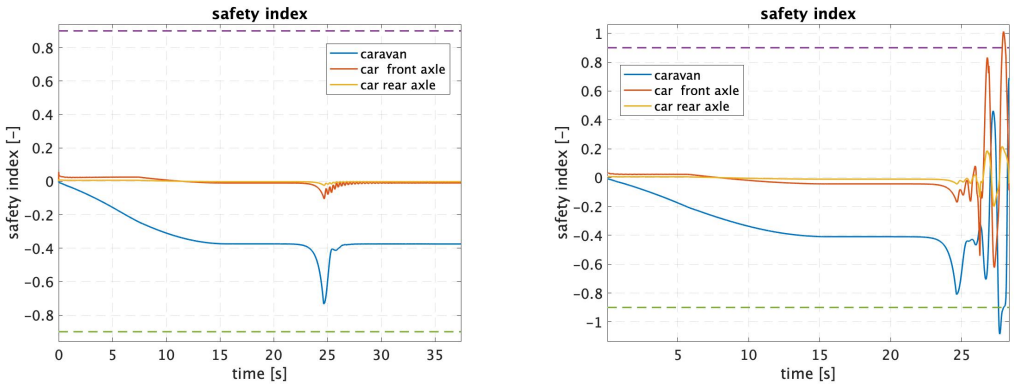

(a) η_i *at 17 m/s and 30°* (b) η_i *at 17 m/s and 35°*

Figure 5.6. η_i comparison for the two cases

Analysing the behaviour of the safety index it is clear that the caravan is the vehicle most affected by aerodynamic loads and which presents the greatest risk of overturning. Considering only the limit condition it is possible to notice that the rear axle of the car is less critical for the rollover. This is due to the load transfer of the caravan that influence the junction pin, and so the influence of the caravan motion and loads are more relevant on the rear part of the car. For the front axle the safety index has a higher variation but it is quite far from the limit condition.
Considering the safety index in critical conditions, it can be seen that the overturning is achieved first by the caravan and then by the car as it is the first to exceed the limit. This result justifies the fact that in order to have a clear overview of the overturning risk, it is sufficient to analyse the caravan safety factor as it is the most sensitive component.
For what concern the car in the critical conditions the front axle present an higher variation and this is due to the fact that the caravan exchange the vertical force on the rear axle so the front axle has a reduction on the vertical load and so it is more sensitive to the wind action.
The graph representing the critical conditions has been limited on the x axis as once the vehicle overturns is reached, the simulation loses its meaning.

An important aspect is the trend of the vertical load on each wheel, the vertical load is a parameter that not only indicates the overturning of the vehicle but also influences the lateral and longitudinal forces exchanged in the contact patch. Analysing the figure 5.7, referred to the unsafe condition, it is possible to notice how the load on the left wheel of the caravan decreases with the wind presence. In the first part, up to 40 seconds, the load is about 40% lower than the static load and has a sharp decline in correspondence with the gust. This indicates that, already in the presence of stationary winds at high speed (in the first part the wind has a constant value of 17 m/s), there is a considerable vertical load loss reaching the overturning in correspondence of the gust.
In the safe case, on the other hand, the percentage of vertical load during the quasi-stationary part is equal to 65% reaching a peak of 48%.

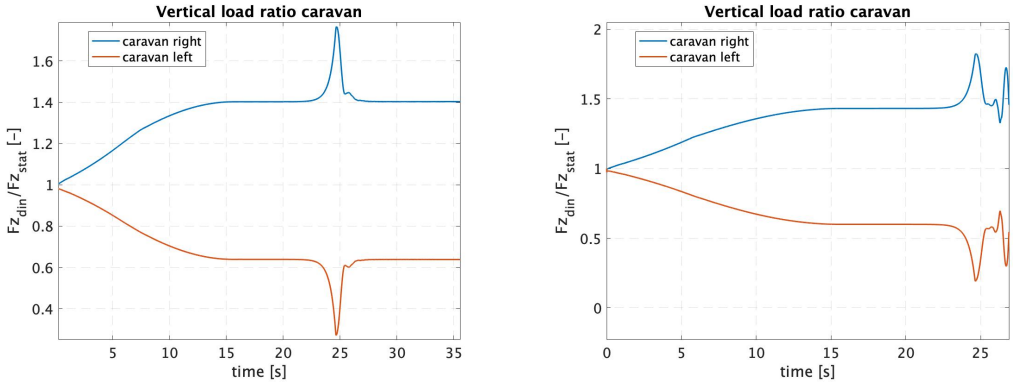

(a) *Vertical load ratio at 17 m/s and 30°* (b) *Vertical load ratio at 17 m/s and 35°*

Figure 5.7. Vertical load ratio comparison for the two cases

The vertical load loss can also be seen by analysing the trajectory carried out by the caravan (figure 5.8), the trajectory of the caravan center of gravity has a deviation from the trajectory carried out by the car of about 0.07 m, reaching the value of 0.15 m during the gust. While in the safe case the deviation from the car trajectory is about 0.06 m reaching a peak of 0.14 m, so there is not a big difference between the safe and unsafe scenarios.

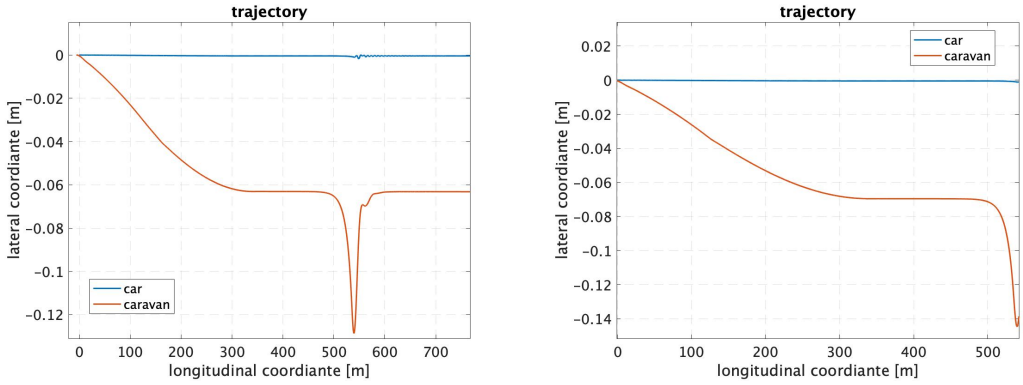

(a) *Trajectory at 17 m/s and 30°* (b) *Trajectory at 17 m/s and 35°*

Figure 5.8. Trajectory comparison for the two cases

Analysing the trajectory it is possible to notice that in correspondence with the gust there are oscillations. These obviously have repercussions on the steering wheel and consequently affect the driver's response. This is a very important aspect as they could catch the driver off guard and cause an incorrect response. This aspect, depends a lot on the experience and reactivity of the rider, cannot be studied systematically, but it remains a very important aspect.
Finally, the roll angle trend of both the car and the caravan has been analysed 5.9.

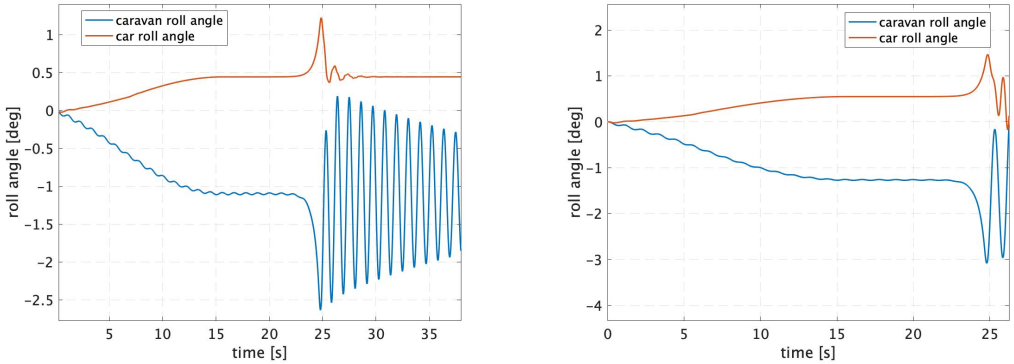

(a) *Roll angle at 17 m/s and 30°* (b) *Roll angle at 17 m/s and 35°*

Figure 5.9. Roll angle comparison for the two cases

The roll angle trend has been analysed first of all to verify if at the aerodynamic level it was necessary to carry out further CFD simulations at various roll angles. Analysing the figure 5.9 it can be seen that in critical conditions the roll angle of the caravan reaches values of 1.4° in the quasi-static area with a peak of about 3°. While in safe conditions it has a constant value of 1.1 ° reaching a peak of 2.55 ° during the gust. Therefore it was not necessary to carry out CFD analyses at different roll angles as the amplitudes reached are in the order of a few degrees.
The interesting thing, however, it is the difference between the roll angle of the car and the roll angle of the caravan, the first in addition to having much smaller amplitudes has higher damping values that allows to have few oscillations. While for the caravan the damping is lower and there is a greater number of oscillations; this is due to the different type of suspension used for the caravan (type leaf spring) and for the car.

5.2.2 Lane change trajectory with external gust wind

While driving on the motorway, an obstacle may be encountered on the carriageway or, due to roadworks, it may be necessary to change lanes. For this reason it was decided to analyse the behaviour of the vehicle during a lane change in conditions of strong side winds. The conditions are shown in figure 5.10 in which it can be seen how the gust wind occurs at approximately half of the lane change.

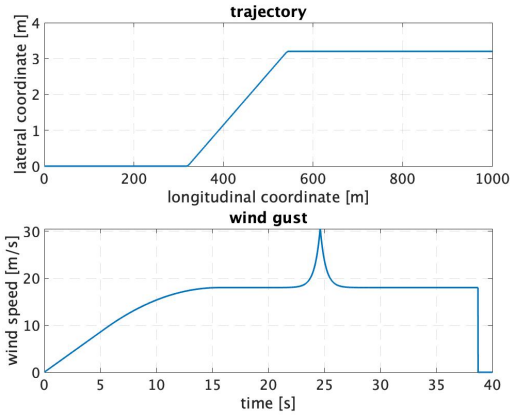

Figure 5.10. Wind profile and trajectory

In this case the mapping has been carried out in a different way than in the previous case as the trajectory carried out by the vehicle is not symmetrical. For this reason winds with negative angles have been analysed in order to study the influence of the wind direction. Furthermore, a wider discretisation has been carried out in the field of wind speeds in order to obtain a denser mapping. In this case, therefore, winds with angles from -90° to 90° with discretisation of 10° have been analysed; while, as regards the speeds, speeds from 4 m/s up to 20 m/s with discretisation of 2 m/s have been analysed.
The results obtained are reported in figure 5.11.

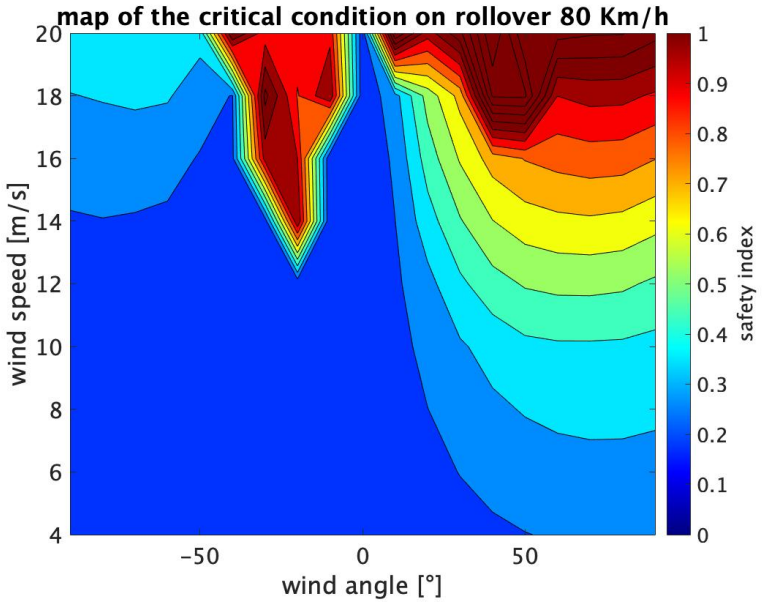

Figure 5.11. Map of safety index of trailer at different wind conditions

From figure 5.11 it is possible to notice that there is an asymmetry of the results. It is noted that for negative angles the safety index exceeds the limit of 0.9 for wind speeds lower than in the case of wind with positive angles.
This means that the worst condition for making a lane change when towing a caravan

it is when the wind direction is the same as the direction followed by the vehicle to make the lane change. This is due to the fact that the gust is located just before the realignment with the arrival lane, so the lateral aerodynamic forces are added to the lateral forces of inertia, increasing the load transfers.
Another difference is that for negative angles less than -70 ° the vehicle remains in safe condition even at high wind speeds. This is due to the fact that the vehicle travels along a trajectory with a certain inclination with respect to the absolute reference system (on which the wind angle is defined), and therefore the relative angle between wind and vehicle speed is lower in modulus and consequently also the lateral aerodynamic loads are lower.
Analysing the limit values it is noted that for wind speed equal to 14 m/s with an angle of -20° the safety coefficient exceeds the limit of 0.9, while for the same wind speed and angles of -30° the safety coefficient remains below the limit.
The safety index trend respect to both safe and unsafe conditions are reported in figure 5.12.

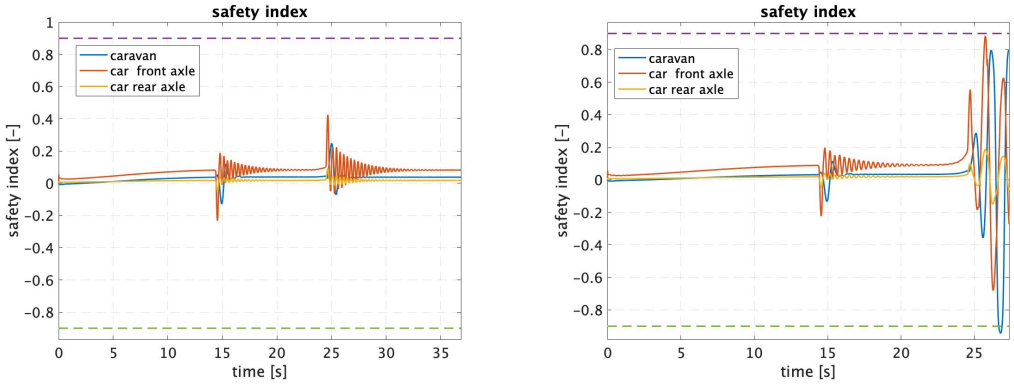

(a) η_i *at 14 m/s and -30°* (b) η_i *at 14 m/s and -20°*

Figure 5.12. η_i comparison for the two cases

Analysing the safety coefficient trend in safe conditions, it can be seen that there are three oscillations, one relative to the start of the lane change maneuver, one relative to the wind gust and one to the end of the maneuver. It is noted that the oscillations with greater amplitude are those relating to the front axle of the vehicle. This is due to the fact that the caravan load is discharged on the rear of the car and so the front axle has a lower vertical load and is more sensitive to inertia and external forces.
While analysing the trend of the safety coefficients in the unsafe condition, it is clear that the wind gust has an influence on the variation of the safety coefficient that is accentuated by the end of the maneuver; it is the sum of the wind gust plus the the load transfer due to the inertia that cause the exceeding of the limit.
Another important aspect is that the front axle safety coefficient is the first to exceed the limit but the safety index of the caravan exceed the limit more time, so the caravan is the component that is critical for the turnover.
It is therefore interesting to analyse the load transfers for each axis normalised with respect to the static load. The results are reported in figure 5.13.

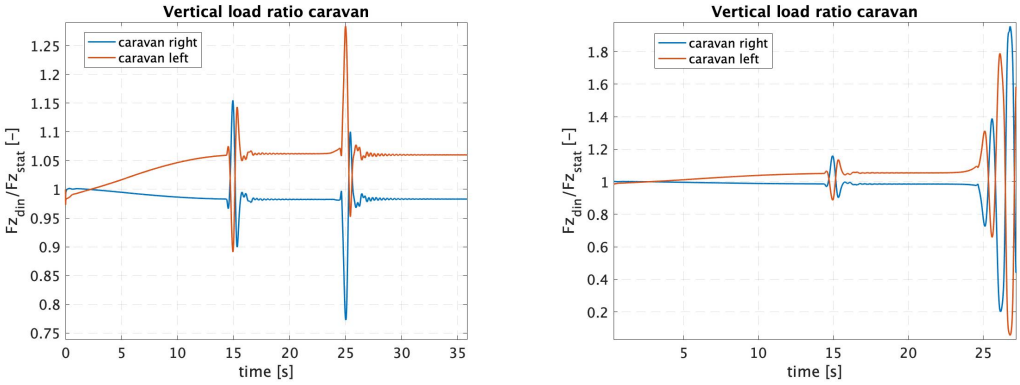

(a) *Vertical load ratio at 14 m/s and -30°* (b) *Vertical load ratio at 14 m/s and -20°*

Figure 5.13. Vertical load ratio comparison for the two cases

Analysing the case under safe conditions, it is possible to see the presence of three areas in which there are oscillations; the first one related to the beginning of the lane change, the second one due to the wind gust and the third one due to the end of the lane change. In particular the third oscillation zone is wider respect to the first one due to the presence of the wind gust just before. There is an important difference between the first oscillating region and the third one, in the first region (without the wind gust) there is an inversion of the vertical load from the left to the right wheel. This is due to the lateral inertia, while, in the third region, the inversion of the load is smaller respect to the previous case due to the presence of the wind gust.
Analysing what happens in the case of unsafe conditions, at the starting of the maneuver the oscillation are quite small, the overturning happens when there is the end of the maneuver. In this case there are the effect due to the wind gust that start the oscillations, and the inertia, due to the change of direction, increase their amplitude until the overturninig.
The wind effects and load transfers effects can be seen on the trajectory shown in the figure 5.14.

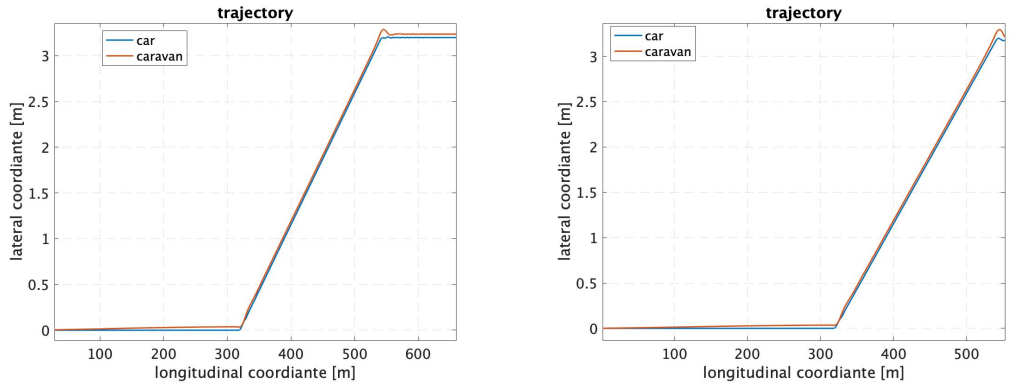

(a) *Trajectory at 14 m/s and -30°* (b) *Trajectory at 14 m/s and -20°*

Figure 5.14. Trajectory comparison for the two cases

Analysing the trajectory in safe conditions, oscillations are always noticed at the beginning and end of the maneuver and are present contained deviations from the

reference trajectory. The oscillations present depend not only on the wind conditions but also on the drive's response. In the event that the driver is caught by surprise or has no experience in driving, these oscillations could cause an incorrect response and therefore aggravate the situation.
While analysing the trajectory in unsafe conditions it is noted that in correspondence with the gust there are deviations of 0.5 m before the caravan overturns. This aspect is very important as before the rollover there is a strong skid, which in a scenario with other vehicles would mean their involvement and therefore an increase in the number of the people involved.
Finally, the roll angle trend in both situations is analysed for both vehicles. The results are reported in figure 5.15.

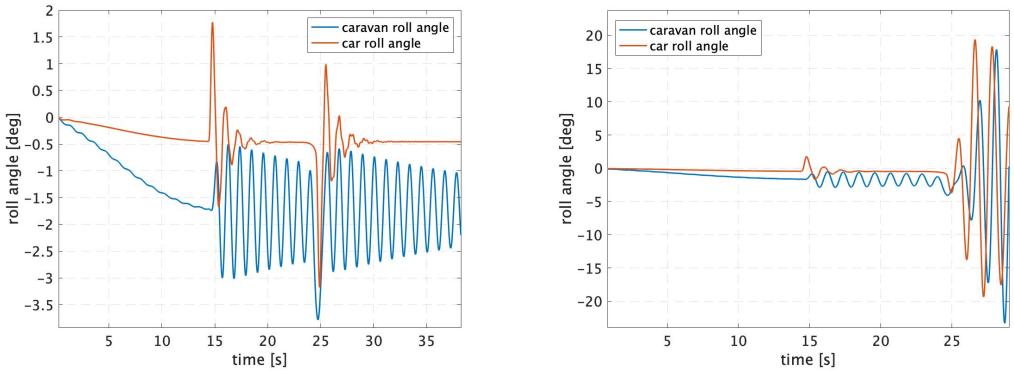

(a) *Roll angle at 14 m/s and -30°*

(b) *Roll angle at 14 m/s and -20°*

Figure 5.15. Roll angle comparison for the two cases

Analysing what happens in the case on the left it can be noticed that just before the starting of the maneuver there is a significant inclination of both the car and caravan due to the presence of cross-wind. At the starting of the maneuver there is a significant inclination followed by an oscillating trend; the first oscillating trend is smaller respect to the second one due to the fact that before the end of the maneuver there is the wind gust that increase the amplitude of the oscillations.
As for the case shown on the right the car has a smaller inclination in the first part before the overturning and small oscillations, this can be dangerous because the driver does not fell that there is a dangerous situation coming.

5.2.3 Double lane change trajectory with external gust wind

One of the other possibilities that have been analysed is the overtaking maneuver. While driving, it is possible to meet a slower vehicle in front and therefore it is necessary to carry out an overtaking maneuver. In this case, the positioning of the gust was carried out just before the maneuver to return to the first lane, as reported in figure 5.16.

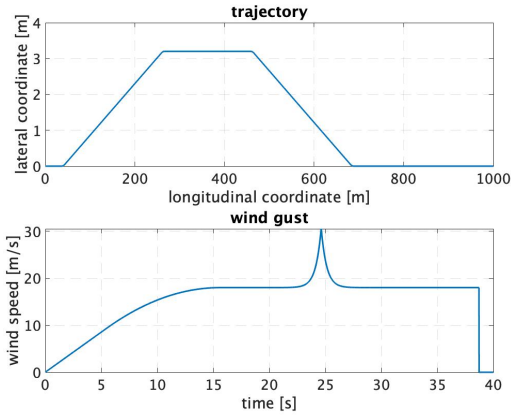

Figure 5.16. Wind profile and trajectory

The simulation strategy used in this case is the same as in the previous case and therefore negative wind angles and a denser discretisation of speeds were used. The results obtained are reported in figure 5.17.

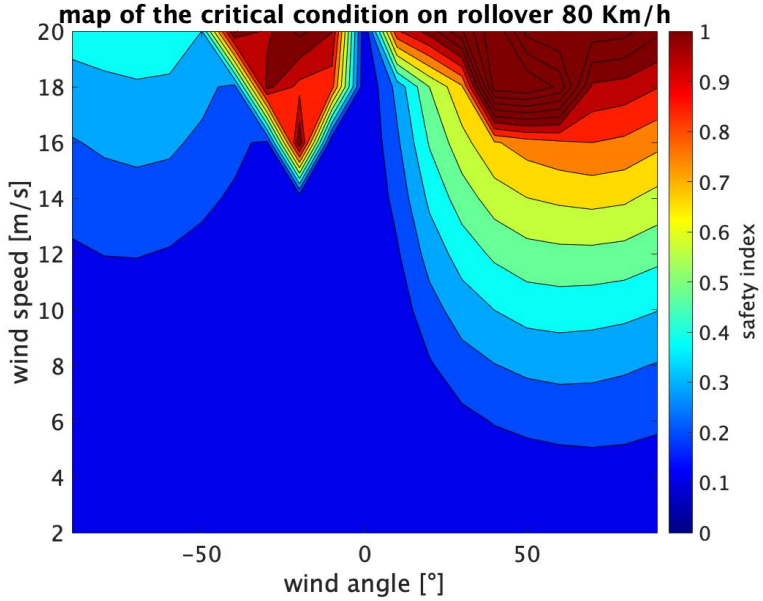

Figure 5.17. Map of safety index of trailer at different wind conditions

In this case the results are similar to the lane change case. There is a critical zone due to low wind speeds for angles between -10° and -40°, while for positive angles the criticality comes for higher wind speeds. The difference with respect to the previous case lies in the fact that critical situations are reached due to higher wind speeds, in this case of 15 m/s compared to 14 m/s in the previous case.
An interesting aspect is the high gradient between the safe zone and the risk zone. In fact, it is noted that in the case of positive angles there is a smaller gradient and there is a transition zone between safety and unsafe regions; while, in the case of negative angles, there is not the transition region but there is a sharp change in the safety coefficient.

Another interesting aspect is that for wind angles smaller than -50° the vehicle is not in critical conditions also for high speed wind, in fact in the map one the up left corner the difference of vertical load between caravan left and right side is less than 50%.
In this case the critical values are encountered for speeds of 15 m/s and angles of -20°, while the limit zone is in correspondence with wind at 15 m/s and an angle of -30°.
The following figure shows the trends of the safety factor with respect to time for the two cases.

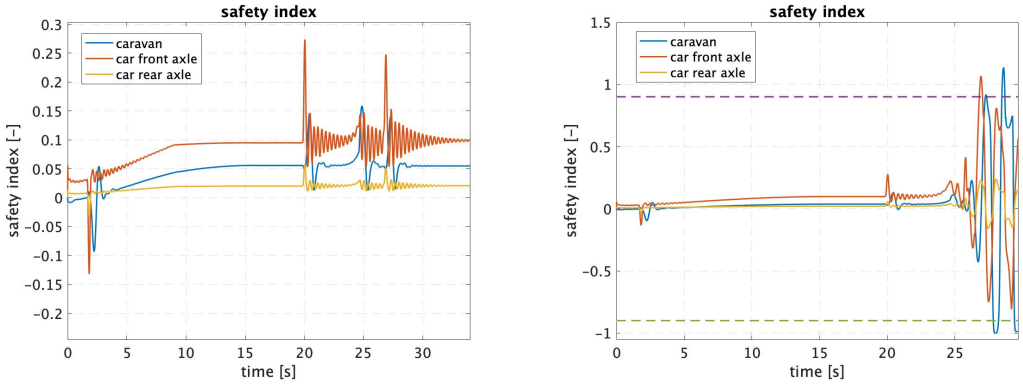

(a) η_i *at 15 m/s and -30°* (b) η_i *at 15 m/s and -20°*

Figure 5.18. Safety coefficients comparison for the two cases

Analysing the graph on the right on figure 5.18, under safe conditions, it is possible to see four regions in which there are oscillations. The first two zones with oscillations are the same as in the previous case, while the third that is encountered it is due to the gust and the last is due to the start of the maneuver to return to the lane. It can be noted that the most sensitive part, respect to the inertia forces, is the front axle, as it presents peaks in correspondence with changes in direction; while the part most stressed by the wind gust turns out to be the caravan which has a marked peak in correspondence with the wind gust. In this situation, the safety factor remains well below the limit threshold.
As for the unstable conditions, it is noted how the wind gust negatively influences the change of direction for the return to the lane. As in the case of lane change, also in this case the front axle is the first to exceed the safety limit, but it only exceeds it once and then remains within the safe range. While the safety coefficient of the caravan exceeds the limit several times, oscillating between values well above the limit, implying a highly dangerous situation.
The rear axle, on the other hand, always remains well below the limit values, indicating that the load variations between the right and left side are limited.
To learn more about the vertical load variations on the most critical vehicle, the vertical load variations for each wheel of the caravan are shown below.

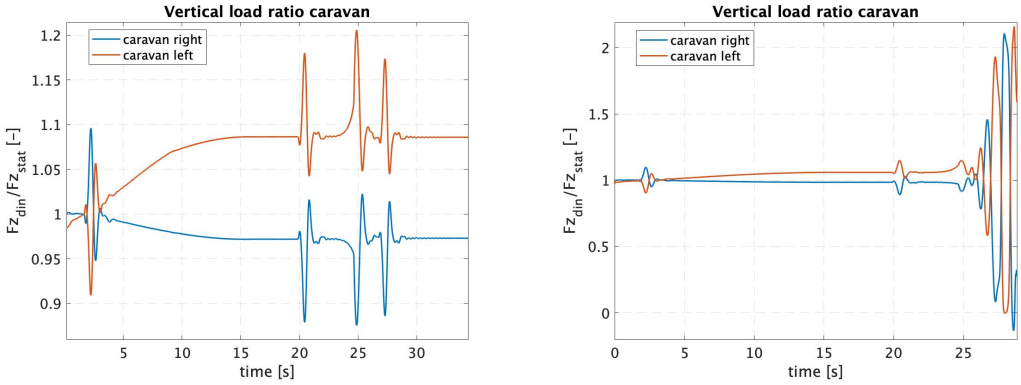

(a) *Vertical load ratio at 15 m/s and -30°* (b) *Vertical load ratio at 15 m/s and -20°*

Figure 5.19. Vertical load ratio comparison for the two cases

In the graph on the left, in figure 5.19, it can be seen that there are the four load transfers due to changes in direction and due to wind gust. An interesting thing is the fact that there are no large oscillations but only some peaks corresponding to the beginning of the trajectory or in the gust presence, followed by small oscillations.
Referring to the graph on the right (unsafe conditions) it is possible to note the presence of the four load transfers that are present also in the graph on the left. The difference lies in the last load transfer, because the oscillations due to the gust have a dampened trend and their amplitude decreases until the change of trajectory occurs. The lateral forces of inertia due to the change of trajectory are added to the load oscillations due to the lateral gust, bringing the vehicle into unsafe conditions. In fact, it is noted how the oscillations present after the change of trajectory have increasing amplitudes going to reach even zero values or the complete detachment of the wheel from the ground.
The lateral wind gust and the associated load transfers also have repercussions on the trajectory.
The figure 5.20 shows the trajectories for the safe and unsafe case.

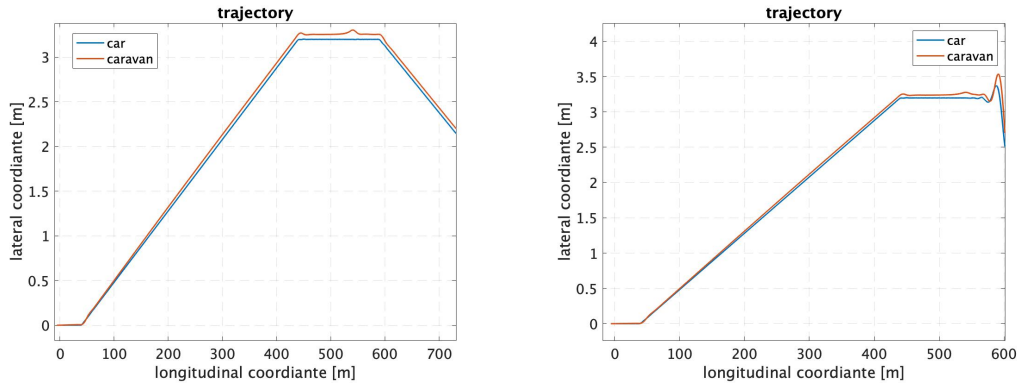

(a) *Trajectory at 15 m/s and -30°* (b) *Trajectory at 15 m/s and -20°*

Figure 5.20. Trajectory comparison for the two cases

Considering the graph concerning the trajectory in safe conditions, no oscillation is noticed but only the skids of the caravan with respect to the car. There is also

an almost constant deviation between the trajectory followed by the car and the one followed by the caravan due to the fact that the caravan has a greater lateral area and is therefore subject to greater lateral aerodynamic loads.
Considering the graph on the right instead, it can be seen that the skid caused by the side wind gust is similar to the case on the left. The difference is present at the beginning of the return in the first lane where there is a significant side slip, about half a meter. Also in this case, before the caravan overturns, there is a significant skid that could lead to the involvement of other vehicles present.
Finally, the roll angle trend is reported for both cases in the figure 5.21.

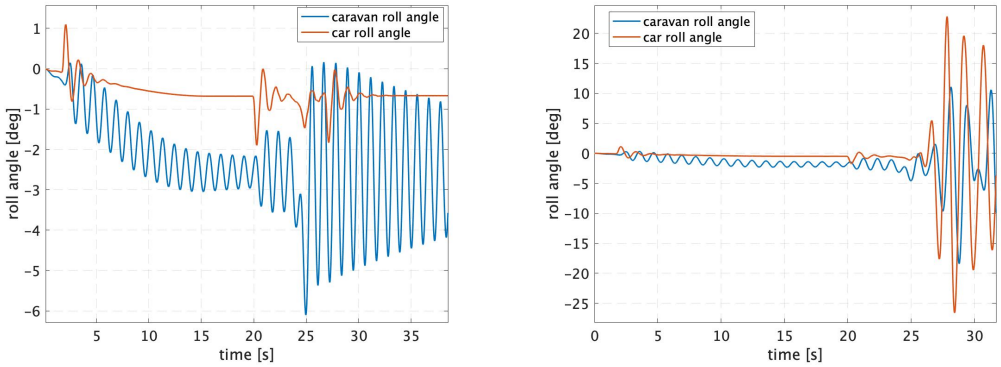

(a) *Roll angle at 15 m/s and -30°*

(b) *Roll angle at 15 m/s and -20°*

Figure 5.21. Roll angle comparison for the two cases

In the graph on the left, regarding safe conditions, it is possible to see that there are oscillations of the caravan from the beginning of the lane change. These oscillations have an increasing average value in the first part and reach a constant value of -2.5° at the end of the initial ramp of the gust. The oscillations undergo a first increase once the second lane is reached and a sharp increase in correspondence with the gust. While in the case of the car there are no oscillations and the roll angle experienced is much lower respect to one of the caravan, safeguarding the comfort on board.
In the graph on the right, the trend up to the gust is almost identical to the left case with a sharp increase in the part following the gust. This trend in the first part is very dangerous as there is no difference between the two situations before the caravan overturns and therefore the driver is not able to notice the imminent danger.

5.2.4 Highway curve trajectory with external gust wind

The last studied trajectory is a highway curve with a large radius of curvature equal to 500 m. In this case the vehicle is on a curve with a constant radius and therefore undergoes a load transfer towards the outside of the curve which could aggravate the effects due to the gust.
The trajectory and the wind profile are reported in the figure 5.22.

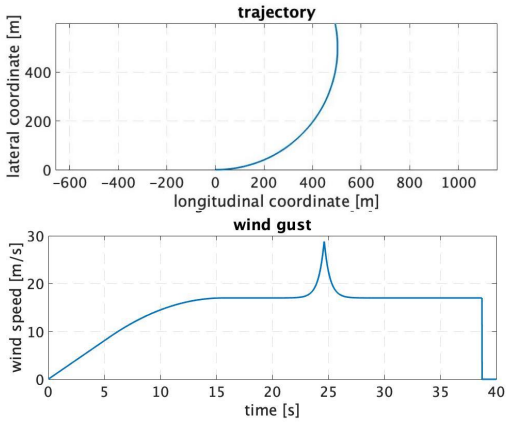

Figure 5.22. Wind profile and trajectory

In this case, the method used for lane change was adopted for mapping the safety index. Winds with angles from -90° up to +90° with 10° pitch and speed from 2 m/s up to 20 m/s with 2 m/s pitch were analysed.
The results obtained are reported in figure 5.23.

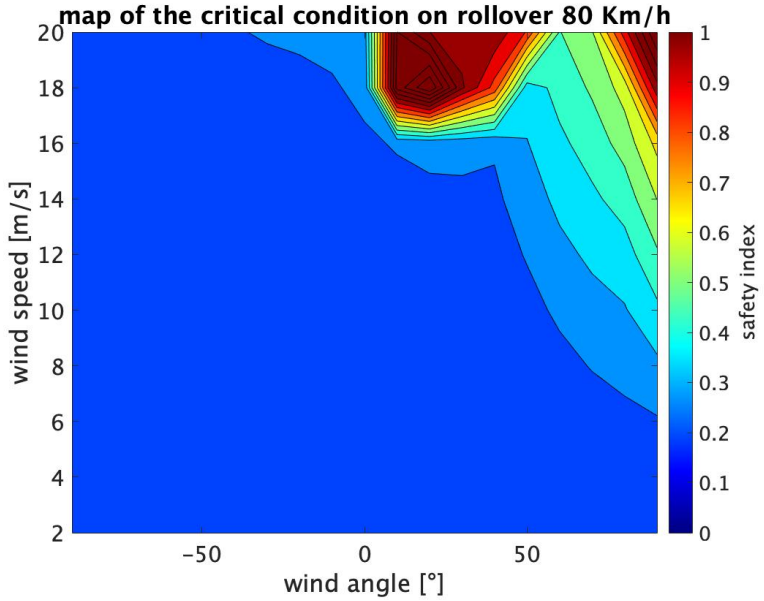

Figure 5.23. Map of safety index of trailer at different wind conditions

Analysing the figure 5.23 it can be seen that it is predominated by safe conditions with safety coefficients quite below the limit threshold. The limit is exceeded for winds with high speeds and positive angles. In particular, the critical conditions occur for winds with speeds higher than 18 m/s and angles between 10° and 40°. There is another zone in which the safety coefficient exceeds the limit, at angles close to 90° and speeds above 18 m/s. The present asymmetry is due to the fact that the vehicle is traveling a curve to the left, therefore it undergoes a load transfer to the right; for positive angles the wind hits the vehicle on the left side, aggravating the load transfers due to inertia forces. On the contrary, for negative angles the wind

impacts on the right surface of the vehicle, compensating for the load transfers due to inertia. In this case, therefore, the external wind can result as a phenomenon that can negatively affects the safety of the vehicle or can affected in a positive way by opposing the overturning.
In this case it is noted that the safety coefficient exceeds the limit for wind speed equal to 18 m/s and angles of 20 °, while for wind with an angle of 50 ° the safety coefficient does not exceed the limit but the vehicle does not have a strong drift with respect to the reference trajectory. For this reason it will be reported the cases with wind speed equal to 18 m/s and angles of 50°, in which the trajectory is followed, and angles of 20° for which drift occurs.
The following figure 5.24 shows the trends of the safety coefficient in the two cases.

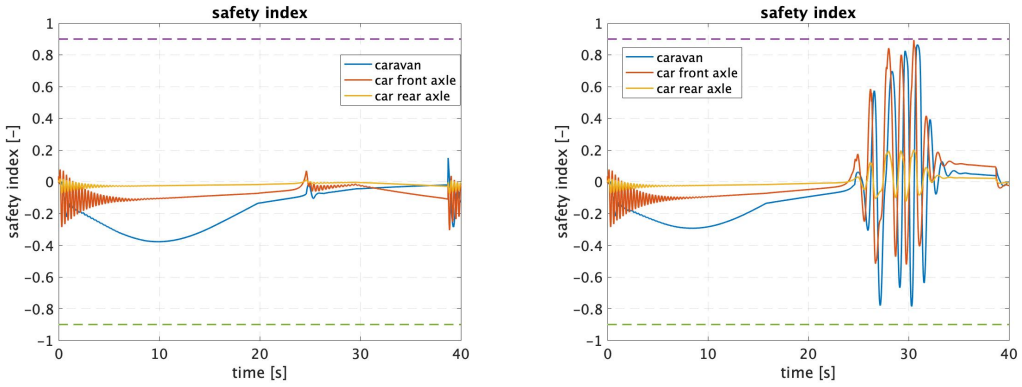

(a) η_i *at 18 m/s and 50°* (b) η_i *at 18 m/s and 20°*

Figure 5.24. Safety coefficients comparison for the two cases

Analysing the graph on the left it is possible to see how the safety coefficient associated with the caravan has a more marked variation than those associated with the car. This is due both to the dynamic characteristics of the caravan and to the fact that the caravan has higher aerodynamic loads having a considerable lateral surface. There is also a peak at about 25 seconds caused by the side gust.
Analysing the graph on the right the trend before the gust is almost identical to the left-hand case, while there are large fluctuations after the gust. It should be noted that the oscillations, even if they have very large amplitudes, never exceed the safety limit; this means that considering only the risk of overturning, the vehicle is in a safe condition even if close to the limit. In any case, the coefficients of the caravan and the front axle of the car reach values very close to the limit, indicating that the vertical load on the wheels undergoes strong decreases.
The following figure 5.25 shows the trends of the vertical loads associated with the caravan for both wheels.

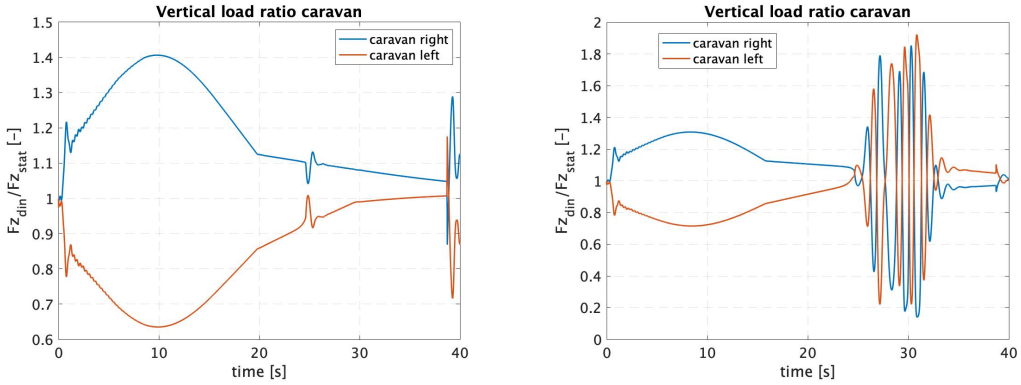

(a) *Vertical load ratio at 18 m/s and 50°* (b) *Vertical load ratio at 18 m/s and 20°*

Figure 5.25. Vertical load ratio comparison for the two cases

With reference to the graph on the left in the figure 5.25, it is possible to notice a strong variation of the vertical load with a peak at about 10 seconds. This trend is due to the establishment of the wind profile which in about 10 seconds runs out of the initial ramp and reaches the average value. In this case the load transfer is accentuated by the presence of the forces due to the curve and therefore the coefficients undergo greater variations than in the previous cases.
While, referring to the case on the right, there are strong oscillations in the presence of the gust which are then dampened after a time span of about 6 seconds. This behaviour is explained by analysing the graph on the right in the figure 5.26 where it is noted that the trajectory undergoes a variation and the vehicle is no longer able to follow the curve to the left but has a very marked drift towards the right.
It becomes very interesting therefore to analyse the trajectory followed by the vehicle in the two cases.

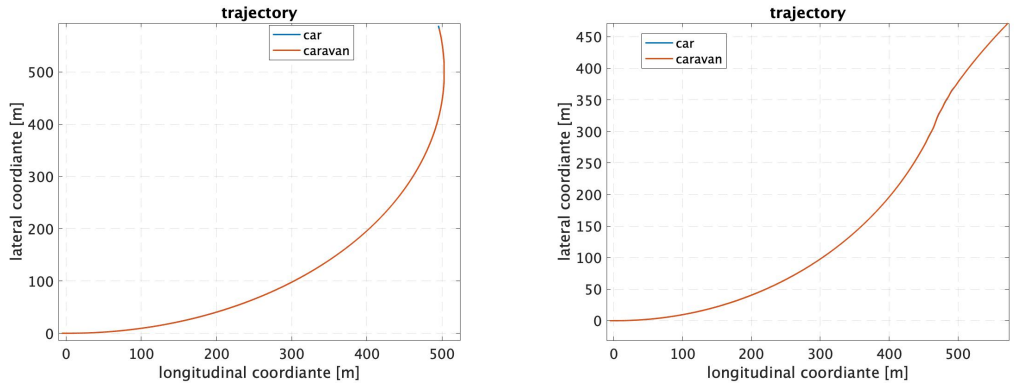

(a) *Trajectory at 18 m/s and 50°* (b) *Trajectory at 18 m/s and 20°*

Figure 5.26. Trajectory comparison for the two cases

Referring to the graph on the left, it can be seen that there are no major variations with respect to the reference trajectory. While analysing the case on the right it is possible to notice that there is a large lateral drift following the gust. This behaviour is very dangerous because although the vehicle is not at risk of overturning, the vehicle behaves abnormally. For this reason it is also important to consider the lateral drift

with respect to the reference trajectory and not exclusively the overturning.
In the following figure are reported the trends of the car and caravan roll angles for both cases.

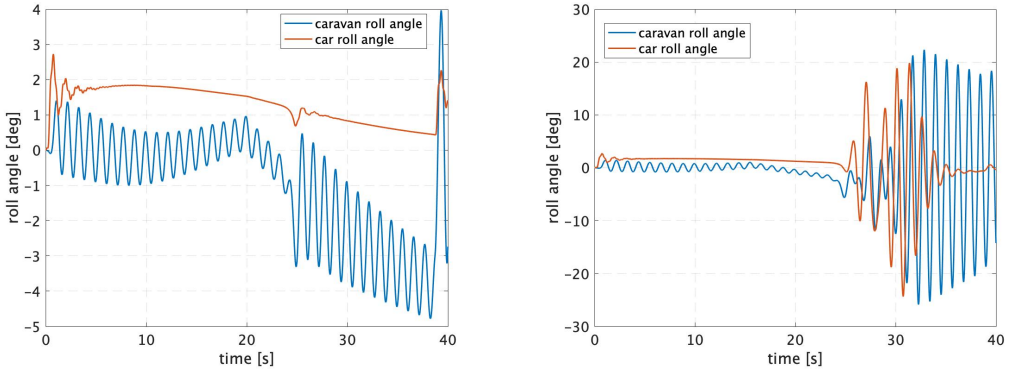

(a) *Roll angle at 18 m/s and 50°* (b) *Roll angle at 18 m/s and 20°*

Figure 5.27. Roll angle comparison for the two cases

With reference to the figure on the left, it is possible to see some oscillations in the roll angle of the caravan right from the start of the maneuver, which increase in correspondence with the gust.
Much more interesting is the behaviour in the case on the right in which it is noted that after the gust, large oscillations occur both on the car and on the caravan. The oscillations of the car are present only in the presence of the gust and have a duration of about 10 seconds, while in the case of the caravan the situation is much more critical. There are large oscillations up to angles of 20°.

5.3 Vehicle speed influence

This section analyses the effects of vehicle speed in all scenarios. Three different speeds have been tested for each trajectory: 60 Km/h, 80 Km/h and 100 Km/h. The results obtained for the different speeds are reported below, considering each trajectory previously exposed.

5.3.1 Speed influence on straight trajectory

In the case of a straight trajectory, three different vehicle speeds are compared: 100 Km/h, 80 Km/h and 60 Km/h.
The figure 5.28 shows the results regarding the safety coefficients relating to the caravan as they are the most severe indicators for analysing the safety of the vehicle. In fact, as seen previously, in the event of an unsafe condition in which the vehicle is close to overturning or is unable to maintain the reference trajectory, the safety factor of the caravan better represents this dangerous condition.

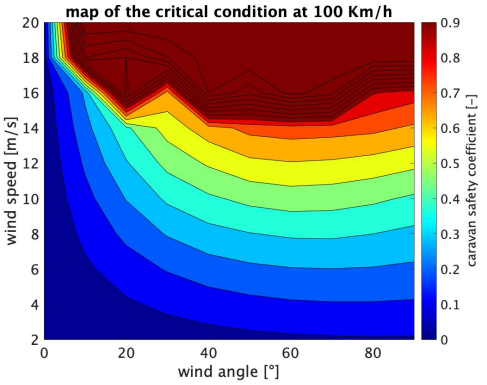

(a) *Caravan safety coefficient at 100 Km/h*

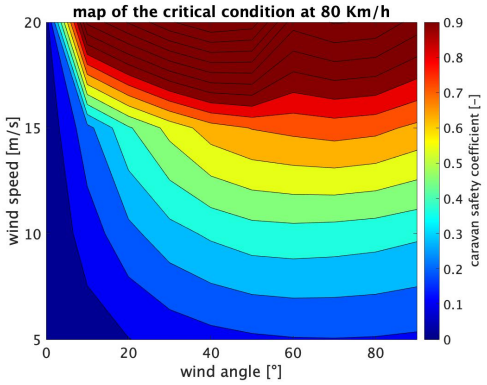

(b) *Caravan safety coefficient at 80 Km/h*

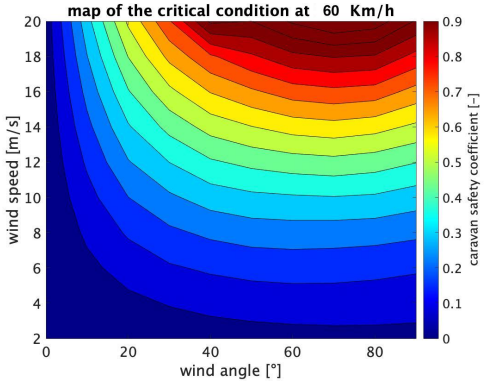

(c) *Caravan safety coefficient at 60 Km/h*

Figure 5.28. Safety coefficients at different speeds

Comparing the three figures 5.28, it can be seen that increasing the vehicle speed leads to obtaining critical conditions even for lower wind speed values. In particular, if the vehicle speed is 60 Km/h, the safety coefficient reaches the limit threshold for wind speeds above 18 m/s, while if the driver travel at a speed of 100 Km/h, the limit is reached for winds at 15 m/s.
A difference between the three cases also lies in the effectiveness of the wind angle. It can be noted that by increasing the vehicle speed the limit is reached for smaller angles than in the case at low speed. This is a very important factor as it increases the range of wind conditions for which the vehicle results in a dangerous condition.

5.3.2 Speed influence on lane change trajectory

Also in this case, the results regarding the safety coefficient of the caravan at different travel speeds have been compared. In this case the trajectory has undergone some slight changes in order to unrelate the results from the dynamic effects. In particular, the distance traveled has been increased at 100 Km/h , while it has been decreased in the case of 60 Km/h.
The following figure 5.29 shows the results.

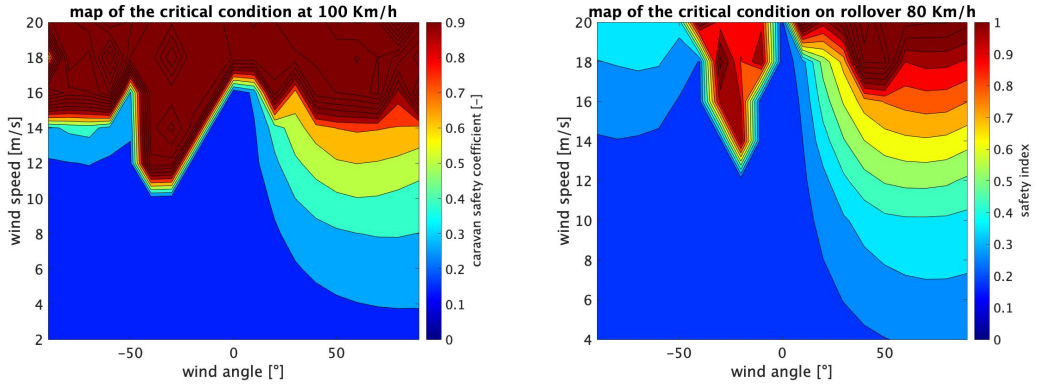

(a) *Caravan safety coefficient at 100 Km/h* (b) *Caravan safety coefficient at 80 Km/h*

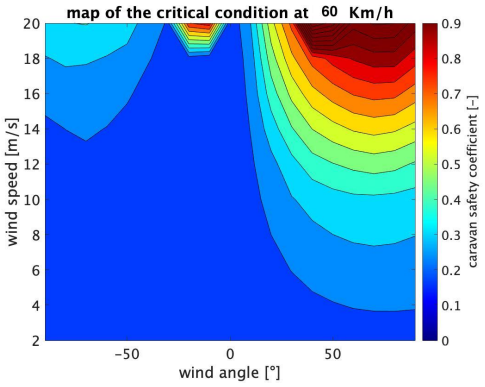

(c) *Caravan safety coefficient at 60 Km/h*

Figure 5.29. Safety coefficients at different speeds

Analysing the results in the figures 5.29 it can be seen that also in this case by increasing the vehicle speed the limit of the safety coefficient is reached for less marked conditions. In particular, it is noted that in the event that the vehicle has a speed of 100 Km/h there is a large expansion of the critical area, also incorporating the area of large negative angles which in the case of 80 Km/h is not present.
The area affected by the exceeding of the limit threshold decreases considerably if the vehicle is traveling at 60 Km/h.
In this case, in fact, it is possible to note that the exceeding of the limit threshold occurs exclusively in very adverse conditions with winds speeds above 18 m/s.

5.3.3 Speed influence on double lane change trajectory

For this trajectory the procedure was the same as the previous one, i.e. the distances to make the two lane changes were modified in order to exclude any effects due to the dynamics.
In the following are reported the results of the safety indexes at different speeds.

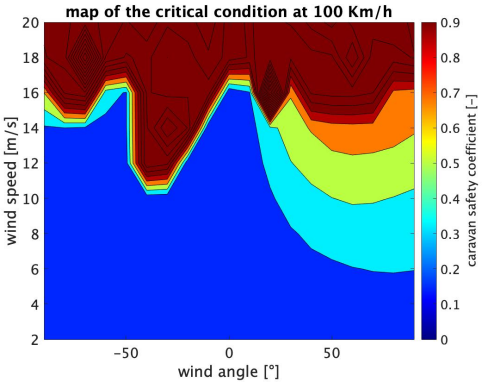

(a) *Caravan safety coefficient at 100 Km/h*

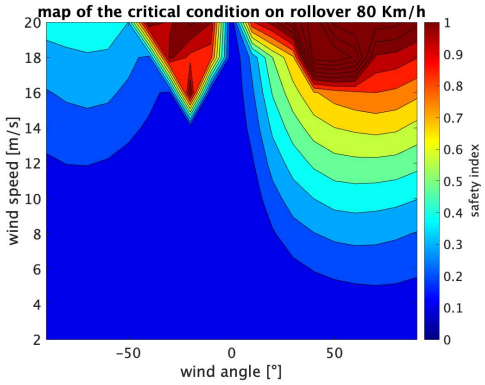

(b) *Caravan safety coefficient at 80 Km/h*

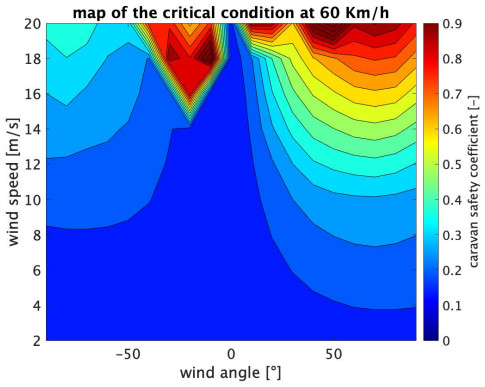

(c) *Caravan safety coefficient at 60 Km/h*

Figure 5.30. Safety coefficients at different speeds

By analysing the figure 5.30 it is possible to notice how an increase in the vehicle speed leads to a sharp increase in the area in which the safety limit is reached. In particular, it is noted that the area in which the safety coefficient of the caravan exceeds the limit value affects all angles from -90 ° to + 90 °, unlike the case at 80 Km/h where it is limited to some particular angles. There is also a strong decrease in the minimum wind speed for which the limit is exceeded, in the case at 100 Km/h this speed drops to about 12 m/s compared to 15 m/s in the case of 80 Km/h.
If the vehicle is traveling at 60 Km/h, the critical area has a smaller area, maintaining the same critical areas as in the case at 80 Km/h. In this case the difference is much less marked than the difference between 100 Km/h and 80 Km/h.

5.3.4 Speed influence on highway curve trajectory

In this case it was not possible to modify the trajectory to compensate for the dynamic effects as it is not a driver-dependent parameter as in the two previous cases. For this reason, the turning radius was kept at 500 m and only the vehicle speeds were changed.
The figure A.3 shows the results obtained.

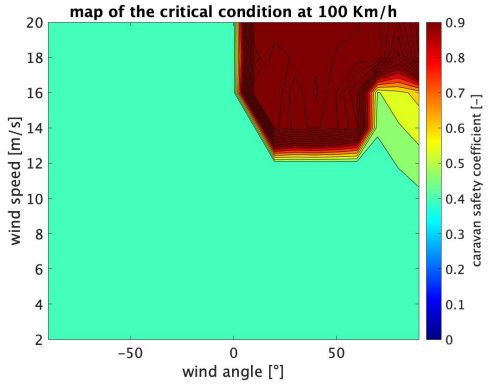

(a) *Caravan safety coefficient at 100 Km/h*

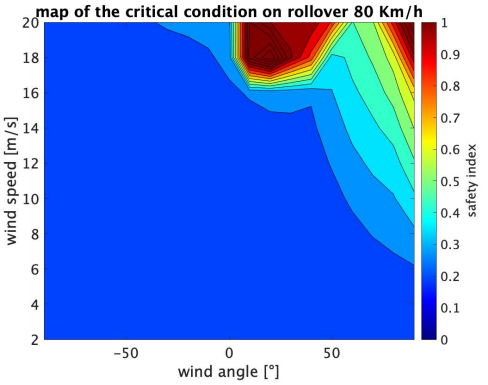

(b) *Caravan safety coefficient at 80 Km/h*

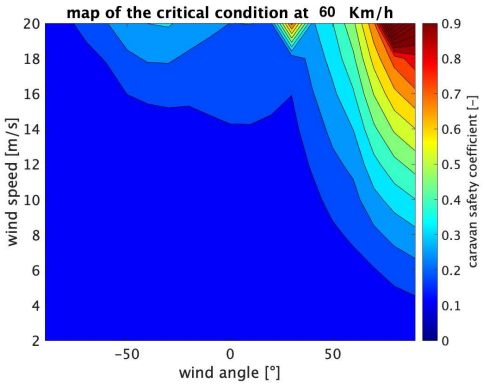

(c) *Caravan safety coefficient at 60 Km/h*

Figure 5.31. Safety coefficients at different speeds

Analysing the map in the upper left corner on figure A.3, it is possible to see how the safety coefficient has a higher average value than the other two cases due to the fact that the dynamic effects are more consistent due to the high speed. There is also an increase in the zone in which the safety coefficient exceeds the limit of 0.9, presenting threshold at 13 m/s. It is interesting to note that in this case, even at high speeds, the critical zone remains confined to the region with positive angles unlike the previous cases.
As regards the graph below in the figure, it can be seen that there is a considerable decrease in the critical area and the critical area corresponding to angles equal to 30° is no longer present. In this case, the criticality is present exclusively for strong wind speeds and marked angles, i.e. for speeds above 18 m/s and angles close to 90°.

5.4 Final considerations

In this section the final considerations are made by grouping all the critical situations based on the speed of the vehicle and the type of trajectories carried out.

Table 5.1. Critical conditions resume

Trajectories\Vehicle speeds	**100** Km/h	**80** Km/h	**60** Km/h
Straight	15 m/s 60°	17 m/s 35°	18 m/s 70°
Lane change	11 m/s - 40°	14 m/s -20°	18 m/s 80°
Double lane change	12 m/s -30°	17 m/s -20°	18 m/s -10°
curve	13 m/s 30°	18 m/s 20°	18 m/s 80°

From the table 5.1 it is clear that the trajectories that are most at risk of overturning are the two trajectories involving lane change. In these two cases, in fact, dangerous situations occur in the presence of gusts of wind with not too high speeds.
It can also be noted that in the case of a straight trajectory and a motorway curve, the critical wind speeds are identical in the case of the vehicle proceeding at 80 Km/h or at 60 Km/h, and the only difference is related to the direction.
Another important aspect is to consider the possibility of skidding, i.e. that due to the side wind gust the vehicle has a drift with respect to the reference trajectory. This aspect becomes of fundamental importance when driving on the road as, if there are significant movements, the vehicle could go off the road or in the worst case hit other vehicles in the vicinity. For this reason, a table is shown below which lists the limit conditions to prevent this from happening.
The results shown in the table 5.2 consider 0.25 m as the maximum permissible displacement with respect to the reference trajectory and are extrapolated from the graphs in the appendix.

Table 5.2. Critical conditions on lateral drift

Trajectories\Vehicle speeds	**100** Km/h	**80** Km/h	**60** Km/h
Straight	14.8 m/s 20°	18 m/s 35°	18 m/s 40°
Lane change	11 m/s -40°	14 m/s -10°	18 m/s -20°
Double lane change	11.8 m/s -40°	15 m/s -20°	18 m/s -10°
curve	16 m/s 80°	17 m/s 20°	18 m/s 40°

Analysing the table 5.2 it is possible to note that the critical conditions for which there is a lateral error greater than 0.25 m are almost identical to those reported in the table 5.1. This similarity indicates that it is correct to consider the safety factor of the caravan as a parameter for evaluating the overall safety of both vehicles.
A very important factor to consider is the driver. The driver model in fact greatly simplifies human behaviour, so the results obtained have a general validity but could vary considerably based on the modelling of the driver.
A factor that has not been considered in this work is the variability of the response based on the type of driver used. All the results obtained are strongly dependent on

the driver's response, therefore an interesting future work could be the study of the driver's influence. In fact, given the nature of the problem, completely different driver responses could occur as the driver's experience and ability to react to the gust vary. Furthermore, the driver could be taken by surprise and consequently could have a response that could accentuate the effects of the gust.
In order to have a rapid overview on the critical conditions, are reported four polar plot representing the limit conditions in all the four trajectory and for all the three different speeds. In these graph the line represent the critical conditions that can not be overcome. For each trajectory are reported three line representing the three different speeds analysed. In order to be sure that the vehicle is not close to overturning it is necessary that the wind conditions, associated whit the traveling speed, are below the represented lines.

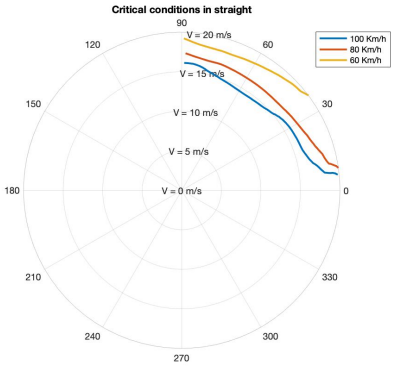

(a) *Safety limit for straight trajectory*

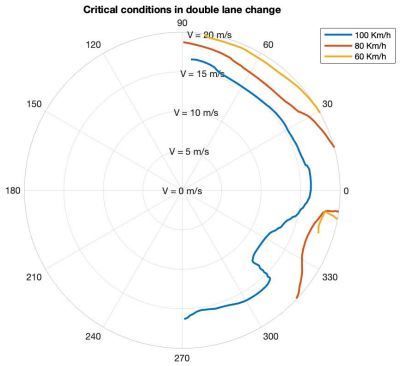

(b) *Safety limit for lane change trajectory*

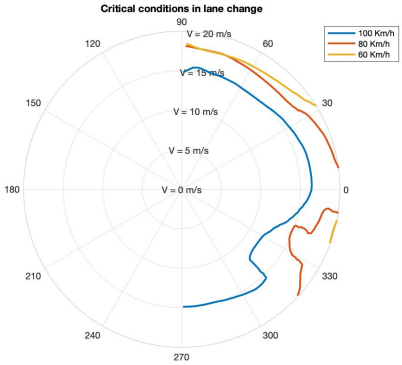

(c) *Safety limit for double lane change trajectory*

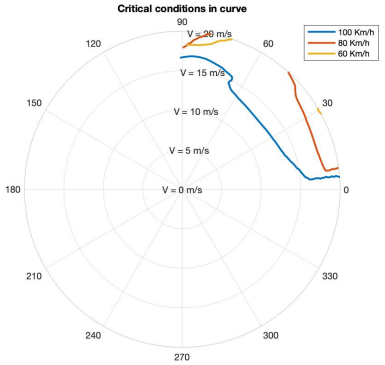

(d) *Safety limit for curve trajectory*

Figure 5.32. Safety limit for all trajectories

Conclusions

The aim of the thesis was to analyse the interaction between cross wind and a car towing a caravan. Three different coefficients were analysed to evaluate the vehicle safety in various cross wind conditions. The first, which is the most significant, analyses the vertical load variation for each axle. The second one studies the vertical load variation for each wheel. The third one analyses the sliding.
In addition, the behaviour of the roll angle in various situations was studied to understand importance of this parameter.
In order to obtain the aerodynamic loads caused by cross wind in multiple conditions, CFD simulations were carried out using the OpenFoam software. Based on these results an experimental campaign was carried out in the wind tunnel with the aim of validating the proposed caravan model.
Through the CFD simulations it was possible to obtain the aerodynamic coefficients associated to the two vehicles separately as function of the incidence wind angle.
For the dynamic analyses, a non-linear model was developed. It allow to study the behaviour of the vehicle subjected to different cross wind conditions. During the model creation phase, it was paid particular attention to three important aspects. Firstly, the definition of the vertical forces acting individually on each wheel. Secondly, the car's motion parallel to the ground. Thirdly, the rolling behaviour.
With the aim of obtaining results for the widest number of situations, four different trajectories were analysed, a straight line, a lane change, an overtaking maneuver and a motorway curve with a large radius of curvature. The wind model used, replicates a cross-wind gust. In particular the Chinese hat model was used.
The results obtained show that the influence of cross wind is of fundamental importance in the analysis of vehicle safety and, therefore, can not be neglected. In case of safe conditions was noted that the roll angle variations remain limited and, therefore, it was not necessary to carry out aerodynamic simulations with models presenting non-zero roll angles.
The results highlight that not only the wind speed during the gust but also the absolute angle associated with the wind is of fundamental importance and is closely related to the type of maneuver.
The most critical conditions arise in case of lane change and overtaking maneuvers, in which the safety limits are exceeded even with lower wind speeds respect to the other maneuvers. In these cases the direction of the wind plays a fundamental role, because it increases or decreases the loads transfer caused by the wind action.
In conclusion, it has been studied the vehicle speed influence, obtaining that a decrease in travel speed leads, in most cases, to a marked decrease in the percentages possibilities of encountering an unsafe condition. While an increase of the vehicle speed leads

to an increase of the loads transfers caused by the wind action, making the vehicle unsafe even for low wind speeds.
Once the critical conditions are known, it is possible to develop new method in order to decrease the effect of the cross-wind on the vehicle. This could be done by studying the effect of side barriers to be installed on the rode side, or by studying the shape of the caravan in order to reduce the aerodynamics loads acting on the caravan.
Another interesting aspect is the driver response; knowing the critical conditions for the different vehicle speeds it is possible to study the response of the driver using a driving simulator in order to study the relation between the type of driver and his response to a wind gust. These two aspects pave the way for new research and future work.

Appendix A

Appendix

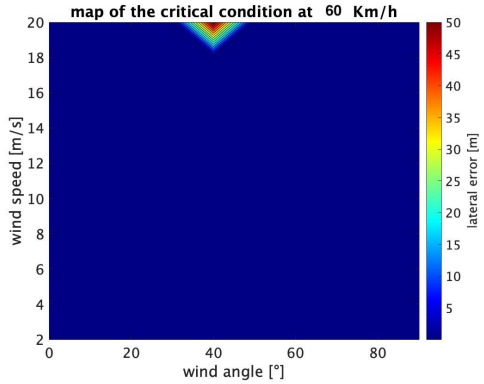

(a) *Car lateral drift straight trajectory*

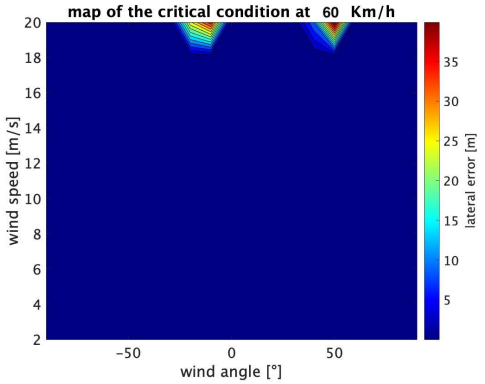

(b) *Car lateral drift lane change trajectory*

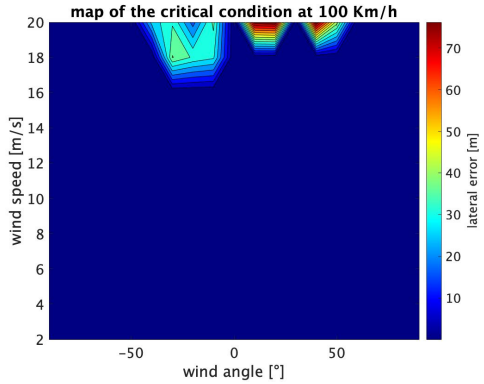

(c) *Car lateral drift double lane change trajectory*

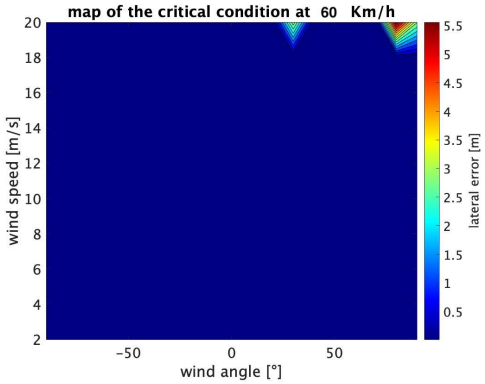

(d) *Car lateral drift highway curve trajectory*

Figure A.1. Lateral drift at 60 Km/h

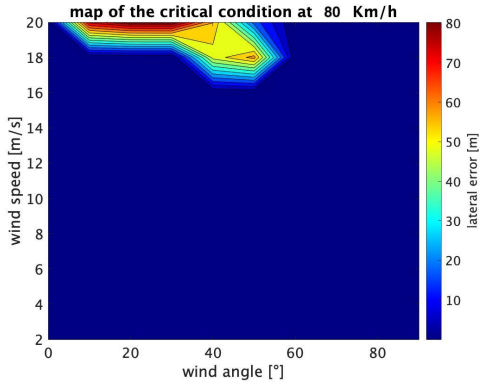

(a) *Car lateral drift straight trajectory*

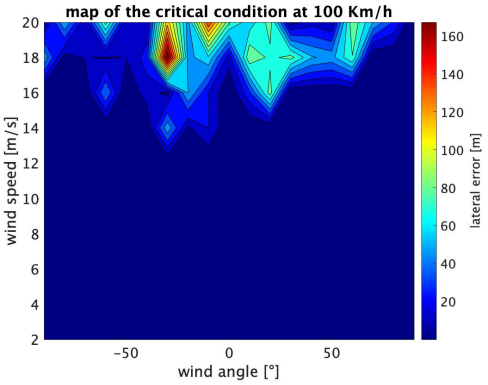

(b) *Car lateral drift lane change trajectory*

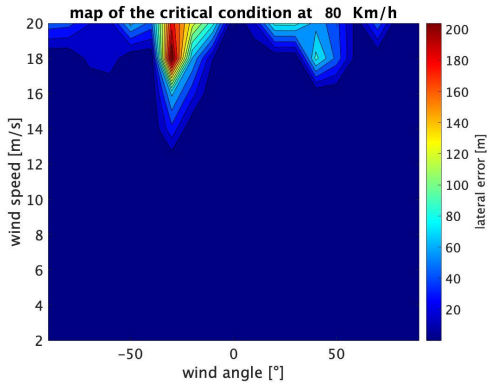

(c) *Car lateral drift double lane change trajectory*

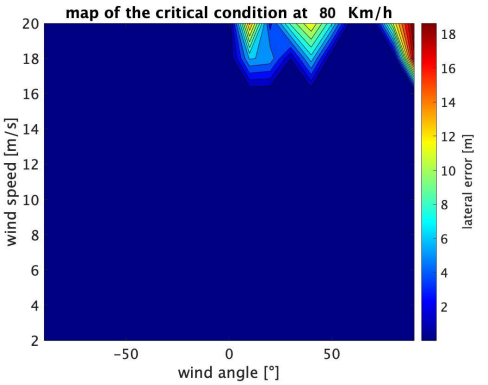

(d) *Car lateral drift highway curve trajectory*

Figure A.2. Lateral drift at 80 Km/h

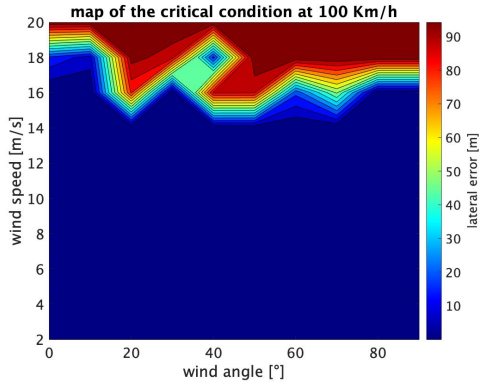

(a) *Car lateral drift straight trajectory*

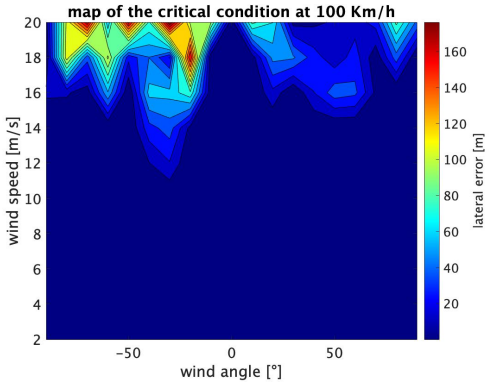

(b) *Car lateral drift lane change trajectory*

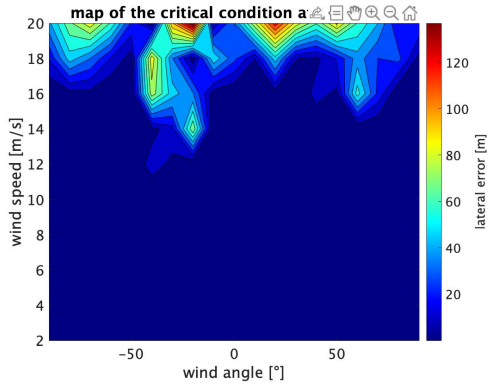

(c) *Car lateral drift double lane change trajectory*

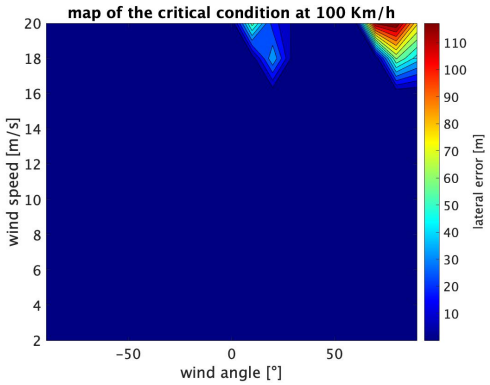

(d) *Car lateral drift highway curve trajectory*

Figure A.3. Lateral drift at 100 Km/h

Bibliography

[1] ISTAT. *INCIDENTI STRADALI IN ITALIA*. URL: https://www.istat.it/it/archivio/245757 (cit. on p. 1).

[2] F. Cheli L. Salati P. Schito. "Strategies to reduce the risk of side wind induced accident on heavy truck". In: (Jan. 2008) (cit. on pp. 1, 31).

[3] Johannes Wojciak et al. "Investigation of Unsteady Vehicle Aerodynamics Under Time-Dependent Flow Conditions". In: June 2011 (cit. on pp. 1, 2, 8, 38).

[4] Skuli Thordarson, Researcher, and Bjorn Olafsson. "Weather induced road accidents, winter maintenance and user information". In: (Jan. 2008) (cit. on p. 1).

[5] David H. Weir, Richard H. Klein, and John W. Zellner. "Crosswind Response and Stability of Car Plus Utility Trailer Combinations". In: *SAE Transactions* 91 (1982), pp. 570–583 (cit. on pp. 1, 4, 7).

[6] J Darling and P M Staden. "A Study of caravan unsteady aerodynamics". In: *Proceedings of the Institution of Mechanical Engineers, Part D: Journal of Automobile Engineering* 217.7 (2003), pp. 551–560 (cit. on pp. 2, 3).

[7] Johannes Wojciak et al. "Experimental Investigation of Unsteady Vehicle Aerodynamics under Time-Dependent Flow Conditions - Part2". In: (2011) (cit. on p. 2).

[8] S. Chen and C. Cai. "Accident assessment of vehicles on long-span bridges in windy environments". In: *Journal of Wind Engineering and Industrial Aerodynamics* 92 (2004), pp. 991–1024 (cit. on p. 2).

[9] R S Sharp and M A Alonso Fernández. "Car—caravan snaking: Part 1: The influence of pintle pin friction". In: *Proceedings of the Institution of Mechanical Engineers, Part C: Journal of Mechanical Engineering Science* 216.7 (2002), pp. 707–722 (cit. on p. 3).

[10] Qianwen Zhang et al. "Numerical Investigation on Handling Stability of a Heavy Tractor Semi-Trailer under Crosswind". In: *Applied Sciences* 10.11 (2020) (cit. on p. 3).

[11] Mr Adrian De Leon. "Improving Caravan Design by Modelling of Crosswind". MA thesis. University of Southern Queensland, Oct. 2016 (cit. on pp. 4, 9).

[12] Jakob Huemer et al. "Influence of unsteady aerodynamics on driving dynamics of passenger cars". In: *Vehicle System Dynamics* 52.11 (2014), pp. 1470–1488 (cit. on p. 5).

[13] M. Eng. Xiaoyu Zhang. “Crosswind stability of vehicles under nonstationary wind excitation”. In: (Apr. 2015) (cit. on p. 5).

[14] Yuping He and Jing Ren. “A Comparative Study of Car-Trailer Dynamics Models”. In: *SAE International Journal of Passenger Cars - Mechanical Systems* 6 (May 2013), pp. 177–186 (cit. on p. 5).

[15] M. Hubner et al. “Lateral stabilization of vehicle-trailer combinations against crosswind disturbances by means of sliding control”. In: *2008 16th Mediterranean Conference on Control and Automation* (2008), pp. 431–438 (cit. on p. 6).

[16] Martin Horn Robert Tafner Markus Reichhartinger. “Robust Vehicle Roll Dynamics Identification based on Roll Rate Measurements”. In: *The International Federation of Automatic Control Rueil-Malmaison, France, October 23-25, 2012* (2012), pp. 72–78 (cit. on p. 6).

[17] TUM. *DrivAer model*. URL: `https://www.mw.tum.de/en/aer/research-groups/automotive/drivaer/` (cit. on p. 8).

[18] Halshaw Hevans. “Best Used Family Cars for Towing Caravans”. In: (2020) (cit. on p. 8).

[19] Jeff Howell and Sumit Panigrahi. “Aerodynamic Side Forces on Passenger Cars at Yaw”. In: (Apr. 2016) (cit. on pp. 9, 38).

[20] A Carrarini. “Reliability based analysis of the crosswind stability of railway vehiclesl”. In: *International Journal of Rail Transportation* 0.0 (2006), pp. 20–25 (cit. on p. 11).

[21] Christian Wetzel and Carsten Proppe. “On reliability and sensitivity methods for vehicle systems under stochastic crosswind loads”. In: *Vehicle System Dynamics - VEH SYST DYN* 48 (Jan. 2010), pp. 79–95 (cit. on p. 11).

[22] Massimiliano Burlando et al. “Wind climate analysis in complex terrains”. In: *Journal of Wind Engineering and Industrial Aerodynamics* 123 (Dec. 2013) (cit. on p. 12).

[23] H. B. Pacejka and I. J.M. Besselink. “Magic formula tyre model with transient properties. Vehicle System Dynamics”. In: (1997), 27:234–249 (cit. on p. 25).

[24] José Neto et al. “Evaluation of the train running safety under crosswinds - a numerical study on the influence of the wind speed and orientation considering the normative Chinese Hat Model”. In: *International Journal of Rail Transportation* (2020), pp. 1–28 (cit. on p. 29).

[25] Wolf-Heinrich Hucho. *Aerodynamics of road vehicle. From fluids mechanics to Vehicle Engineering*. Vogel-Verlag, Würzburg, West Germany, 1987 (cit. on p. 33).

[26] Humberto Medina et al. “Open source Computational Fluid Dynamics using OpenFOAM”. In: Nov. 2015 (cit. on p. 34).

[27] Walter Frei. *Which Turbulence Model Should I Choose for My CFD Application?* URL: `http://precog.iiitd.edu.in/people/anupamahttps://www.evanshalshaw.com/blog/best-used-cars-for-towing-caravans/` (cit. on p. 34).

[28] Pelin Yılmazer. “Design of a Low-Speed Subsonic Portable Wind Tunnel for Educational Purposes”. In: (Jan. 2019) (cit. on p. 47).